Design of Composite Die for Wire Drawing

by

Rasheed Ahmed Butt

A Thesis Presented to the

FACULTY OF THE COLLEGE OF GRADUATE STUDIES

KING FAHD UNIVERSITY OF PETROLEUM & MINERALS

DHAHRAN, SAUDI ARABIA

In Partial Fulfillment of the
Requirements for the Degree of

MASTER OF SCIENCE

In

MECHANICAL ENGINEERING

January, 1994

Order Number 1360399

Design of composite die for wire drawing

Butt, Rasheed Ahmed, M.S.

King Fahd University of Petroleum and Minerals (Saudi Arabia), 1994

U·M·I
300 N. Zeeb Rd.
Ann Arbor, MI 48106

DESIGN OF COMPOSITE DIE FOR WIRE DRAWING

BY

RASHEED AHMED BUTT

A Thesis Presented to the

FACULTY OF THE COLLEGE OF GRADUATE STUDIES

KING FAHD UNIVERSITY OF PETROLEUM & MINERALS

DHAHRAN, SAUDI ARABIA

In Partial Fulfillment of the
Requirements for the Degree of

MASTER OF SCIENCE

In

MECHANICAL ENGINEERING

JANUARY 1994

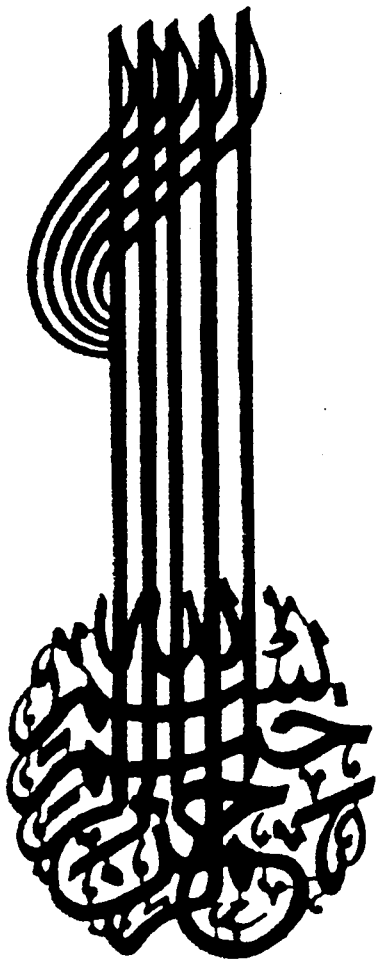

KING FAHD UNIVERSITY OF PETROLEUM AND MINERALS

DHAHRAN, SAUDI ARABIA

This thesis, written by

RASHEED AHMED BUTT

under the direction of his thesis committee, and approved by all the members, has been presented to and accepted by the Dean, College of Graduate Studies, in partial fulfillment of the requirements for the degree of

MASTER OF SCIENCE IN MECHANICAL ENGINEERING

Thesis Committee:

Ravi S. Rao
Chairman (Dr. Ravi S. Rao)

Anwar Khalil Sheikh
Member (Dr. A. K. Sheikh)

RR Guntur
Member (Dr. R. R. Guntur)

Dr. Muhammad O. Budair
Department Chairman

Dr. Ala H. Rabeh
Dean, College of Graduate Studies

Date: 5 · 6 · 94

Dedicated to

My Parents,

Brothers and Sisters

Acknowledgment

In the name of Allah, Most Gracious, Most Merciful. Read in the name of thy Lord and Cherisher, Who created. Created man from a { *leech-like* } clot. Read and thy Lord is Most Bountiful. He Who taught { the use of } the pen. Taught man that which he knew not. Nay, but man doth transgress all bounds. In that he looketh upon himself as self-sufficient. verily, to thy Lord is the return { of all }.

(The Holy Quran, Surah 96)

First and foremost, all praise to the Almighty Allah Who gave me the courage and patience to carry out this work. I am happy to have had a chance to glorify His name in the sincerest way through this small accomplishment and ask Him to accept my efforts. May He guide us and the whole humanity to the right path *(Aameen)*.

Acknowledgement is due to King Fahd University of Petroleum and Minerals for providing support to this work.

My deep appreciation goes to my major thesis advisor Dr. Ravi S. Rao for his constant help, guidance and the countless hours of attention he devoted throughout

the course of this work . His priceless suggestions made this work interesting and learning for me. He was always kind, understanding and sympathetic to me. Working with him was indeed a wonderful and learning experience which I thoroughly enjoyed.

Thanks are also due to my thesis committee members Dr. A. K. Sheikh and Dr. R. R. Guntur for their interest, cooperation, advice and constructive criticism.

I am also indebted to the department chairman, Dr. M. O. Budair and other faculty members for their support.

Lastly, but not the least, thanks are due to my family members for their understanding, throughout my academic career, and also to my fellow graduate students, and all my friends in the campus from whom I learned a lot and who made the long work hours pleasant.

Contents

List of Tables

List of Figures

Abstract

Name: **Rasheed Ahmed Butt**

Title: **Design of Composite Die for Wire Drawing**

Major Field: **Mechanical Engineering**

Date of Degree: **January, 1994**

In the present work a design methodology is developed to protect brittle ceramic materials from failure during drawing operations. Analytical and Finite Element techniques are employed to study straight taper and contoured dies respectively. Variation of shrink-fit pressure is studied by systematically varying some important process parameters. It is found that area reduction and exit wire velocity significantly affect shrink-fit pressure. Effect of radial thickness is significant only for small thicknesses. Semi die angle and die length have almost no effect on shrink-fit pressure. A comparison between the analytical and Finite Element approach shows that the analytical approach produces good results for small reductions and die angles.

Master of Science Degree

King Fahd University of Petroleum and Minerals

Dhahran, Saudi Arabia

January, 1994

خلاصة الرسالة

الاسم: رشيد أحمد بت

عنوان الرسالة: تصميم قالب صوغ مركب لسحب الأسلاك

التخصيص: الهندسة الميكانيكية

تاريخ الشهادة: يناير ١٩٩٤م

في هذا البحث تم تطوير طريقه تصميم معينة لحماية المواد السيراميكيه السريعةالانكسار من الانهيار أثناء عمليات السحب. حيث تم توظيف طريقين للحل أحدهما تحليلي و الأخر ذوفروق محددة و ذلك لدراسة قوالب السحب المستقيمة المستدقة و كذلك قوالب السحب المنفرجة المستدقة. ولقد تمت دراسة تغير الضغط الانكماشي بين قالب السحب والاسطوانه الخارجية المحيطة به وذلك بالتغييرالمنتظم لبعض المقادير الهامه في عملية السحب حيث وجد أن عملية تقليص المساحة وسرعة خروج السلك توثر بشكل كبير في الضغط الانكماشي. أما تأثير السمك القطري فقد وجد أن له تأثيرا واضحا فقط في حالة السماكات الصغيرة. أما زاوية قالب السحب وطوله فقد وجد أنها غالبا لا يؤثران على الضغط الانكماشي. لقد أظهرت المقارنه بين الحل التحليلى والحل ذو الفروق المحددة أن الحل التحليلى يعطى نتائج جيدة اذا ما كان زاوية القالب ومقدار تقليص المساحة صغيران.

درجة الماجستير فى العلوم
جامعة الملك فهد للبترول و المعادن
الظهران – المملكة العربية السعودية
يناير ١٩٩٤م

Chapter 1

Introduction

Wire is one of the most important products required by modern man. The near-endless lengths of wire used in the form of conductors in communication and power fields, the enormous quantities of wire drawn for fencing in farms and in cities, and spun into cables for bridges and hoists, give us an imperfect idea of the immense bulk of this material which is produced and utilized every day. Some of the products are made to exact specifications in dimension, surface finish and mechanical properties. Their sizes may vary in diameters from fraction of an inch down to diameters of a few thousandths. All of the products are commonly produced by the process known as *wire drawing.*

1.1 Wire Drawing Process

Among all metal forming processes, wire drawing is the most well-understood from the view point of process mechanics. The past several decades have witnessed the development, refinement, and utilization of a variety of analyses and models which now enable the process engineer to control metal flow, prevent defects and optimize process efficiency.

Drawing operations involve pulling metal through a tapered die by means of a tensile force applied to the exit side of the die. Most of the plastic flow is caused by compression force which arises from the reaction of the metal with the die.

The raw material for wire drawing is generally a rolled wire or rod. Although many shapes are produced by this process, this study is restricted to circular cross sections. The dimensional accuracy and surface finish obtained by drawing are superior to those for rolling. When these characteristics are required, drawing follows rolling. All kinds of ductile materials can be processed by drawing.

The raw material is first cleaned of scale, from the previous hot rolling or of rust, by mechanical or chemical treatment. It then might be coated with a good lubricant. For drawing, the end is chamfered to enter the die so that it can be clamped and pulled. Several kinds of equipment are used for drawing, depending upon the size of wire to be drawn; these can be classified into two groups. One type is draw bench, for drawing wires of larger diameters, as shown in Figure 1.1; the other is a

drawing block with a drum to pull and coil the wire, as shown in Figure 1.2. As is known, both from practice and from theory, only a small reduction in size can be achieved by the use of one die. For the larger sizes, a wire drawing machine is constructed as a single block unit. For finer wire, blocks in tandem are used. The drawing tool may be constructed from an assembly of blocks to form the shape of the product. Wire as fine as 0.0004 *in.* in diameter is drawn. Since wire drawing is a cold forming process, an intermediate anneal is often required before the final diameter is reached. Controlled atmosphere furnaces are common equipment in a wire drawing plant. The hardness and ductility of the finished wire are controlled by the amount of reduction effected from the last re-crystallization anneal to the final product. Final heat treatment and coating can be given to the wire if desired.

1.2 Wire Drawing Dies

Every one, in the field of metal forming, is aware of the importance of a good die. Even the best wire drawing equipment, the best lubricant will fail, when a set of poor die is used. The wire drawing die has been aptly described as being outstanding among all devices employed by man in that it presents a very remarkable combination of simplicity and effectiveness, causing plastic flow of metal obtainable by no other method. It changes the physical properties of the material and provides

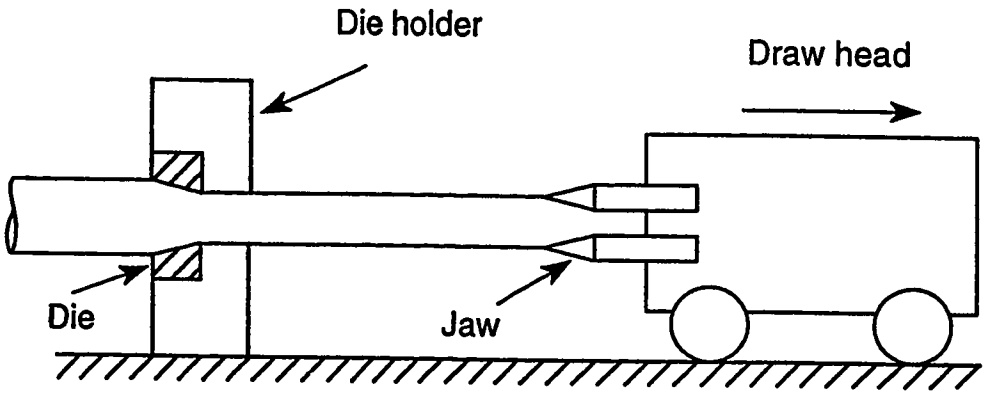

Figure 1.1: Schematic drawing of a draw bench.

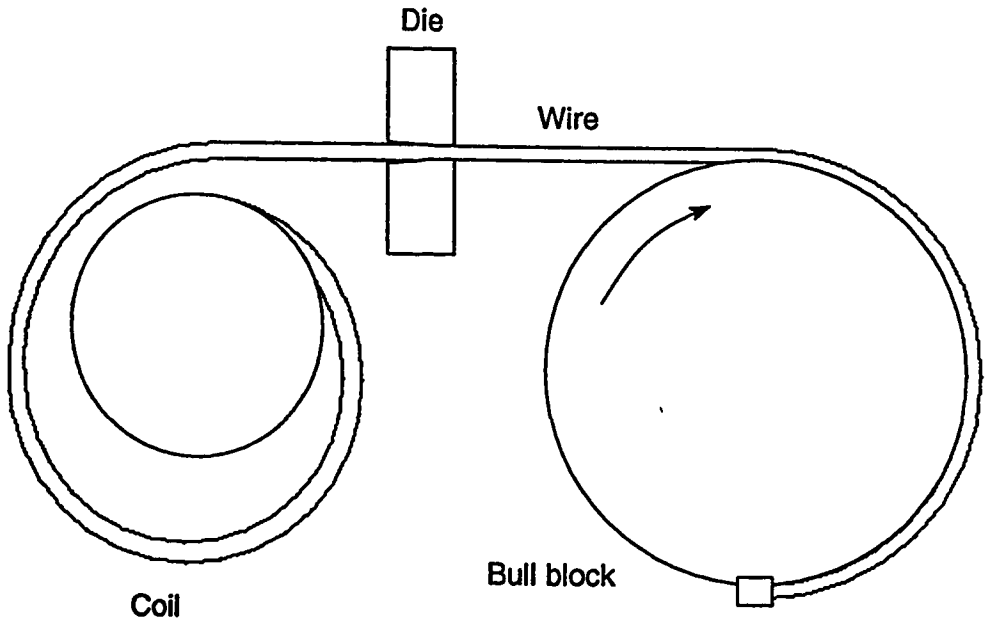

Figure 1.2: Schematic drawing of a block drawing equipment.

wire with a degree of accuracy of size and section obtainable by few other methods. To the metal it imparts a dense structure, a hard surface, and a high degree of polish.

To obtain the properties described above the drawing die must have a special profile, which in general consists of five different important parts, as shown in Figure 1.3. These are described briefly in the following sections.

1.2.1 Entrance Angle

The function of the entrance angle is to direct the flow of lubricant into the die approach angle where the lubricant is compacted onto the wire surface during drawing. The entering wire should be guided directly into the approach angle without making contact with the entrance angle, except when paying off from a coil. This region can be left in the rough-cored condition. In general angles can vary from 40° to 80°.

1.2.2 Bell Radius

This section of the die is used to guide the incoming rod only if it enters the die contour in a spiral path. The rod contacts this surface for a moment before entering up in the conical approach angle. This region can also be left in the rough-cored condition. Angles vary from 30° to 40°.

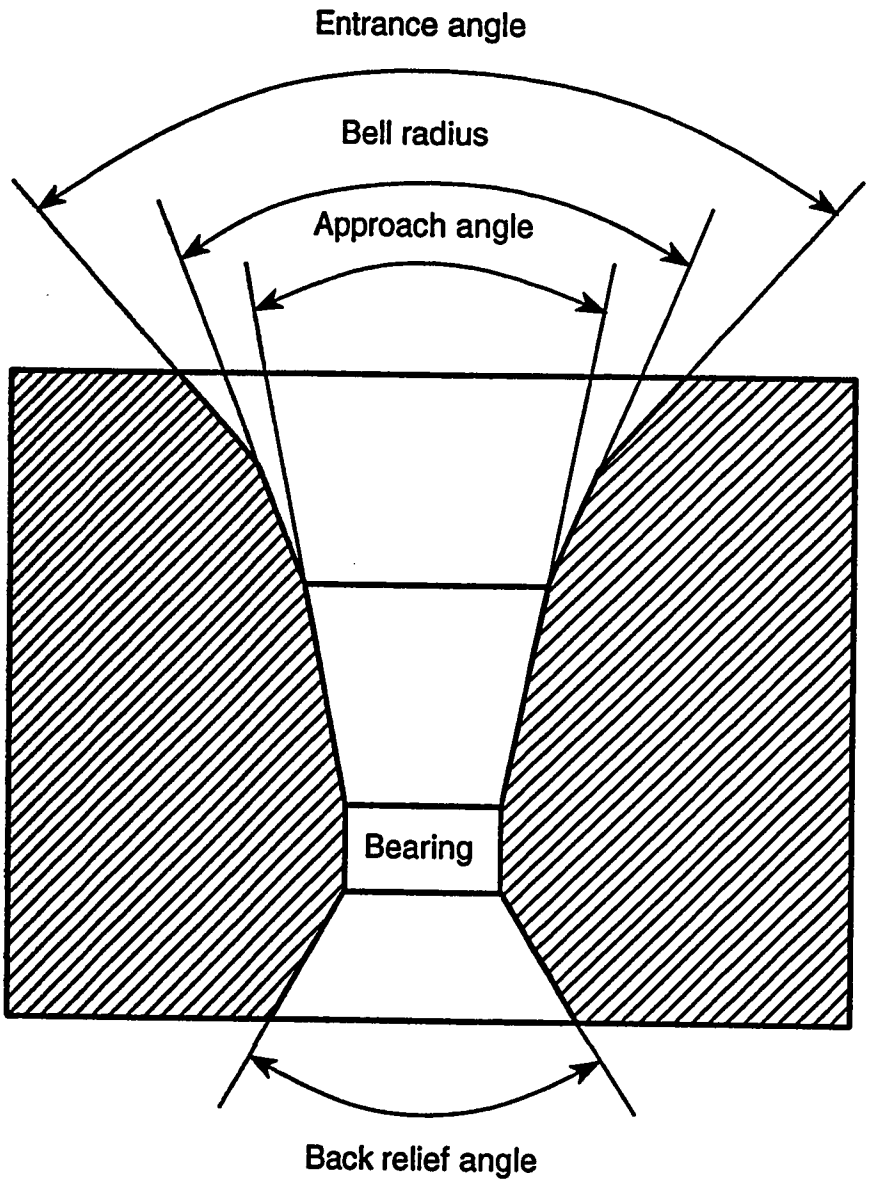

Figure 1.3: Die nomenclature.

1.2.3 Approach Angle

The approach angle is the most important section of a wire drawing die. The entire reduction in area and the compacting of lubricant onto the incoming wire occur here. The efficiency of any wire drawing die is determined by the design and accuracy of this approach area which must be cut to a specified die profile with a smooth surface finish. The angle must be precision-machined on equipment designed to assure that the approach angle and bearing diameter surfaces have a common center line; in addition, these surfaces must be concentric with the outside diameter of the die. Angles vary from 10° to 20°.

1.2.4 Bearing

The function of the bearing in a wire drawing die is the final control of the diameter of the drawn wire and to guarantee its roundness, straightness, and flat, smooth surface finish. For this reason the surface must be accurately machined to ensure roundness and finish to close dimensional tolerances. To prevent the die from rapidly wearing oversize, the length of parallel bearing surface should be from 35 to 50 percent of the bearing diameter. The correct length of parallel bearing surface helps to extend die life when wire drawn through the die is pulled off-line, causing additional pressure to one side of the bearing surface.

1.2.5 Back Relief

The back relief conical area is designed to strengthen the exit of the die and prevent breakage of the die. The back relief angle is usually preformed in a rough cored die. In most cases, it is large enough in diameter to accommodate the re-cutting of larger sizes without the necessity of enlarging the angle. Angles can vary from 30° to 70°.

To achieve a smooth flow of the material through the die, the five regions of the profile, mentioned above, are carefully blended into each other and the die mirror-polished as near perfect as possible to minimize friction and heat caused during the wire drawing process. The portions of these five different regions in a die profile considerably depend on the materials to be drawn. As a general rule, one can say that harder wire materials demand a profile with smaller reduction and longer bearing lengths than softer ones. Naturally, there are exceptions to this rule and controversial opinions of die experts exist, but the majority of wire drawing applications has confirmed such drawing die profiles.

When wire dies have worn beyond the accepted bore tolerance, it is a normal practice to open them up to a larger diameter. This requires a high degree of quality because any holes revealed by re-working will result in rejection.

1.3 Die Materials

In the Middle Ages, drawing tools of rather primitive design and made from materials like hard wood, iron plate dies, and later on from rubies were in use. Tools of that primitive kind certainly did not allow great improvements in quality and performance of wire drawing. After that period, tool steels were supposed to be the main die materials. The need to draw materials of higher strength, compelled researchers to find ways to make dies from more harder materials available at that time.

Sintered carbides were first used in 1914 as a die material. The succeeding applications as wire drawing dies did not give sufficiently encouraging results until 1922. Today this material is available in a varied selection of sintered carbides for the wide range of wire drawing applications.

Natural single crystal diamond is the hardest material known. Accordingly, it is the most suitable material to be used in dies, because of its wear resistance. Natural diamond has been used for wire drawing since the second half of the 19th century for drawing round wires up to 0.1 *in* maximum diameter.

In particular, diamond has a chemical affinity with ferrous materials and at high temperatures tends to form carbides, which can lead to premature wear of the die bore. Therefore iron or steel wires are generally drawn with carbide dies.

Synthetic poly-crystalline diamond dies consists of randomly oriented single crys-

tals of synthetic diamond giving virtually constant hardness in all directions. This endows them with a wear resistance better by a factor of 5 than natural diamond in wire drawing, and a much greater resistance to fracture.

1.4 Scope of the Present Study

Ceramic materials, like Alumina(Sapphire, Al_2O_3) and Zirconia(Z_rO_2) are hard and have good wear resistance. Such properties are attractive for selecting these materials for forming dies. However they are brittle in nature and have very low toughness. Hence, they must be protected from failures due to any excessive tensile stresses produced during the drawing operation. This can be done by supporting it with a high strength steel holder.

The question, why one wants to use these ceramic materials?, has been answered partially in the above paragraph. In addition to the above mentioned properties ceramic materials have,

- a high melting point
- chemically inert at high temperatures
- retains strength at high temperatures

These physical properties, together with a method to protect them from tensile failure, give the following advantages when ceramics are used as a die material.

- improved surface finish of the product
- lower die maintenance
- higher drawing ratios
- decreased die wear
- increased drawing speeds

Another very important factor, observed from experiments [1], appealing the wire manufacturers, is a lower coefficient of friction between the die and work-piece as compared with the traditional carbide dies.

A design methodology for utilizing these brittle ceramic materials effectively, as a wire drawing die material, has been developed. A brief discussion of the above mentioned methodology is given in the following paragraph. Mathematical details will be presented in later chapters.

There are, in general, three ways of protecting these brittle materials from failure, namely;

1. Providing pre-stress by shrink-fit,
2. Providing pre-stress by ribbon wound,
3. Providing pre-stress by wire wound.

We have used the simplest and most economical technique to pre-stress a ceramic die, i.e the shrink-fit technique. By pre-stressing a short cylinder (having high strength

and toughness properties) over such a die material, a residual circumferential stress is introduced into the die. This residual stress significantly reduces the magnitude of any tensile circumferential stress that is introduced during the drawing operation. The net effect of pre-stressing is longer life, from a fracture stand point and it improves fatigue loading.

Stress analysis of a composite pre-stressed die is performed. First, by using the Lame's thick walled cylinder theory, for dies of small semi angle and secondly by using a Finite Element software for contoured dies(Cosine and Convex die). This software is employed for the first time to solve the shrink-fit composite die design problem of contoured dies. For a given set of process parameters, e.g area reduction, exit wire velocity, semi die angle, axial die length, optimization of the die dimensions is also carried out. Because of the classified nature of the problem, not much information is available in the literature regarding die design. From the available literature it is found that until now the wire drawing process and wire drawing die design have been studied independently. In the present study integration of the process with die design is also carried out through a Fortran program (valid for small area reductions and small semi die angles), so that the input to the design part comes from the actual process. The terms small reductions and small die angles stands for reductions of up to 15 % and semi die angles of about 7°.

Chapter 2

Literature Review

2.1 Wire Drawing Process

Up to the mid of 19th century the process of wire drawing and extrusion was considered within the framework of classical time-independent plasticity theory . Drawing stresses and die pressures were calculated using slab analysis and force balance techniques. In 1955, an extensive experimental study of wire drawing process was carried out by Wistrech [2]. He not only measured drawing forces but also the mean die pressure and the mean coefficient of friction. The investigation revealed weaknesses in all wire drawing theories. A simple relation between tool-stock configuration and non-homogeneity of deformation was also discovered. The assumption that the deformation is independent of the properties of the wire was found invalid for annealed wires drawn with very light reductions.

Although the results obtained were in good agreement with experiments for low to moderate drawing speeds. With the introduction of high speed drawing machines, experimental results did not support this theory very well. Avitzur [3, 4] employed upper bound technique to calculate drawing stresses for small and large angle dies. Results, when compared with [2], shows good agreement for low drawing speeds.The need to develop a theoretical background for the effect of drawing speed on various drawing parameters was emphasized by Davies and Austin [5] through their experimental findings.

In 1975 Cristescu [6] introduced a new theory for wire drawing, using a visco-plastic constitutive equation. It was shown that the drawing stress is increased when the speed of the process or when the viscosity coefficient of the material is increased or when the diameter of the die is increased or when the mean yield stress of the billet is reduced. It was also shown that the optimum semi cone angle depends on the speed of the process. Cristescu performed a number of experiments [7] and justified his theory by concluding that the drawing speed has a significant effect on drawing stress even for small velocities. At the same time Tirosh and Kobayashi [8] presented an approximate analysis for estimating the external load required for deforming a time-independent, perfectly plastic material at different time rates. In their analysis they also found two fundamental non-dimensional numbers, one was related to the speed at which the deforming load was applied (the speed effectiveness parameter) and second was related to the acceleration of the deforming tool and its contact

area with the flowing metal (the dynamic head). Therefore they concluded that the effect of these two parameters should be considered even for moderate speeds. Most materials were found strain-rate sensitive. So that an increase of the speed was usually associated with an increase in the yield stress. Camnschi, et al. [9] solved the same problem using the same visco-plastic constitutive equation [6] by perturbation series method. They obtained an expression for drawing stress as a function of drawing speed, friction coefficient, die angle, plastic and viscous property of the work metal. Results when compared with [6, 7] gave an excellent agreement. Since the perturbation series method gives drawing stress as a function of a number of process parameters, Sandru and Camenschi [10] solved the drawing problem using perturbation series method. They also found drawing stress as a function of a number of process parameters. The results were in good agreement with [6, 7]. Kohser and Cronister [11] studied the wire drawing process from a different but important view point. They conducted wire drawing experiments on a verity of engineering alloys to determine the effect of the forming operation and its various process parameters upon the resulting properties of the metal. They observed that, in all curves of draw stress versus die angle, an optimal die angle exists which minimizes the required drawing stress for the particular material and reduction being studied. The curves for product density showed that, in general, dies with large cone angles tended to produce a less dense product than those with smaller angles. The magnitude of density variation was strongly dependent upon the nature of the

material being deformed.

In 1980 Cristescu [12] used the same visco-plastic constitutive relation [6], and showed how the optimum die angle, i.e the angle which would give the minimum drawing force, can be calculated for different drawing speeds, wire diameters, frictional conditions and mechanical properties of the billet material. He concluded that an optimum drawing process can be obtained only by a very accurate determination of the die angle required for each particular drawing condition.

The straight cylindrical portion of the die had not been considered seriously as a parameter influencing final properties of the product until 1981. Vannes and Theirry [13] carried out a theoretical-experimental analysis for the case of low angle dies and moderate reductions. The problem was examined particularly taking into account the effect of the cylindrical portion of the die. Experiments were carried out on three dies each with a different bearing length. They concluded that for moderate reductions, dies with longer cylindrical portion produce good quality products.

Durban [14] investigated the effects of material strain rate sensitivity on steady forming processes (sheet and wire drawing) of plastic solids. He obtained explicit expressions for the stress field within the working zone, valid only for long and tapered dies. He concluded that the strain rate sensitivity of the material is related to the dependence of the driving stress on the Bingham number. Results compared with analytical studies and with experimental results showed good agreement.

2.2 Contoured Dies

As evidenced from experiments that die contour has a strong effect on the ductility of the final product. First theoretical work on contoured dies for strip drawing was carried out by Richmond and Devenpeck [15]. Using slip-line field theory they showed that it is possible to achieve the same efficiency and uniformity of the product in a strip drawing operation as can be achieved by uniform compression. This was done by shaping the die in such a way that the direction of flow in the plastic region was every where coincident with the direction of principal stress.

In another study [16] they perform a number of strip drawing experiments to evaluate a sigmoidal die profile which, according to slip-line theory, can achieve perfect work efficiency and uniform deformation. On the basis of the criteria examined - drawing efficiency, strain uniformity, product strength, product ductility, and product fatigue life - the sigmoidal die profile proved best of the straight, convex, and concave die profile, each designed for a similar reduction and axial length. The surface contours of the above mentioned dies are shown in Figure 2.1.

Samanta [17] employed a new technique to design die profiles which yield high process efficiency during axi-symmetric wire drawing. The upper bound on the average drawing stress was calculated for small to large reductions and optimal die lengths. It was shown that up to 55 percent reduction the normalized drawing stress was same for both the convex and cosine die. Also the efficiency of the proposed

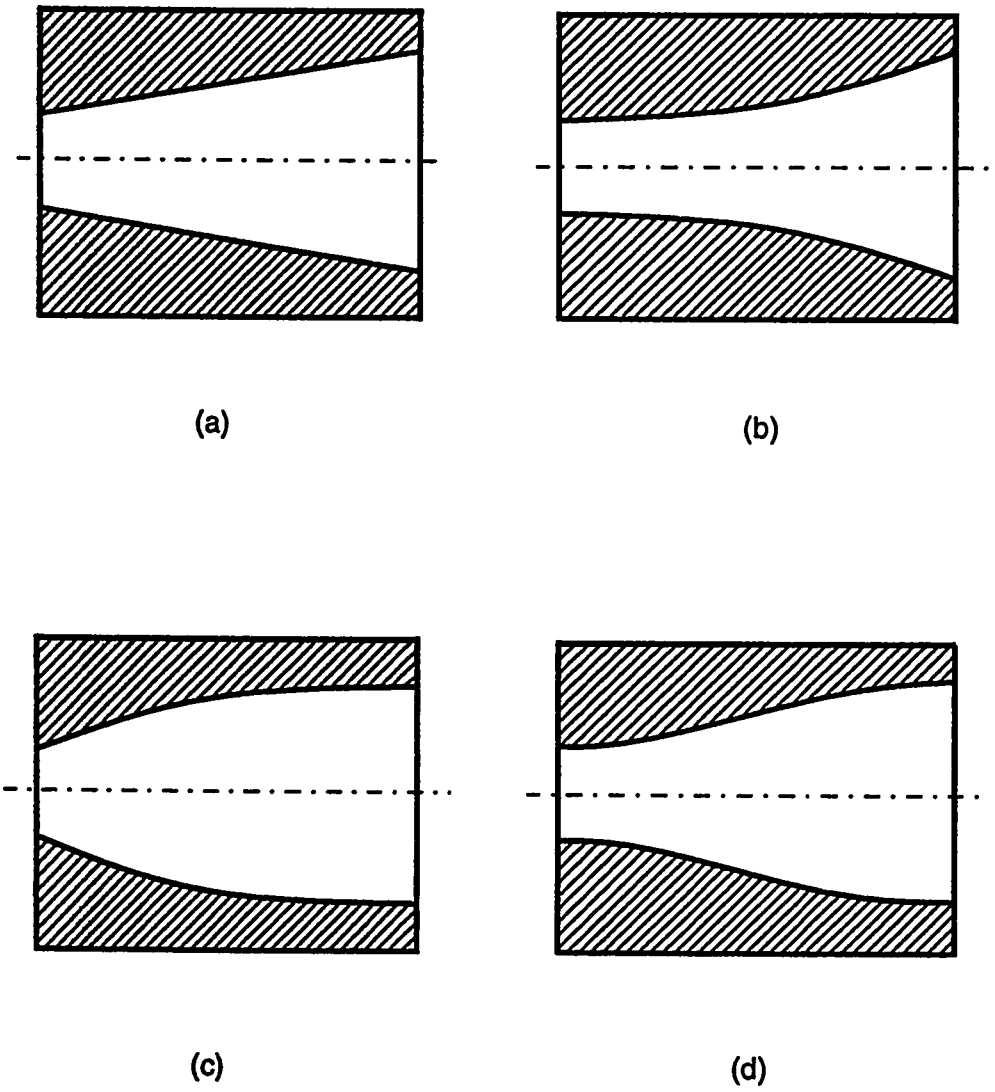

Figure 2.1: Schematic drawings of (a) Straight taper (b) Convex (c) Concave and (d) Sigmoidal die profile

convex die exceeds those of conventional conical dies.

Richmond [18] extended his previous work to the case of axi-symmetric deformation and gave some new examples of streamlined dies. He concluded that streamlined dies showed slight improvement in efficiency and product tensile strength, and a more significant improvement in product ductility and fatigue strength. With the introduction of NC and CNC machines, now it is possible to produce dies of any profile by just writing down a program [19, 20]. Also Finite Element Method is playing an important role in studying metal forming processes. Oh [21] make use of the rigid plastic FEM, which was developed by Lee and Kobayashi [22], to establish the theoretical foundation of the rigid visco-plastic FE analysis of metal forming processes with arbitrarily shaped dies. Solutions obtained using this technique were in good agreement with experimental results.

2.3 Shrink-Fit Dies

As has been said earlier in chapter 1 that, because of the classified nature of the problem, very little information on the mechanics of wire drawing die is available in the literature. Instead a lot of qualitative discussion on drawing dies is available [23, 24, 25, 26, 27].

The idea to pre-stress drawing dies has come from high pressure vessels and high pressure concrete pipes [28, 29, 30, 31, 32, 33], where this technique is basically used

to reduce the weight of the container, to increase the pressure bearing capacity and because of space limitations. In forming industry the main objective of pre-stressing is to provide additional strength to the die and in some instances because of space limitations. Most of the time a pre-stress is required for extrusion dies because of the tremendous internal pressure generated by pushing the working material through an orifice. Recently a stress analysis of such a die has been performed using Lame's theory [34] and also by a Finite Element code [35]. Usually drawing dies are designed by assuming that the internal pressure is uniformly distributed in the working zone. Lang [36], using FEA, performed the stress analysis of extrusion dies by assuming a linear pressure variation in the working zone. A different pre-stress technique was used by Gronbaek and wanheim [37] but they also used the Lame's solution and did not consider the effect of taper.

2.4 Sapphire Dies

The use of sapphire in metal forming processes emerged from earlier work on machining by Doyale, et al. [38] and Wright [39]. First use of sapphire as a die material in strip drawing was by Rao, et al. [40]. The objective of employing these dies was to observe and photograph the work material as it passes through the working zone. The photographs were then used to provide incremental displacement boundary conditions for input to the analysis. In another study of strip drawing Lu, et al. [41]

employed Finite Element Analysis, using measured boundary conditions at the work-piece die interface with the help of transparent sapphire dies. Appleby, et al. [42] performed a theoretical experimental comparison for plane strain strip drawing using experimentally determined stress strain curve and measured die-interface velocities. Predicted values of drawing force, separating force, global friction, and residual stresses were in good agreement with the experimental values. Rao, et al. [1] performed a number of experiments on carbide and sapphire dies by systematically varying different process parameters. The data obtained from these experiments were used as the prescribed boundary conditions in a large strain elastic-plastic Finite Element Analysis of the strip drawing process. With this information it was not necessary to assume a friction model. Instead, the solution provided information on the local friction as well as on the stress and strain distributions, drawing load, and residual stresses in the work material. Finally they concluded that transparent dies were very useful for observing the tribological conditions along the tool work-piece interface during the deformation process. By using this technique it was also possible to determine the relative velocity profile at the interface, which in turn was used as input to a model of the process. Another important result was that sapphire dies exhibit lower coefficient of friction than carbide dies, but the variations with the process parameters were similar for both die materials. Rao [43] performed a theoretical-experimental analysis for strip drawing using prestressed sapphire dies. The strip drawing analysis was based on the force balance method and includes

redundant shearing. He also studied the effect of back tension on drawing, which in turn affect die design. Results obtained were in good agreement with experiments and showed that simple strip drawing analysis provided an adequate estimate of forces and pressure acting on the die. Finally he concluded that, because of low coefficient of friction, these dies would reduce the frictional forces and power consumption in metal working processes.

Chapter 3

Design of Composite Dies

3.1 Introduction

The majority of drawing dies are conical in nature and are usually analysed by assuming cylindrical geometry. When the internal pressure is low, the wall thickness of the cylinder is not great and the tangential and radial stresses are almost uniformly distributed through the wall from its inner to its outer surface. Although thin walled cylinders can not be used for metal forming, they may be used for some other applications. Under these conditions, the relation between the tensile, tangential(hoop) stress in the cylinder wall and the internal pressure p_i is

$$\sigma_t = \frac{P_i r_m}{t}$$

For a given mean radius r_m and a tensile stress in the wall at the elastic limit, the pressure may be increased if the wall thickness is increased proportionately. As the

wall thickness is increased to withstand higher internal pressure, the distribution of tensile stress throughout the wall becomes nonuniform and the wall thickness must be increased more than in proportion to the pressure. The calculation of the stresses and strains in a thick walled cylinder must allow for the nonuniform distribution of stresses throughout the wall and to do this a more rigorous analysis is required. More effective use of the strength of material can be made in several ways. The wall may be constructed in layers pre-stressed by the proper amount, so that the initial residual stress must be overcome and reversed by the application of internal pressure. The wall may be constructed of layers of wire, tape, sheets, or of two or more concentric cylinders (shrink-fit construction). Since we are interested in the later construction, because of its economic advantages, we will discuss in detail the mechanics of shrink-fit construction.

3.2 Shrink-Fit Cylinders

The theory of this is complicated at the outset by the fact that it is virtually impossible to mate a pair of tubular components in this way without setting up stresses in the axial direction; and these stresses must depend on many factors. The usual practice is to assume that, until the internal working pressure is applied, there is no axial stress. It might be possible to achieve it with a duplex cylinder if the inner cylinder(insert) is subjected to an axial force which would extend it by the same

amount as the temperature had extended the length of the outer cylinder(holder), and then gradually to reduce this force as the two components approached the same temperature. In practice, therefore, we must accept an inevitable axial stress. The only reasonable assumption about it is that it will generally be intermediate algebraically between the tangential and radial stresses, so that the maximum shear stress will still be controlled by these two.

Crossland and Burns [44] carried out an experimental investigations with small duplex cylinders and showed that the assumption of no initial axial stress is justified, although axial stresses certainly were set up as might be expected. They also showed that these stresses did not interfere to any serious extent with the theoretical treatment.

3.3 Elastic Stresses in Thick Walled Cylinders

Figure 3.1 illustrates the general case of a radially loaded thick walled cylinder in that it is subjected to an internal pressure P_i, and an external pressure P_o. Since the loading is two dimensional, only plane stresses will be involved initially. When $sin(d\theta/2)$ is replaced by $d\theta/2$, the equation of equilibrium of radial forces acting on an element of length dL is

$$\sigma_r(r d\theta\, dL) + 2\sigma_t(dr\, dL)\frac{d\theta}{2} - (\sigma_r + d\sigma_r)(r+dr)\, d\theta\, dL - F(r\, d\theta\, dr\, dL) = 0 \quad (3.1)$$

Where

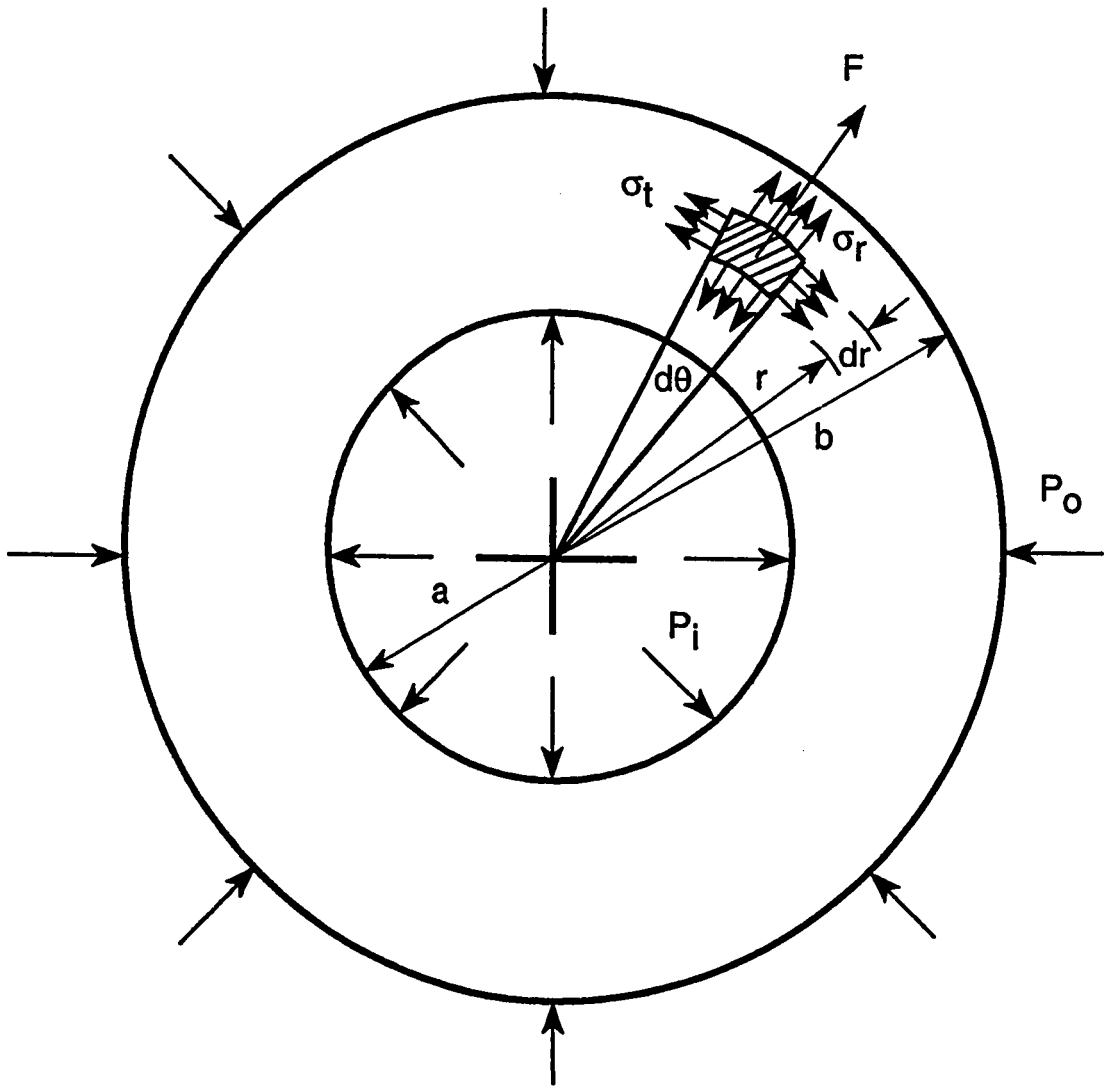

Figure 3.1: Thick walled cylinder with internal and external pressure.

σ_r radial stress

σ_t tangential stress

F body force

After dividing by $rdrd\theta dL$ and dropping terms of higher order differential, this expression reduces to

$$\frac{\sigma_t - \sigma_r}{r} - \frac{d\sigma_r}{dr} - F = 0 \tag{3.2}$$

The sign convention for normal stresses are regarded as positive when tensile. All stresses acting on the element in Figure 3.1 are shown in the positive direction.

Equation (3.2) involves two unknown stresses, σ_r and σ_t. In order to develop equations expressing each of these separately as a function of r, other known relationships must be invoked.

The displacement of an element of the material under the specified conditions is in the radial direction, as shown in Figure 3.2. The element subtends the same angle $d\theta$ before and after displacement. The radial dimension of the element dr increases during displacement by the amount du_r, while the tangential element dimension $r\ d\theta$ increases by amount $u_r\ d\theta$. Hence the strains involved are

$$\epsilon_r = \frac{du_r}{dr} \quad and \quad \epsilon_t = \frac{u_r}{r} \tag{3.3}$$

The stress strain relationships for plane stress situation are

$$\sigma_t = \frac{E}{1-\nu^2}(\epsilon_t + \nu\epsilon_r)$$

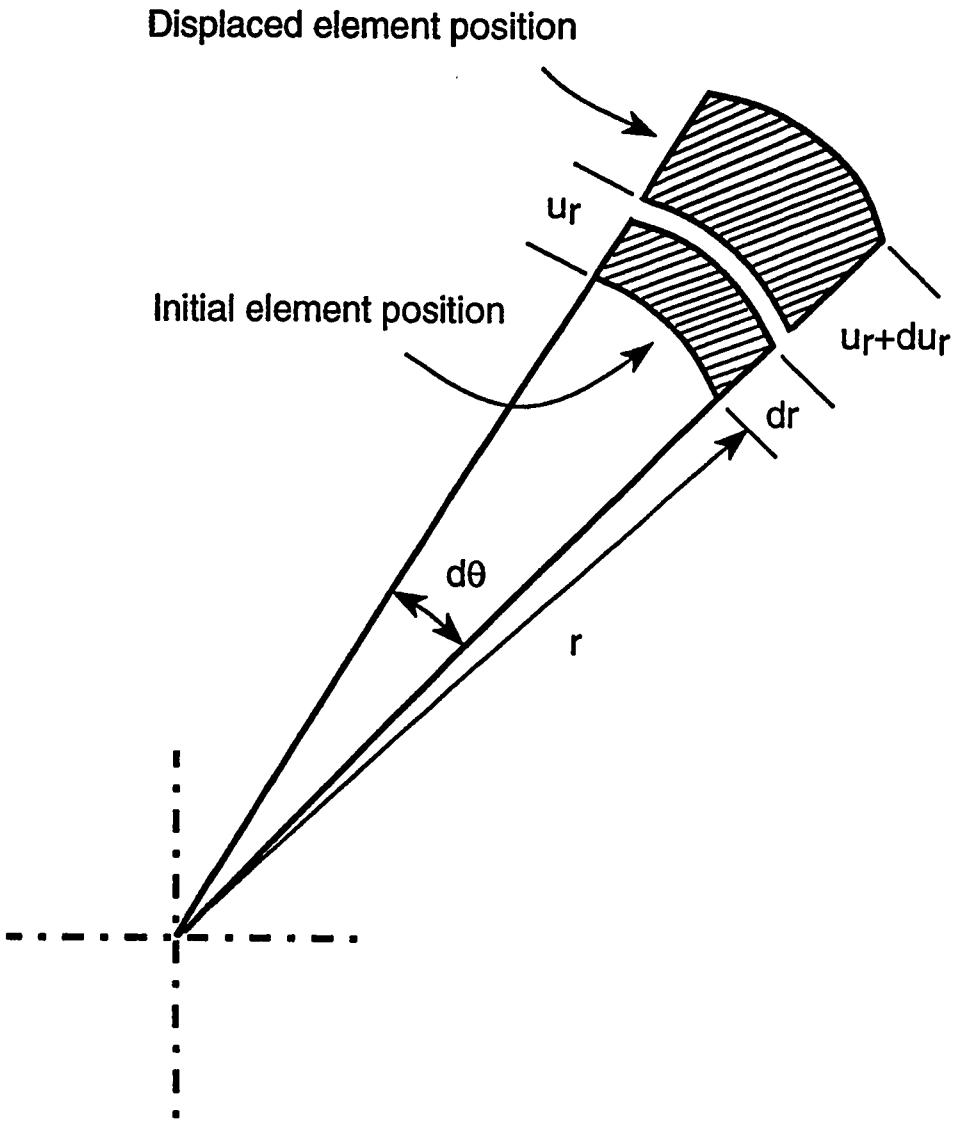

Figure 3.2: Displacement of an element of a thick walled cylinder.

and

$$\sigma_r = \frac{E}{1-\nu^2}(\epsilon_r + \nu\epsilon_t) \tag{3.4}$$

Substitution of equations (3.3) into equations (3.4) yields

$$\sigma_t = \frac{E}{1-\nu^2}\left(\frac{u_r}{r} + \nu\frac{du_r}{dr}\right)$$

and

$$\sigma_r = \frac{E}{1-\nu^2}\left(\frac{du_r}{dr} + \nu\frac{u_r}{r}\right) \tag{3.5}$$

Substitution of equations (3.5) into equation (3.2) yields

$$\frac{E}{1-\nu^2}\left(\frac{u_r}{r^2} + \frac{\nu}{r}\frac{du_r}{dr} - \frac{1}{r}\frac{du_r}{dr} - \frac{\nu u_r}{r^2}\right) - \frac{E}{1-\nu^2}\left(\frac{d^2u_r}{dr^2} + \frac{\nu}{r}\frac{du_r}{dr} - \frac{\nu u_r}{r^2}\right) - F = 0$$

which reduces to

$$\frac{d^2u_r}{dr^2} + \frac{1}{r}\frac{du_r}{dr} - \frac{u_r}{r^2} = -\frac{1-\nu^2}{E}F \tag{3.6}$$

Equation (3.6) is the differential equation relating u_r and r. Assuming negligible body forces, i.e. $F = 0$, the general solution of equation (3.6) is;

$$u_r = Ar + \frac{B}{r} \tag{3.7}$$

which can be verified by substitution. The constants A and B are determined from the conditions at the inner and outer surfaces of the cylinder where the pressure, i.e., the normal stress σ_r, are known. Substituting equation (3.7) into equations (3.5), we obtain

$$\sigma_t = \frac{E}{1-\nu^2}\left[A(1+\nu) - B\frac{1-\nu}{r^2}\right]$$

and

$$\sigma_r = \frac{E}{1-\nu^2}\left[A(1+\nu) + B\frac{1-\nu}{r^2}\right] \tag{3.8}$$

Applying the boundary conditions as indicated in Figure 3.1 i.e;

$$(\sigma_r)_{r=b} = -P_o \;\; and \;\; (\sigma_r)_{r=a} = -P_i$$

Substitution of these boundary conditions in the equation for σ_r gives the values of constants A and B;

$$\begin{aligned} A &= \frac{1-\nu}{E}\,\frac{a^2P_i - b^2P_o}{b^2-a^2} \\ B &= \frac{1+\nu}{E}\,\frac{a^2\,b^2(P_i-P_o)}{b^2-a^2} \end{aligned} \tag{3.9}$$

With these values for the constants in equations (3.8) the general expressions for the normal stresses σ_t and σ_r become

$$\begin{aligned} \sigma_t &= \frac{a^2P_i - b^2P_o}{b^2-a^2} + \frac{(P_i-P_o)a^2\,b^2}{r^2(b^2-a^2)} \\ \sigma_r &= \frac{a^2P_i - b^2P_o}{b^2-a^2} - \frac{(P_i-P_o)a^2\,b^2}{r^2(b^2-a^2)} \end{aligned}$$

or in terms of radius ratio the above equations can be written as

$$\begin{aligned} \sigma_t &= \frac{P_i - \rho^2P_o}{\rho^2-1} + \frac{(P_i-P_o)\,b^2}{r^2(\rho^2-1)} \\ \sigma_r &= \frac{P_i - \rho^2P_o}{\rho^2-1} - \frac{(P_i-P_o)\,b^2}{r^2(\rho^2-1)} \end{aligned} \tag{3.10}$$

where $\rho = b/a$

It is important to note that the sum of these two stresses remains constant, so that the deformation of all elements in the direction of the axis of the cylinder is the same, and cross-section of the cylinder remains plane after deformation.

3.4 Optimum Design to Withstand Internal Pressure Alone

The work presented here is concerned with the problem of designing a composite die for maximum strength. In the present analysis the insert(inner cylinder) is taken to be absolutely brittle, i.e. to fail only due to fracture. Furthermore, it is assumed that fracture in tension occurs when the maximum principal stress reaches a certain critical value f_t which is independent of transverse stresses (maximum principal stress theory), and that fracture in uni-axial compression occurs at a stress of magnitude f_c which in our case is much larger than f_t and the die will not fail in compression. Optimization of the die dimensions, which will be carried out in the following sections, is based on the maximum allowable strength of the insert and holder material.

3.4.1 Assumptions

In an actual composite die the bore of the insert is not constant but has the die profile; the region of pressure during drawing extends over only part of this profile and the pressure is not uniform; the insert may be shorter than the holder(outer cylinder); and the interface between the holder and the insert is either cylinderical or slightly conical.

Following are the assumptions made to simplify the analysis;

1. The holder and the insert are uniform hollow cylinders of the same length.

2. A uniform pressure acts on the entire bore of the insert.

3. The axial stress σ_z is zero every where.

Thus the problem is reduced to one of plane stress. All the basic expressions required for stresses and strains are set out in previous sections and these are now applied to the present optimization problem.

3.4.2 Determination of Internal Pressure

In the literature review it was found that there were two groups of researchers working in this field. One discussed the mechanics of drawing process and developed a number of process models and no attention was given to the die design. The other group discussed the die design part using uniform cylinder theory without getting an input from the process model. A secondary objective of this research was to integrate the drawing process with die design. By doing this, the internal pressure, which is a primary input parameter to the die design problem, is fed directly from a process model to the design part.

Two process models are employed to determine the internal pressure at the bore. It is appropriate to mention first that how we are determining internal pressure for such dies.

Avitzur [3] employed upper bound approach based on admissible velocity field to

calculate the drawing stress. The expression, he obtained for drawing stress, is as follows,

$$\sigma_d = \sigma_b + 2\,Y_m\,f(\alpha)\,ln\,(\frac{R_o}{R_f}) + 1.1547\,Y_m \times \left\{\frac{\alpha}{sin^2\,\alpha} - cot\,\alpha + m_f\,cot\,\alpha\,ln\,(\frac{R_o}{R_f}) + m_f\frac{L}{R_f}\right\} \qquad (3.11)$$

where

Y_m mean flow stress of work material

σ_b back tension

R_o initial wire diameter

R_f final wire diameter

α semi die angle

m_f constant friction factor

L bearing length

and

$$f(\alpha) = \frac{1}{sin^2\,\alpha}[\,1 - cos\,\alpha\,\sqrt{1 - 0.9167\,sin^2\,\alpha} + 0.087 \times ln\,\frac{1 + \sqrt{0.9167}}{\sqrt{0.9167}\,cos\,\alpha + \sqrt{1 - 0.9167\,sin^2\,\alpha}}\,]$$

For small die angles it is a justified approximation to assume that the internal pressure at the die bore is acting at right angle to the drawing stress or in other words neglect the die angle, as shown in Figure 3.3. For plane strain, both the Von Mises and Tresca criteria give;

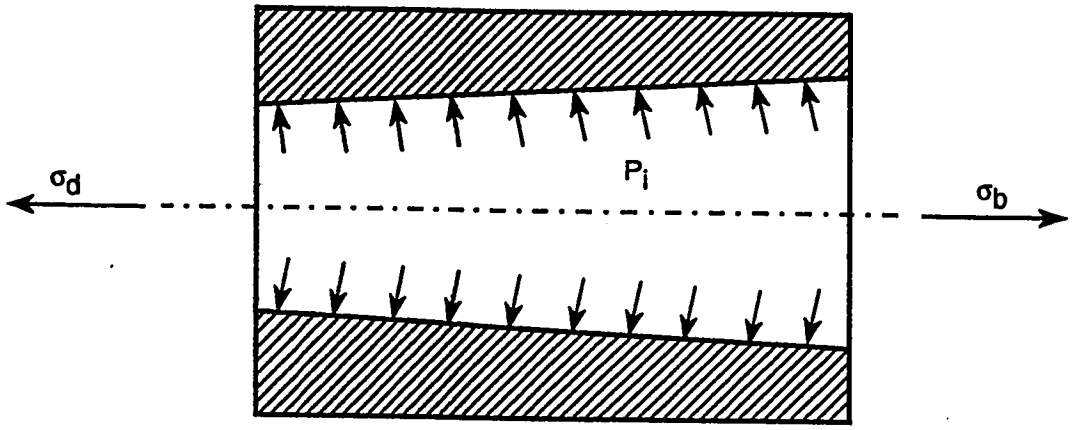

Actual Die Shape

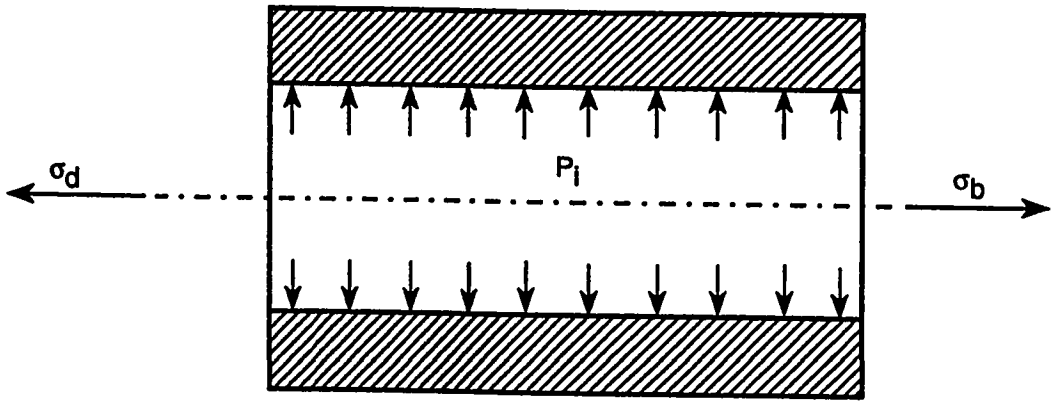

Assumed Die Shape

Figure 3.3: Schematic diagrams of actual and assumed drawing dies.

$$\sigma_d - (-P_i) = 2K$$

where the shear yield stress, K, is $\frac{Y}{2}$ for Tresca and $\frac{Y}{\sqrt{3}}$ for Von Mises. Thus;

$$P_i = 2K - \sigma_d \tag{3.12}$$

In determining internal pressure using this process model, the back tension σ_b is assumed to be zero and the bearing length is also not taken into account.

The second model employed to calculate the internal pressure is based on a visco-plastic constitutive equation and is proposed by Cristescu [6]. This model is suitable to calculate internal pressure for dies of large angle. Another important point to note is that the model proposed by Avitzur did not take into account the effect of drawing speed. From the visco-plastic model it is found that the drawing speed is also an important parameter which affects significantly a number of other process parameters. The internal pressure in this model varies from entry to exit. Therefore a mean value for internal pressure will be used in the current analytical approach. Variation of internal pressure will be taken into account in the Finite Element Model. The expression for pressure at die bore in the visco-plastic model is as follows;

$$\begin{aligned} P_i = {} & 0.5222\, Y_m\, ln\left[cos\alpha + \sqrt{cos^2\alpha + 0.091}\,\right] - \frac{V_f r_f^2 \eta_v}{3}\left(\frac{4}{r^3} + \frac{14}{r_o^3}\right) \\ & + \frac{Y_m}{\sqrt{3}}\, 4.041\, ln\frac{r_o}{r} + \sigma_b - 0.5222\, Y_m \\ & \times ln\left[1 + \sqrt{1 + 0.091}\,\right] - Y_m \end{aligned} \tag{3.13}$$

where

η_v viscosity coefficient of work material

V_f exit wire velocity

r_o outer radii from apex of the cone

r_f inner radii from apex of the cone

r any intermediate radius

The pressure obtained from this expression is limited by the condition that the drawing stress must not exceed mean flow stress of the work material. The expression for drawing stress, as obtained by Cristescu, is given in the following equation;

$$\begin{aligned}\sigma_d &= \sigma_b + Y_m \left[2\, ln\frac{R_o}{R_f}\, f(\alpha) + \frac{2}{3}\frac{\eta_v V_f}{R_f}\frac{1}{sin\alpha}[1 - cos\alpha + \frac{11}{3}\,(1 - cos^3\alpha)] \right. \\ &\quad \times \left[1 - \left(\frac{R_f}{R_o}\right)^3\right] + \frac{2}{\sqrt{3}}\, m_f\, cot\alpha \left\{ ln\frac{R_o}{R_f} + \frac{\eta_v V_f}{R_f}\frac{sin\alpha}{\sqrt{3}}\sqrt{11cos^2\alpha + 1} \right. \\ &\quad \times \left[1 - \left(\frac{R_f}{R_o}\right)^3\right] \Big\} + \frac{1}{sin^2\alpha}\left\{ \frac{2}{\sqrt{3}} + 3.3\frac{\eta_v V_f}{R_f} sin\alpha \left[1 + \left(\frac{R_f}{R_o}\right)^3\right] \right\} \\ &\quad \left. \times [\alpha - \frac{1}{2} sin2\alpha] \right] \end{aligned} \tag{3.14}$$

For more clarity, the variables involved in the above equations are shown in Figure 3.4.

3.4.3 Insert Under External Pressure Alone

First it is necessary to ensure that the insert is not crushed during die manufacture by the interference pressure P_s exerted by the holder. From equations (3.10), after

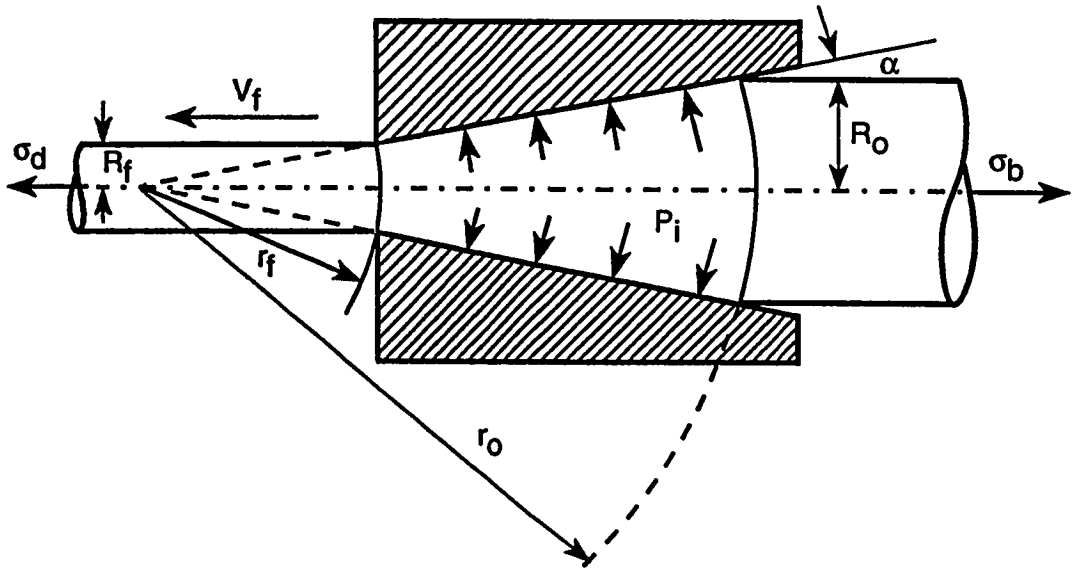

Figure 3.4: Schematic diagram of a large angle die.

putting $P_i = 0$, $P_o = P_s$ and $r = a$, we get;

$$\sigma_t = \frac{-\rho_1^2 P_s}{\rho_1^2 - 1} + \frac{-P_s b^2}{r^2(\rho_1^2 - 1)}$$
$$\sigma_r = \frac{-\rho_1^2 P_s}{\rho_1^2 - 1} - \frac{-P_s b^2}{r^2(\rho_1^2 - 1)}$$

From the above expressions it is found that the maximum compressive stress on the insert is the hoop stress at die bore, i.e;

$$\sigma_h = \frac{2P_s\rho_1^2}{\rho_1^2 - 1} \tag{3.15}$$

Where $\rho_1 = b/a$

Therefore it is reasonable to assume that fracture, if it occurs, will start at the bore. In order to avoid fracture, we must have

$$\sigma_h < f_c \tag{3.16}$$

Where f_c is the allowable compressive strength of the insert material.

3.4.4 Composite Die Under Internal Pressure

Insert

It follows from equations (3.10) that for tensile stresses to occur in the insert, the internal pressure P_i must be greater than the interfacial pressure between the insert and the holder. B is then positive in equations (3.10), and hence the maximum tensile stress is the hoop stress at the bore surface. The shrink-fit pressure P_s

and the internal applied pressure P_i combine to produce an interfacial pressure $(P_s + nP_i)$, as shown in Figure 3.5. Where n is derived in Appendix A. Hence, from equations (3.10), after putting $P_i = P_i$, $P_o = P_s + nP_i$ and $\rho_1 = b/a$, we get;

$$\begin{aligned} \sigma_t &= \frac{P_i - \rho_1^2(P_s + nP_i)}{(\rho_1^2 - 1)} + \left(\frac{P_i - (P_s + nP_i)}{(\rho_1^2 - 1)}\right)\rho_1^2 \\ \sigma_t &= \frac{(\rho_1^2 + 1)P_i - 2\rho_1^2(P_s + nP_i)}{(\rho_1^2 - 1)} \end{aligned} \tag{3.17}$$

where σ_t is the hoop stress at $r = a$

Fracture of the insert will occur in tension when

$$\sigma_t > f_t \tag{3.18}$$

Holder

The total internal pressure on the holder when the composite die is under internal pressure P_i is the interfacial pressure $(P_s + nP_i)$. For optimum design this pressure must be limited, so that the maximum stress should not exceed the allowable yield stress of the holder material. Let us denote this pressure by P_o;

$$P_s + nP_i < P_o \tag{3.19}$$

where P_o is the total external pressure for insert and total internal pressure for the holder material. Assuming that the holder is initially stress free before being fitted to the insert, it yields first on the inside. Again from equations (3.10), after putting

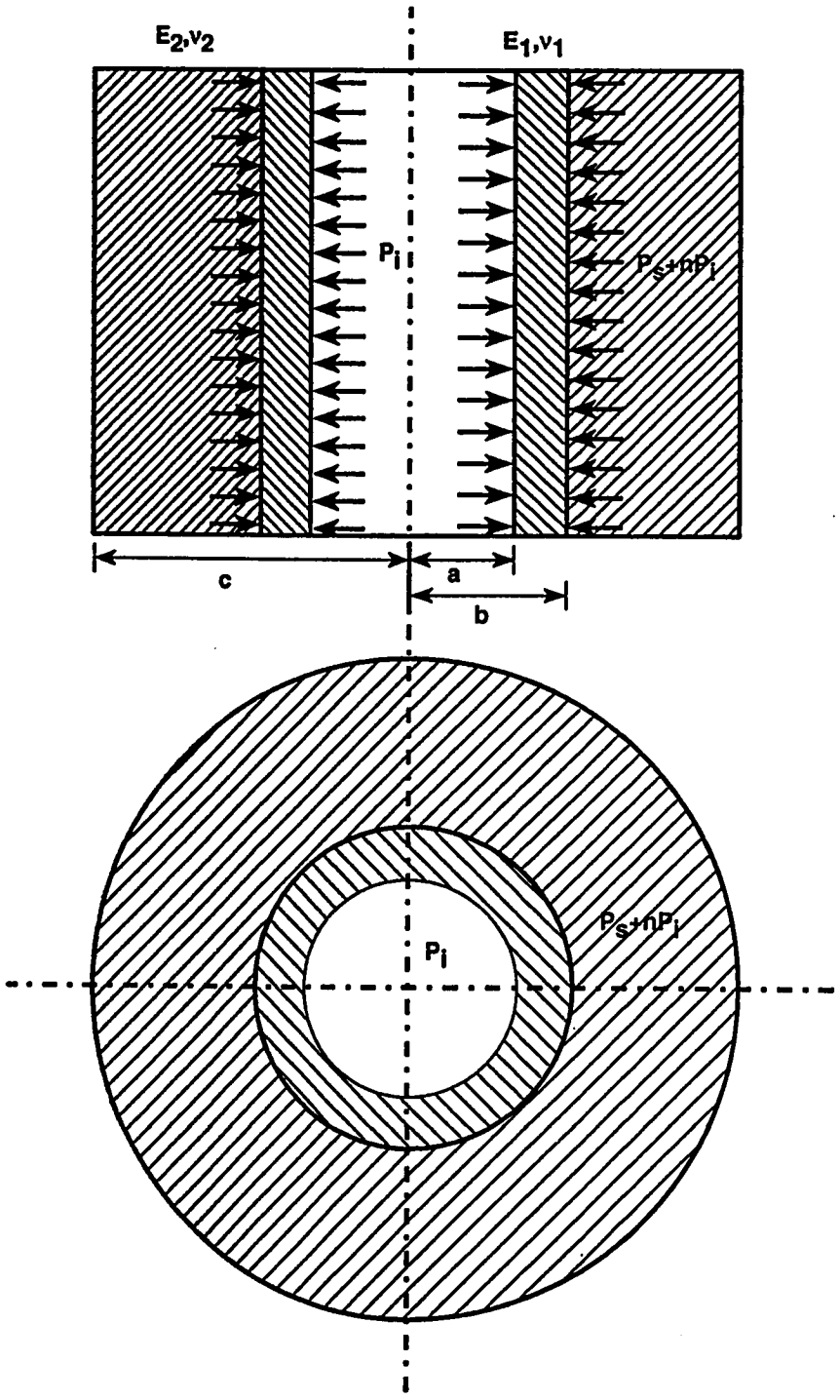

Figure 3.5: Composite cylinder; inner(ceramic material) outer(tool steel).

$P_i = P_o$ and $P_o = 0$, we get;

$$\sigma_t = \frac{P_o}{\rho_2^2 - 1} + \frac{P_o \rho_2^2}{\rho_2^2 - 1}$$
$$\sigma_r = \frac{P_o}{\rho_2^2 - 1} - \frac{P_o \rho_2^2}{\rho_2^2 - 1}$$

Now applying Tresca criteria, we have;

$$\frac{1}{2}Y = \frac{P_o \rho_2^2}{\rho_2^2 - 1}$$
$$P_o = \frac{Y}{2}\left(1 - \frac{1}{\rho_2^2}\right) \tag{3.20}$$

Where

Y yield stress in tension of the holder material

ρ_2 radius ratio of the holder (c/b)

3.5 Optimization for Maximum Internal Pressure

According to equation (3.17) and equation (3.18) the insert will fracture in tension when

$$f_t = \frac{(\rho_1^2 + 1)P_i - 2\,\rho_1^2\,(P_s + nP_i)}{(\rho_1^2 - 1)}$$

$$P_i\,(\rho_1^2 + 1) = f_t\,(\rho_1^2 - 1) + 2\,\rho_1^2\,(P_s + nP_i) \tag{3.21}$$

Moreover P_s is limited by either

1. the need to avoid crushing the insert, equation (3.15) and (3.16) or

2. the aim of avoiding yielding of the holder, equation (3.19) and (3.20).

It is clear from equation (3.21) that the value of P_i at which tensile fracture occurs is a maximum when P_s is just below one or the other of these limits.

3.5.1 Avoiding Failure of the Insert in Compression

To avoid failure of the insert in compression during die manufacture, shrink-fit pressure must be equal or lower than the allowable compressive strength of the insert. Therefore, equating equation (3.15) and (3.16), we get;

$$f_c = \frac{2P_s\rho_1^2}{(\rho_1^2 - 1)}$$

$$P_s = \frac{f_c(\rho_1^2 - 1)}{2\rho_1^2} \tag{3.22}$$

and hence from equation (3.21), in order to avoid tensile fracture of the insert during drawing operation;

$$P_i \leq \frac{(f_t + f_c)(\rho_1^2 - 1)}{(\rho_1^2 + 1) - 2n\rho_1^2} = F_1 \tag{3.23}$$

3.5.2 Avoiding Failure of the Holder in Tension

To avoid failure of the holder in tension during die manufacture, shrink-fit pressure must be equal or lower than the allowable tensile strength of the holder. Therefore,

equating equation (3.19) and (3.20), we get;

$$P_s = \frac{Y}{2}\left(1 - \frac{1}{\rho_2^2}\right) - nP_i \tag{3.24}$$

Again substituting in equation (3.21), we get

$$P_i \leq \frac{f_i(\rho_1^2 - 1) + Y\rho_1^2[1 - (1/\rho_2^2)]}{(\rho_1^2 + 1)} = F_2 \tag{3.25}$$

Thus, the maximum possible strength of the composite die as represented by the upper limits to P_i defined by the inequalities (3.23) and (3.25) is given by F_1 or F_2 whichever has the lower value. It still remains to make the best choice of ρ_1 and ρ_2 and hence of P_s for given internal pressure.

3.6 Selection of Radius Ratios

The insert inner radius a is normally known from the given process conditions. From experiments [28] it is also known that for a two cylinder shrink-fit construction after an overall radius ratio of 6 there is not much gain in internal pressure. Therefore, as an upper limit, the overall radius ratio is set equal to 6. The computer program developed during this research is capable of selecting the outer radius of the holder depending upon the given material and the insert inner radius. The program also suggests a range of yield stress for the holder material for a given insert material and given process parameters, if one selects a holder material having very small or very large yield strength compared to the required yield strength.

As shown in Figure 3.5 c is the outer radius of the holder. Let us suppose that $\rho_3 = c/a = \rho_1\rho_2$. The problem remaining now is to select the intermediate radius b or ρ_1 in a way that we can utilize the maximum possible strength of both the insert and the holder material. For a given internal pressure(which we already know from a given process model) to obtain optimum dimensions of the insert and of the holder, equation (3.23) or (3.25) must be satisfied. Plotting these equations against ρ_1 for its practical range i.e $1 < \rho_1 < \rho_3$. It is found that equation (3.23) has a positive slope throughout the practical range. While equation (3.25) has a maximum value as shown in Figure 3.6.

Since ceramic materials usually have very high compressive strength, it will be very rare that they will fail in compression (due to applied shrink-fit pressure), so the limiting condition here in our case will be to avoid the failure of the insert in tension due to internal pressure and to avoid the failure of the holder which is in tension due to the applied shrink-fit pressure on the insert. In case, the insert failure is expected to be in compression then the optimum value of ρ_1 will be the value which satisfies both, equation (3.23) and (3.25), point N in Figure 3.6. Otherwise equation (3.25) will usually govern the dimensions, point M in Figure 3.6.

In particular, from the point of view of die manufacture, the amount of interference required to produce a specified shrink-fit pressure must also be known. This matter is discussed in detail in Appendix B.

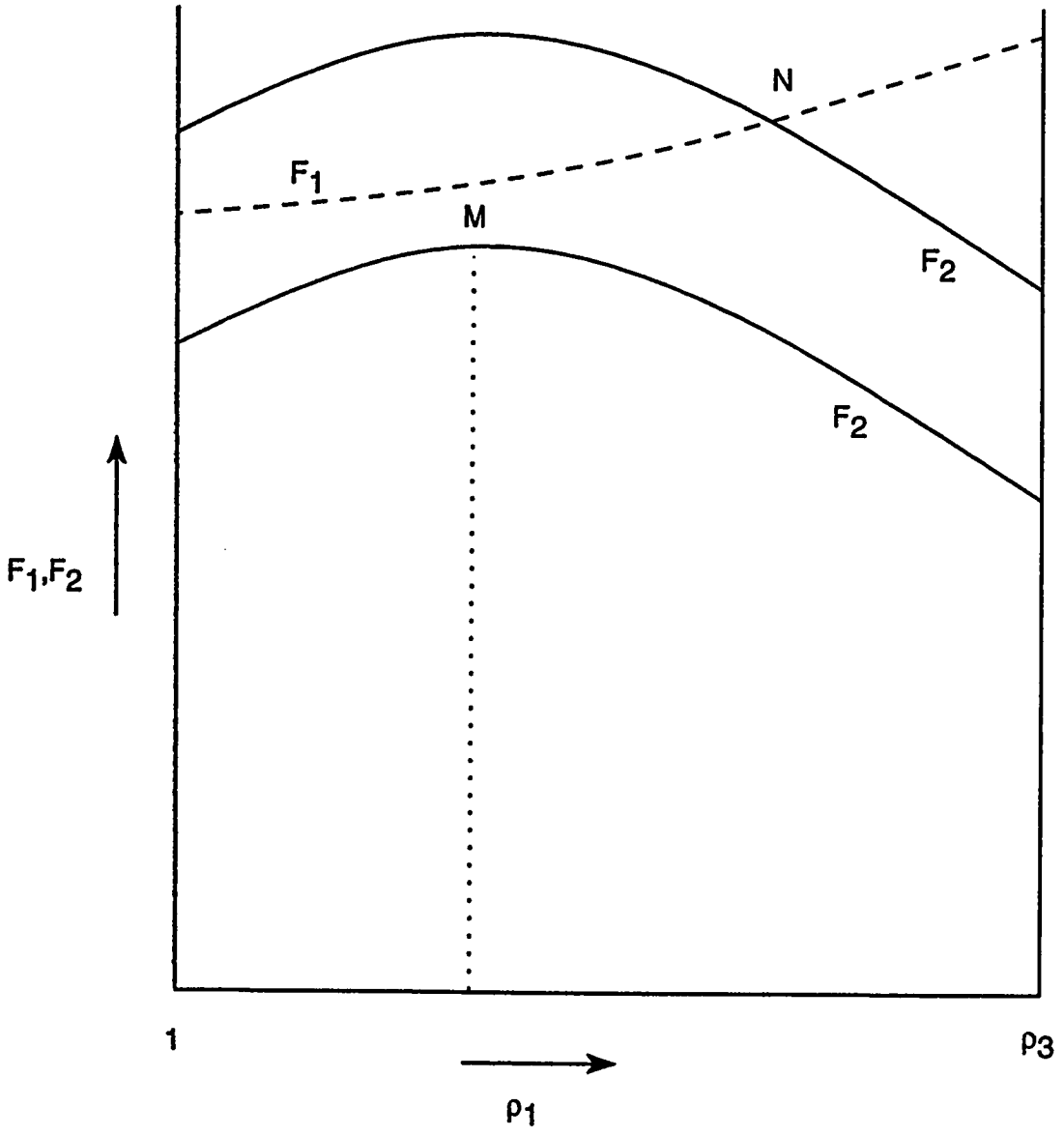

Figure 3.6: Schematic representation of the variation of F_1 and F_2 with radius ratio ρ_1.

3.7 Effect of Shear Stress on the Stress State at the Bore

As has been said earlier that for small die angles the internal pressure at the bore can be assumed to be acting normal to the drawing stress. In this situation the radial and tangential stresses produced by the internal pressure are also the principal stresses for the case of plane stress. But when a shear stress is superimposed at the bore, the problem becomes three dimensional. In order, not to allow the principal stresses to exceed the allowable limit at the die bore, after the application of shear stress, a compressive axial stress is also applied. The magnitude of which is determined by trial and error. Now the state of stress at the bore looks like shown below;

$$\begin{pmatrix} \sigma_r & 0 & \tau_{rz} \\ 0 & \sigma_t & 0 \\ \tau_{rz} & 0 & \sigma_z \end{pmatrix}$$

The principal stresses of the newly formed stress tensor at the bore can easily be calculated using matrix operations;

$$\lambda_1 = \sigma_1 = \sigma_t \tag{3.26}$$

$$\lambda_2 = \sigma_2 = \frac{(\sigma_r + \sigma_z) + \sqrt{(\sigma_r - \sigma_z)^2 + 4\tau_{rz}^2}}{2} \tag{3.27}$$

$$\lambda_3 = \sigma_3 = \frac{(\sigma_r + \sigma_z) - \sqrt{(\sigma_r - \sigma_z)^2 + 4\tau_{rz}^2}}{2} \tag{3.28}$$

The shear stress τ_{rz} in the above analysis is found using a constant friction factor m_f, i.e

$$\tau_{rz} = m_f K$$

where K is the shear yield stress of the work material. m_f in the above expression varies from 0 to 1. $m_f = 0$ indicates no friction at the die bore and $m_f = 1$ indicates maximum or sticking condition at the die bore.

From the above analysis it is seen that one of the principal stress becomes equal to the tensile hoop stress and is independent of the applied shear stress. Fortunately the principal stress σ_2 is compressive, therefore when a shear stress is superimposed at the die bore it first comes to zero and then becomes tensile, whereas the third principal stress σ_3 comes out to be compressive. Since the compressive strength of the insert is very high, there is very little chance of failure in compression. It is found that, for the practical range of friction factor(0.03 to 0.1), the shear stress has no significant effect on the principal stresses. Therefore we do not need to supply the axial compressive stress σ_z. However, for higher m_f values(near to 1) axial compressive stress is needed to constrain the principal stress σ_2 from exceeding the allowable tensile limit.

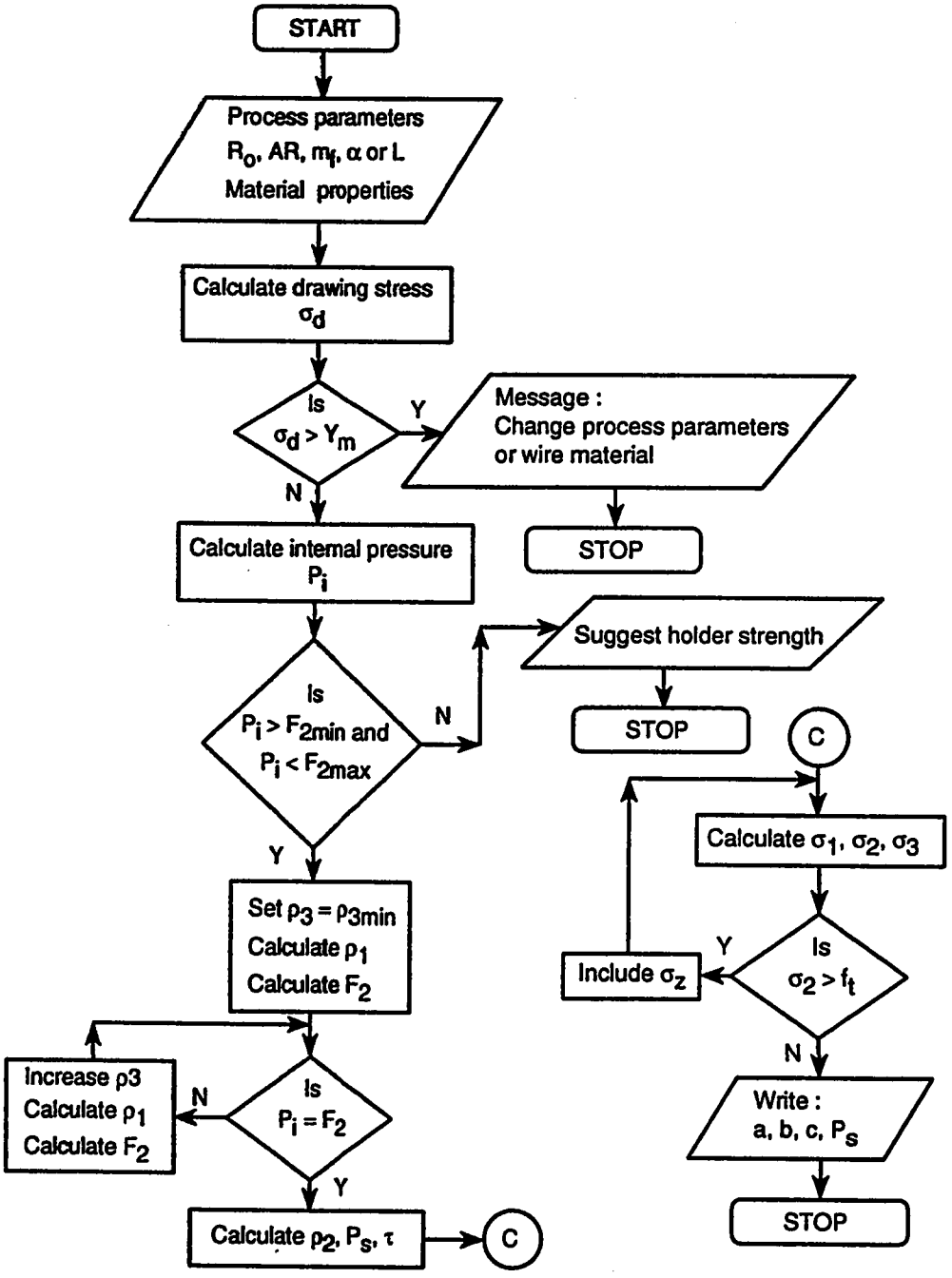

Figure 3.7: Flow chart of the computer program based on analytical procedure.

3.8 Description of the Program

The flow chart of the computer program developed to evaluate the optimum die dimensions and shrink-fit pressure requirements and to integrate dawing process with die design is shown in Figure 3.7. Although most of the things are clear in the flow chart, for more clarity it is described in the following paragraphs.

The input variables of the program are, viscosity coefficient and yield and ultimate tensile strength of the work material, exit wire velocity, semi die angle, friction factor, and mechanical properties of the insert and holder material.

Strain hardening coefficient and strain hardening exponent of the work material are calculated as follows;

$$\sigma = K_h \, \epsilon^{n_h}$$

$$UTS = K_h \, n_h^{n_h}$$

$$Y_{2\%} = K_h \, (0.002)^{n_h}$$

Ultimate tensile strength UTS and 2 % yield strength of the work material are known, therefore solving by iteration K_h and n_h can be found out easily. Using these values mean flow stress is found out from the following expression;

$$Y_m = \frac{K_h \, \epsilon^{n_h}}{n_h + 1}$$

where $\epsilon = 2 \, ln \frac{R_o}{R_f}$

Drawing stress is then calculated by employing suitable process model (Cristescu's

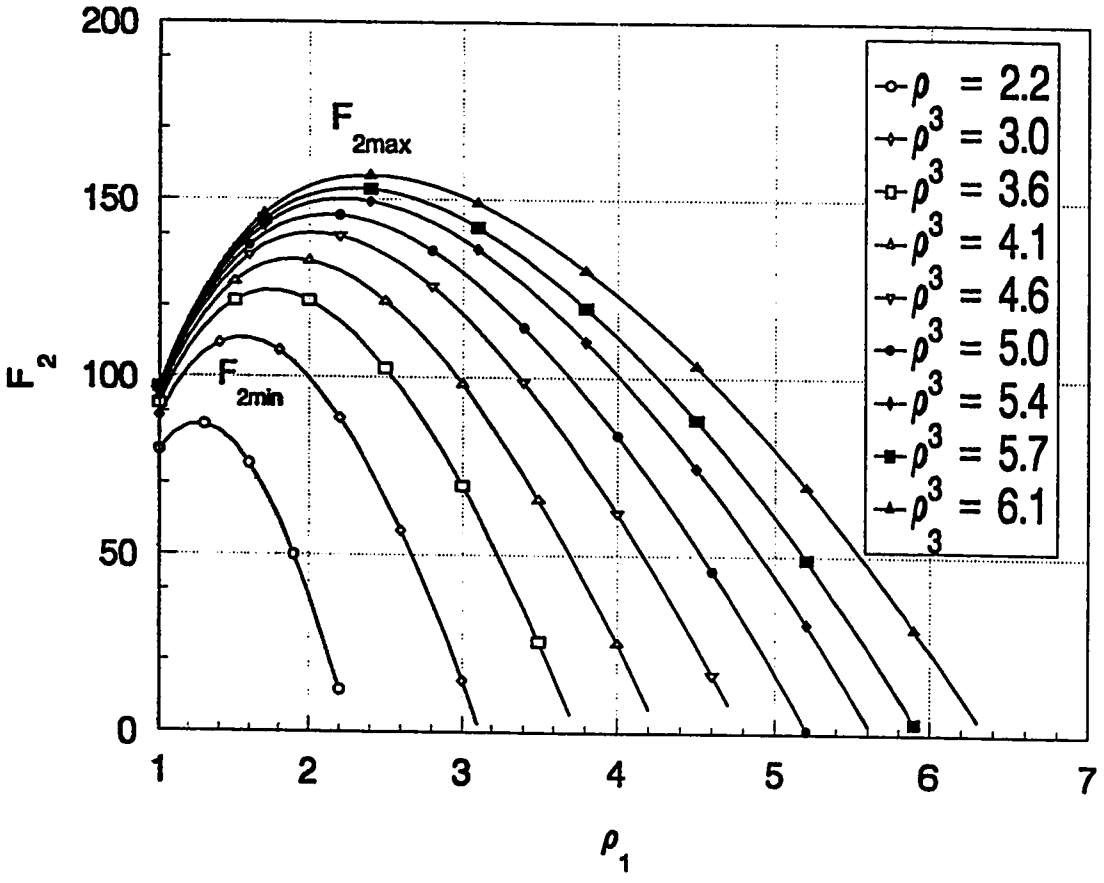

Figure 3.8: Variation of F_2 with ρ_1 for $Y = 200\ Ksi$ and $f_t = 18\ Ksi$.

visco-plastic model equation (3.14) or Avitzur's plasticity model equation (3.11)). This is used as a check, so that for given process conditions and work material the drawing stress must not exceed the mean flow stress of the work material. If drawing stress is lower than the mean flow stress then the internal pressure P_i at die bore is calculated using equation (3.13) or equation (3.12). If P_i lies within the maximum and minimum limits of F_2, as shown in Figure 3.8, then ρ_1 and ρ_3 are optimized iteratively otherwise holder strength needs to be modified. Intermediate radius or ρ_2, shrink-fit pressure, multiplying factor for P_i are then calculated. Finally frictional shear stress is superimposed on the calculated stresses and new principal stresses are calculated in a way such that no principal stress exceeds the allowable limit.

Chapter 4

Finite Element Formulation

4.1 Introduction

As the semi die angle increases, the analytical approach presented in the previous chapter will not hold. The two main assumptions made for small angle dies, that

- the internal pressure acts at right angles to the drawing stress, and
- it is uniformly distributed throughout the working zone

will not hold for dies of large semi angle. Also the assumption of uniform inner radius will not be valid.

There is no analytical solution available to handel such a typical large angle die. The problem becomes more complex when contoured dies, which are more suitable for drawing operation with respect to the final product quality, are under consideration.

Recently Frater [35] performed a Finite Element Analysis to calculate stresses and deformations in shrink-fit dies. His work is limited to calculate the stresses and deflections for dies of uniform inside radius and dies having straight taper. Also the pressure exerted by the work material on the die is assumed to be uniformly distributed.

To handle the problem of large angle dies with mathematically contoured profile surface and variable internal pressure we have used Finite Element approach. Before going into the details of Finite Element Analysis (F.E.A.), it is appropriate to have a general view of F.E.A.

The Finite Element Analysis is a very powerful technique for numerically solving many complex problems. It has been successfully applied to the solution of a wide range of problems in a number of engineering fields. The central idea of the Finite Element Analysis is that a real continuum which has an infinite number of degrees of freedom can be replaced for the purpose of analysis by a discretized analogue, called the Finite Element Model. The model is composed of a linear combination of a finite number of subregions of the continuum, called *elements*, with a finite number of identifiable points within and on the boundaries of each element, called *nodes* or *joints*. Each joint has associated with it a finite number of degrees of freedom. The characteristic behavior of each element can be developed as if it were isolated from all other elements in the model, and the behavior of the entire model is obtained as the sum of the contributions of all of its elements.

4.2 Displacement Method

In the displacement method, the displacement field within each element is defined in terms of displacement functions;

$$\{u\} = [f(x,y,z)]\{q\} \tag{4.1}$$

where

$$\{u\} = \begin{Bmatrix} u(x,y,z) \\ v(x,y,z) \\ w(x,y,z) \end{Bmatrix}, \quad \{q\} = \begin{Bmatrix} q_1 \\ q_2 \\ \vdots \\ q_n \end{Bmatrix}$$

and n is the number of generalized coordinates, q, which is equal to the number of degrees of freedom of the element.

Equation (4.1) can be solved for the generalized coordinates, q, in terms of generalized nodal displacements. By using the strain-displacement relation and the constitutive law, the stresses within each element can be calculated in terms of the generalized nodal displacements.

The contribution of each element to the strain energy of the system can be calculated from the distribution of the strains and stresses within each element. The strain energy of the entire system is then obtained by adding the contributions of all of its elements. Employing the principal of minimum potential energy yields a set of linear algebraic equations relating the generalized nodal loads, p, to the generalized

nodal displacements, u,

$$p = K\,u \tag{4.2}$$

which is the set of the equilibrium equations of the system. K is the stiffness matrix of the entire system. By solving equation (4.2), after modifying it by incorporating the boundary conditions, the spatial description of the displacements can be recovered from equation (4.1). With the displacements known every where within the model, all other quantities, such as stresses and strains, can be routinely evaluated wherever desired.

The procedure described above provides a set of displacements for the idealized model which is generally different from that of the real continuum. By increasing the number of nodes, i.e. by increasing the total number of degrees of freedom of the finite element model, a more realistic and acceptable approximation can be obtained.

4.3 Linear Three Dimensional Element

The general formulation of the linear three dimensional element is described here, while the details of the element stiffness formation and stress calculation are dealt with in subsequent sections.

A local curvilinear set of coordinates, ξ_i, is established such that each coordinate varies from -1 to 1 between opposite faces of the element, as shown in Figure 4.1. A

transformation of coordinates between the global and local coordinates is effected by using shape functions N^m, thus

$$X_i = N^m X_i^m \tag{4.3}$$

where

X_i	global coordinate in direction i
$N^m = N^m(\xi, \eta, \zeta)$	shape function for node m
X_i^m	global coordinate of node m in direction i

Here i ranges over the number of cartesian coordinates of the problem, and m ranges over all the nodes in the element. Some of the important characteristics of the shape functions, introduced above, are;

1. each shape function has a value of one at its own node and zero at other nodes.

2. sum of the shape functions of an element is equal to one.

using the same shape functions as used in the definition of coordinates, the displacement field in the element is defined as,

$$u_i = N^m u_i^m \tag{4.4}$$

where

u_i	displacement of any point in the element, in direction i, and
u_i^m	displacement of node m in direction i

The shape functions for a linear three dimensional element, shown in Figure 4.1, are

$$N^m = \frac{1}{8}(1+\xi\xi^m)(1+\eta\eta^m)(1+\zeta\zeta^m) \tag{4.5}$$

where $\xi^m, \eta^m, \zeta^m = \pm 1$ and $m = 1, 2, \cdots, 8$.

4.4 Element Stiffness Matrix

The strain displacement relation in indicial notation is defined as,

$$\epsilon_{ij} = \frac{1}{2}\left(\frac{\partial u_i}{\partial x_j} + \frac{\partial u_j}{\partial x_i}\right) \tag{4.6}$$

or using the Kronecker delta,

$$\epsilon_{ij} = \frac{1}{2}(\delta_{ik}\delta_{jl} + \delta_{il}\delta_{jk})\frac{\partial u_k}{\partial x_l} \tag{4.7}$$

substituting equation (4.4) into equation (4.7) we obtain,

$$\epsilon_{ij} = \frac{1}{2}(\delta_{ik}\delta_{jl} + \delta_{il}\delta_{jk})\frac{\partial N^m}{\partial x_l} u_k^m \tag{4.8}$$

The stress-strain law of elesticity is

$$\sigma_{ij} = E_{ijkl}\,\epsilon_{kl} \tag{4.9}$$

Where E_{ijkl} is the material properties tensor which is symmetric with respect to each of the two pairs of indices ij and kl. Substituting from equation (4.8) into equation (4.9) we obtain,

$$\sigma_{ij} = \frac{1}{2}(E_{ijkl} + E_{ijlk})\frac{\partial N^n}{\partial x_l} u_k^n \tag{4.10}$$

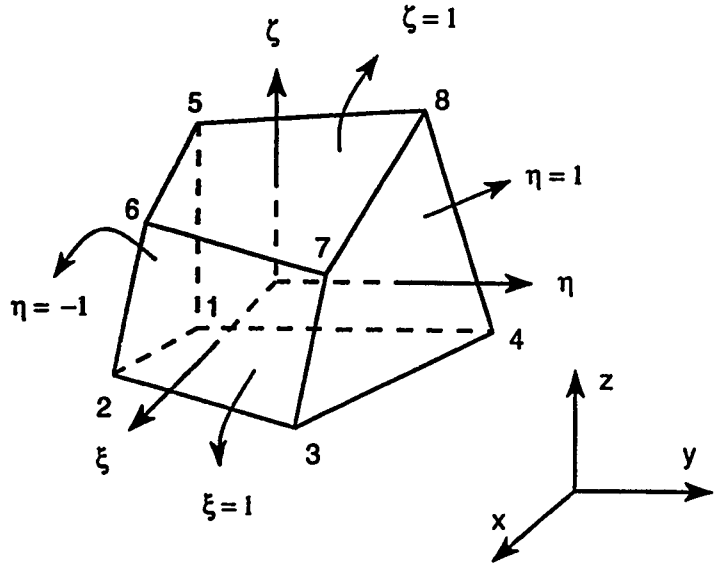

(a) Cartesian Coordinates

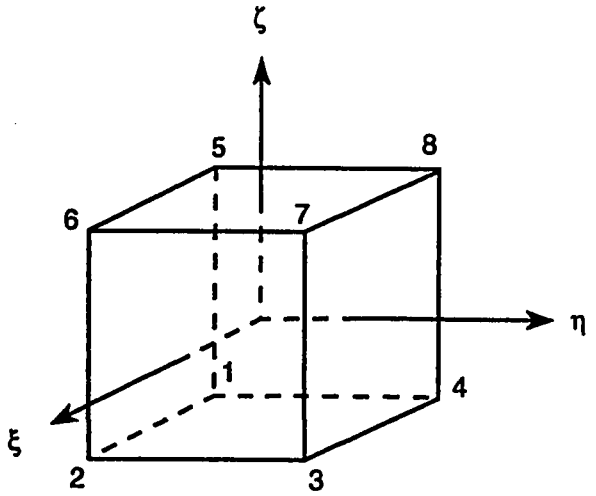

(b) Local coordinates

Figure 4.1: Linear three dimensional brick element.

In view of the symmetry of E with respect to the pair lk, we have

$$E_{ijkl} = E_{ijlk} \tag{4.11}$$

which when substituted into equation (4.10) yields,

$$\sigma_{ij} = E_{ijkl} \frac{\partial N^n}{\partial x_l} u_k^n \tag{4.12}$$

Now, if the element nodes are given virtual displacements δu_i^m, the virtual internal work expended in going through these displacements is,

$$W^{(e)} = \int_V \sigma_{ij} \delta \epsilon_{ij} dV \tag{4.13}$$

where the integration is performed over the entire volume of the element. Upon substituting equations (4.8 and 4.12), the above equation becomes,

$$W^{(e)} = \frac{1}{2} \int_V (E_{ijkl} + E_{jikl}) \frac{\partial N^n}{\partial x_l} \frac{\partial N^m}{\partial x_j} u_k^n \, \delta u_i^m \, dV \tag{4.14}$$

Again due to symmetry $E_{ijkl} = E_{jikl}$, which upon substitution in the above equation yields,

$$W^{(e)} = \left(\int_V E_{ijkl} \frac{\partial N^n}{\partial x_l} \frac{\partial N^m}{\partial x_j} dV \right) u_k^n \, \delta u_i^m \tag{4.15}$$

The external forces, expressed as equivalent nodal forces, also do work in going through the same virtual displacements. This work is calculated as,

$$W_p^{(e)} = -p_i^m \, \delta u_i^m \tag{4.16}$$

where p_i^m is the force at node m in direction i. For the element to be in equilibrium, the net work performed by all forces going through the same virtual displacement

must vanish. Hence,

$$W^{(e)} + W_p^{(e)} = 0 \tag{4.17}$$

Substituting for $W^{(e)}$ and $W_p^{(e)}$ from the respective equations, equation (4.17) becomes,

$$p_i^m \, \delta u_i^m = \left(\int_V E_{ijkl} \frac{\partial N^n}{\partial x_l} \frac{\partial N^m}{\partial x_j} \, dV \right) u_k^n \, \delta u_i^m$$

Since the displacements are virtual, we have

$$p_i^m = \left(\int_V E_{ijkl} \frac{\partial N^n}{\partial x_l} \frac{\partial N^m}{\partial x_j} \, dV \right) u_k^n \tag{4.18}$$

The expression between parenthesis in the above equation is defined as the element stiffness matrix.

$$K_{ik}^{mn} = \int_V E_{ijkl} \frac{\partial N^n}{\partial x_l} \frac{\partial N^m}{\partial x_j} \, dV \tag{4.19}$$

Since the material is assumed to be homogeneous, the material properties tensor is independent of the position coordinates. Therefore it can be taken out of the integral sign i.e.

$$K_{ik}^{mn} = E_{ijkl} \int_V \frac{\partial N^n}{\partial x_l} \frac{\partial N^m}{\partial x_j} \, dV \tag{4.20}$$

The material properties tensor can be expressed in terms of Lame's constants λ_l and μ_l as;

$$E_{ijkl} = \lambda_l \delta_{ij} \delta_{kl} + \mu_l (\delta_{ik} \delta_{jl} + \delta_{il} \delta_{jk}) \tag{4.21}$$

The Lame's constants are computed from the modulus of elasticity and Poisson's ratio, thus

$$\lambda_l = \frac{\nu \, E}{(1+\nu)(1-2\,\nu)} \quad \mu_l = \frac{E}{2\,(1+\nu)} \tag{4.22}$$

The stiffness matrix obtained cannot be evaluated in closed form. Integration is then carried out numerically in the local coordinates. In the Finite Element Analysis, only nodal forces can be handled. Therefore whenever distributed loads occur, they must be replaced by equivalent nodal forces. This equivalence is established through the equivalence of the work that each must do in order to deform the structure into the same configuration.

4.5 Boundary Conditions

The only boundary conditions that can be treated in the displacement formulation of the Finite Element Analysis are displacement boundary conditions. These conditions must be satisfied exactly by the solution of the problem. The stiffness matrix obtained in the previous section is singular. In order to obtain a solution of the equilibrium equations (4.2), the structure must be supported at a sufficient number of nodes to remove this singularity.

Only one type of support is considered during this research, the type that completely constrains the displacement in a certain direction.

4.6 Calculation of Stresses

The Finite Element procedure of discretizing continua, reduces the analysis to that of solving a set of linear simultaneous algebraic equations. These are the discretized

equilibrium equations (4.2). When these equilibrium equations are solved, the displacements may be substituted in the strain displacement relation and subsequently into the constitutive law. This yields expressions for the stresses everywhere in the element. By substituting the coordinates of a point, we can readily evaluate the stress tensor at that point.

4.7 Solution Procedure

In the current study, a comparison between the analytical approach, presented in the preceding chapter, and Finite Element approach is carried out for small angle dies. After a satisfactory comparison of the results for small angle dies, two different, mathematically contoured, die profiles are studied with reference to the shrink-fit problem by employing a Finite Element software. Linear three dimensional brick elements are employed to create Finite Element models for both profiles. All of the steps performed in pre-processing, processing and post processing are described in the form of a flow chart in Figure 4.2.

In particular these die profiles (Cosine, Convex, Sigmoidal, Polynomial and etc) are attractive to the wire manufacturers because of the low drawing stresses and a good product finish. Low drawing stresses are encountered in these dies because of the elimination of a considerable amount of redundant work.

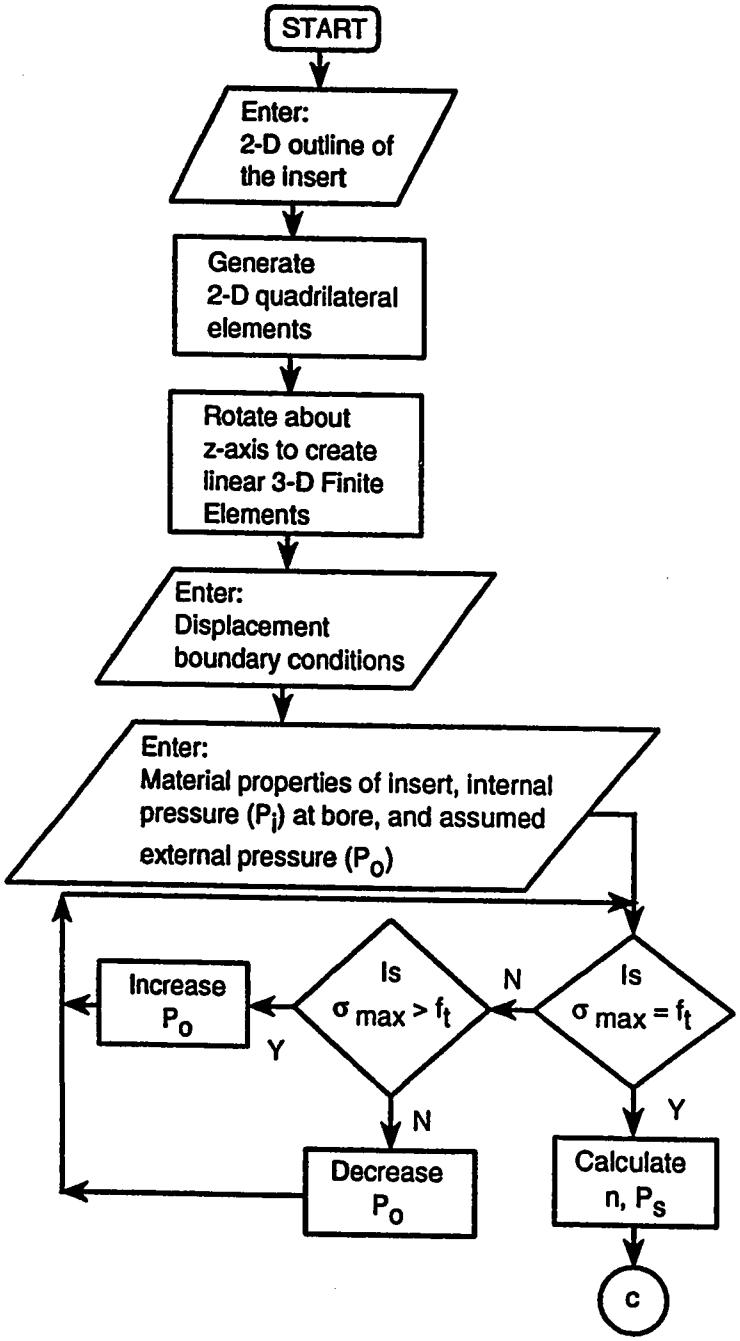
START
Enter:
2-D outline of
the insert
Generate
2-D quadrilateral
elements
Rotate about
z-axis to create
linear 3-D Finite
Elements
Enter:
Displacement
boundary conditions
Enter:
Material properties of insert, internal
pressure (P_i) at bore, and assumed
external pressure (P_o)
Is
$\sigma_{max} = f_t$
N
Y
Is
$\sigma_{max} > f_t$
Y
N
Increase
P_o
Decrease
P_o
Calculate
n, P_s
c

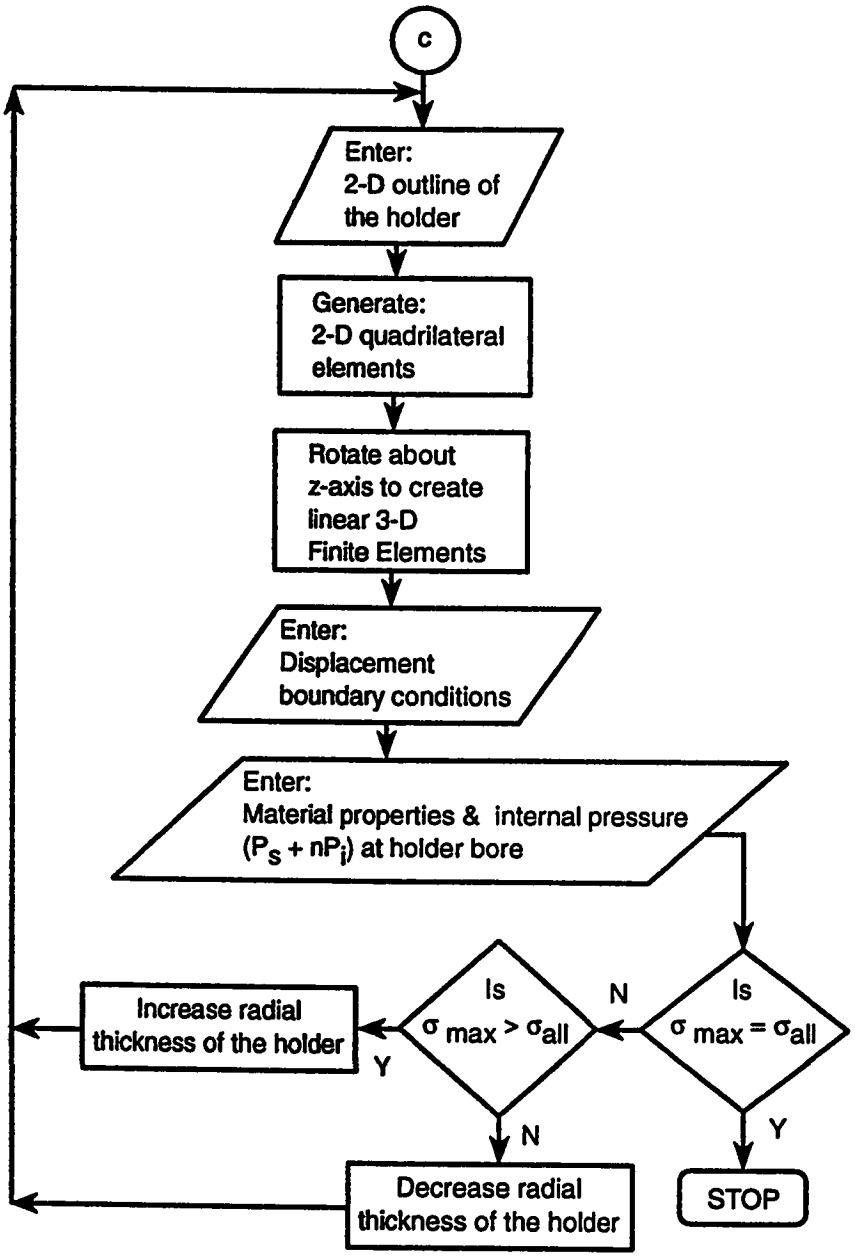

Figure 4.2: Flow chart of the solution procedure for contoured dies.

4.7.1 Cosine Die

The profile equation for cosine die is as follows;

$$R = \frac{R_o + R_f}{2} + \frac{R_o - R_f}{2} \cos\left(\frac{\pi z}{L}\right) \tag{4.23}$$

where

R_o wire radius at entry

R_f wire radius at exit

L axial die length

R wire radius at any length z

A 2-D outline of the die geometry is fed into the computer program which automatically generates the 2-D mesh and then convert this 2-D mesh to 3-D brick elements by rotating it about the z axis. The angle of rotation is 4° for all the models studied. To explain how the boundary conditions and loads are applied on the model a schematic drawing of a slice of straight taper die is shown in Figure 4.3. To calculate stresses and displacements, the model must be supported at some nodes. The bottom surface of the model is constrained to move in the z direction. Since geometry and loading are symmetric with respect to the tangential direction the displacements in this direction are zero. To feed this information to the computer program, boundary elements are used to constrain the tangential displacements of

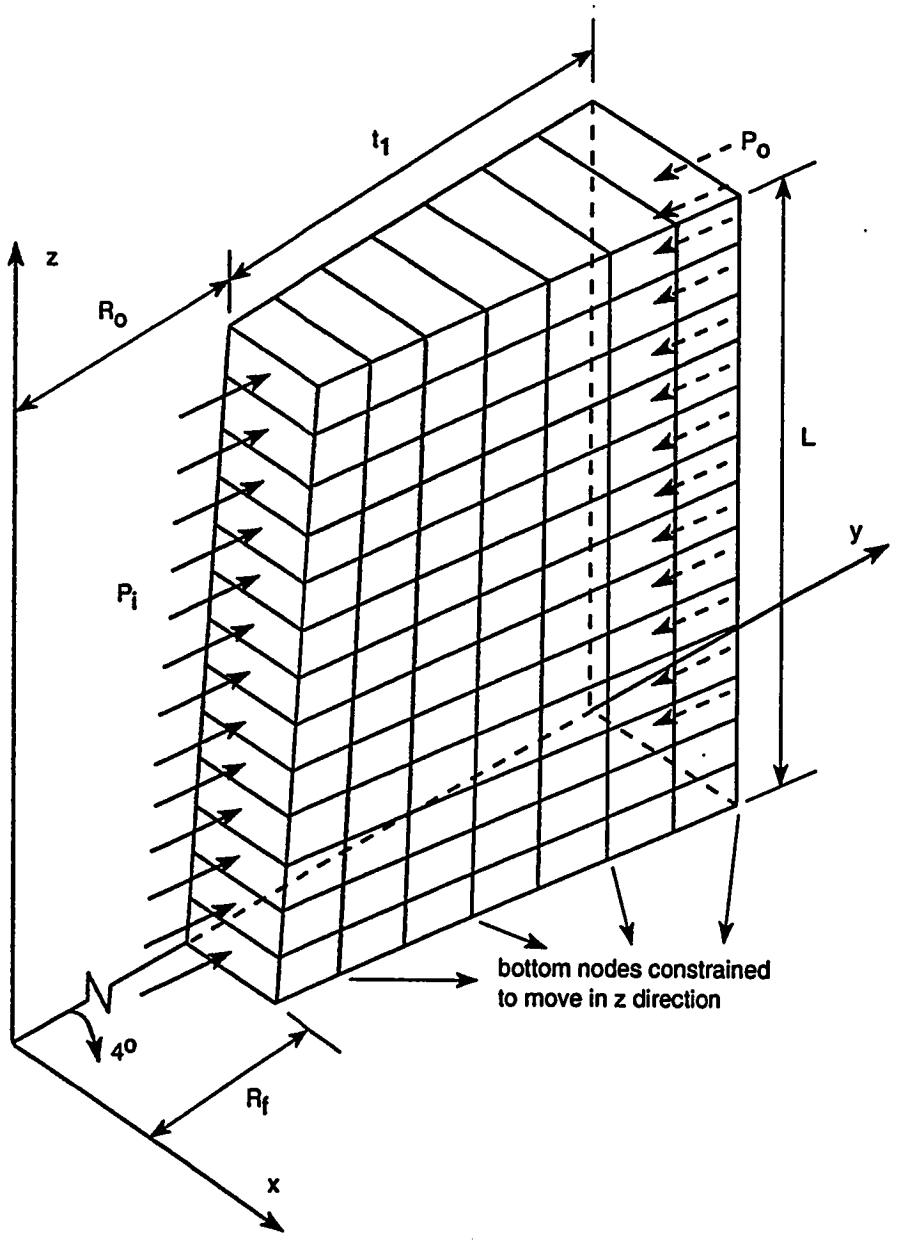

Figure 4.3: Schematic diagram of the Finite Element model for straight taper die

the model. The internal pressure is varying from entry to exit. Therefore we take an average value of pressure over each element, i.e; by summing up the corresponding values of pressure at the top and bottom nodes of that element and dividing by two. For clarity a two dimensional view, instead of a three dimensional isometric view of the Finite Element mesh used for cosine die, for a particular reduction, is shown in Figure 4.4.

4.7.2 Convex Die

The profile equation for convex die is as follows;

$$R = R_o \left[1 + \frac{(R_o/R_f)^2 \, z}{L}\right]^{-1/2} \tag{4.24}$$

The same procedure, as explained for cosine die, is repeated for the convex die. A two dimensional Finite Element mesh of convex die for the same process conditions is also shown in Figure 4.5. The external pressure P_o is then found by an iterative procedure in a way that the maximum principal stress should not exceed the allowable limit of the material at any point in the die. Then some of the process parameters are systematically varied and the external pressure is noted for these variations. To calculate the shrink-fit pressure, we first have to find the multiplying factor n, so that the reaction of the internal pressure can be separated out. To do this, we discretize the die into thin rings, and calculate n value in the same way as has been calculated in the analytical solution. Then we select a n value which is minimum. If

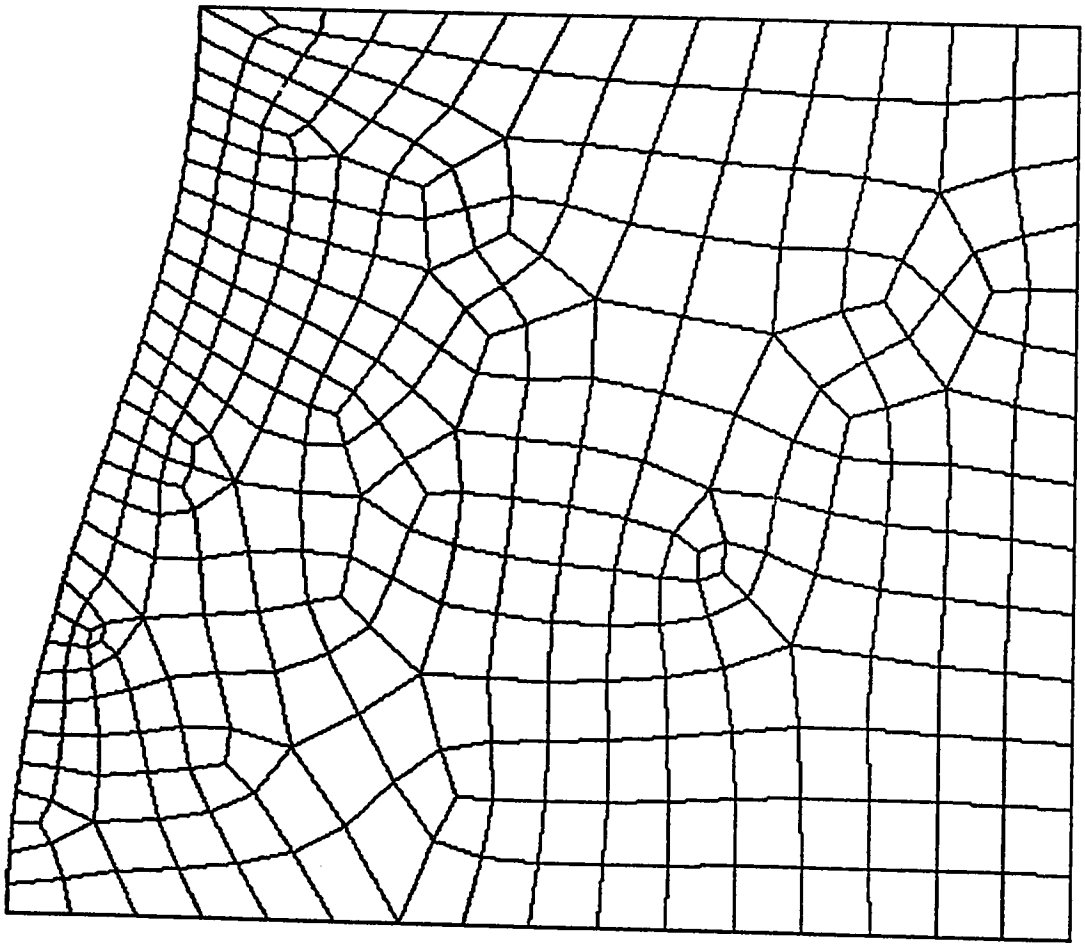

Figure 4.4: Finite Element mesh for cosine die, $AR = 30\%$, $R_o = 0.3937\ in$, $L = 0.3\ in$ and $t_1 = 0.3\ in$.

we choose a higher value then there is a possibility, that at some point the principal stress may exceed the allowable limit. The results obtained from the analytical approach for small die angles and the Finite Element results of mathematically contoured cosine and convex dies are presented and discussed in the next chapter.

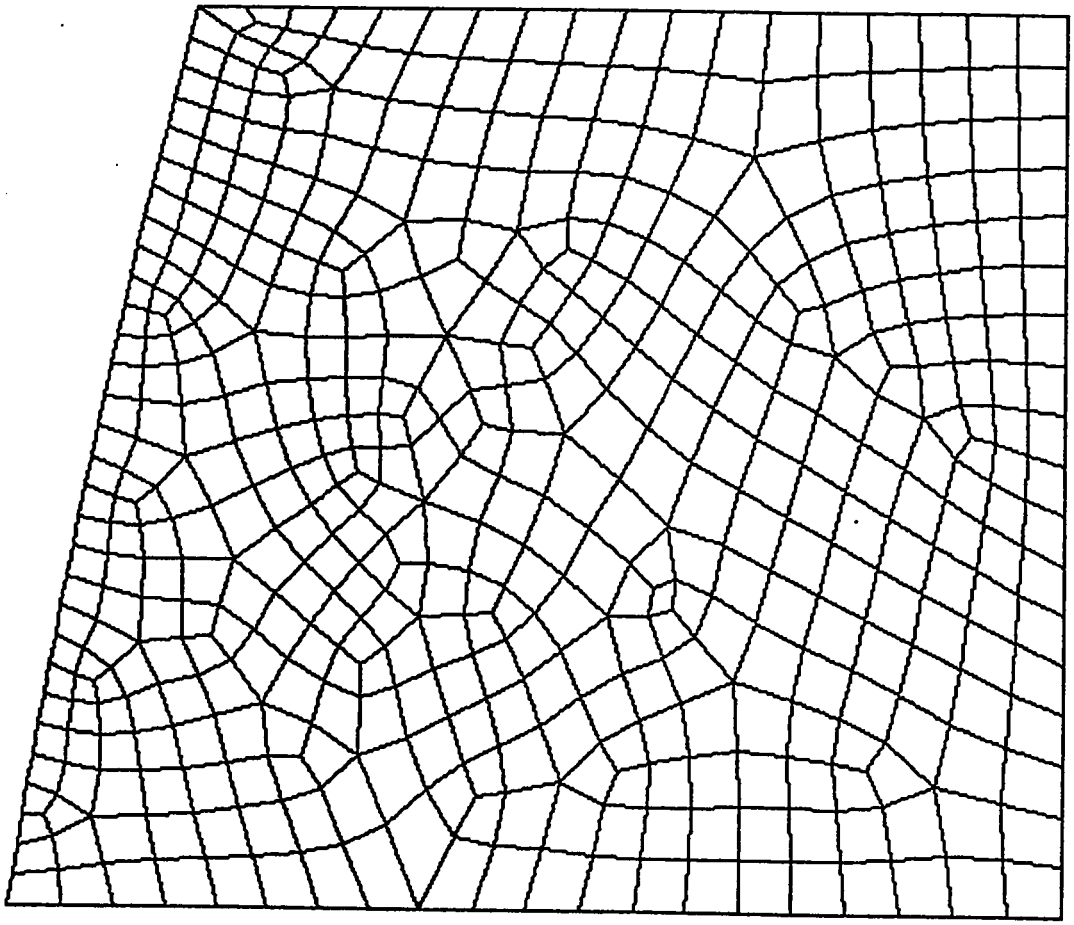

Figure 4.5: Finite Element mesh for convex die, $AR = 30\%$, $R_o = 0.3937$ *in* $L = 0.3$ *in* and $t_1 = 0.3$ *in*.

Chapter 5

Results and Discussions

After analysing the resulting equations of the analytical approach and using Finite Element software for complex die shapes, we have found many interesting results related to the die design. The results show the effects of different process parameters on the shrink-fit pressure required to pre-stress the composite die. In order to present and discuss these results systematically, this chapter is divided into three sections.

In the first section, results of the analytical approach, developed in chapter 3, are presented. To verify some of the assumptions, made during the analytical approach, a comparison between the analytical and Finite Element approach is also performed for maximum principal stresses in the die. The second section contains Finite Element results for contoured dies(Cosine and Convex die). Finally, in the third section, a comparison between the analytical and Finite Element approach is carried out in

order to check the validity of the analytical approach.

Before going into the details of the analytical and Finite Element results, it is appropriate to mention the mechanical properties of the materials used in calculations. All of the plots , which will be presented in the following sections, are for one insert and one holder material, unless otherwise specified. The insert is made up of sintered Alumina(Al_2O_3), with typical mechanical properties as shown in Table 5.1 [45];

Tensile yield strength	38	Ksi
Compressive yield strength	427	Ksi
Modulus of elasticity	46,700	Ksi
Poisson's ratio	0.24	
Allowable tensile yield strength	18	Ksi
Allowable compressive yield strength	200	Ksi

Table 5.1: Mechanical properties of the insert.

The holder is made up of a shock-resisting tool steel(AISI No. S7) with mechanical properties shown in Table 5.2 [46];

Yield strength	200	Ksi
Tensile strength	264	Ksi
Modulus of elasticity	30,000	Ksi
Poisons ratio	0.29	
Allowable yield strength	100	Ksi

Table 5.2: Mechanical properties of the holder.

The wire material, for all cases studied, is an alloy steel(AISI No. 4340) having mechanical properties, as shown in Table 5.3 [46];

Yield strength	68.5	Ksi
Tensile strength	108	Ksi
Strain hardening coefficient	138.15	Ksi
Strain hardening exponent	0.113	

Table 5.3: Mechanical properties of the work material.

In the determination of internal pressure, using Cristescu's visco-plastic model [6], the coefficient of viscosity η_v of the work material is taken as $0.725Ksi - s$ [47]. Initial wire radius R_o for all cases is $0.3937in$.

5.1 Results of the Analytical Approach

Figure 5.1 shows the variation of shrink-fit pressure, required to pre-stress the brittle ceramic die, with area reduction, for exit wire velocities ranging from $1in/s$ to $30in/s$. Semi die angle is kept constant at 4°. For area reductions of up to 15%, the shrink-fit pressure increases a little and then it goes down with further increase in area reduction. This is logical if we observe the variation of the intermediate radius b. Let us take an example of the curve for $V_f = 10in/s$. Variation of the intermediate radius and average internal pressure (P_i) with area reduction (AR) is given in Table 5.4.

Table 5.4 shows that as AR increases the average value of P_i begins to decrease after 15% area reduction. The moment P_i starts decreasing, b must decrease to remain an optimum dimension, as can also be observed in Figure 3.8. The reason, for the

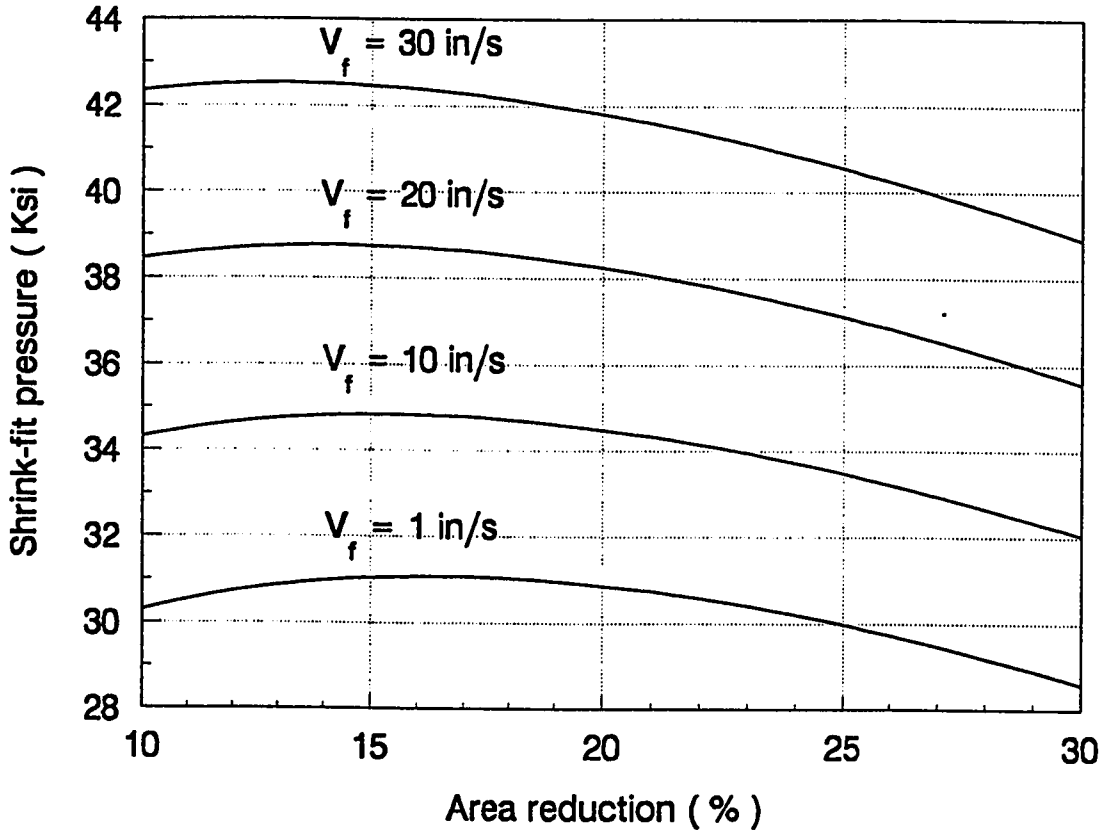

Figure 5.1: Variation of shrink-fit pressure with area reduction for $\alpha = 4°$.

AR %	b in	$P_{i(avg)}$ Ksi
10	0.5398	96.354
15	0.5437	97.199
20	0.5414	96.691
25	0.5341	95.104
30	0.5230	92.627

Table 5.4: Variation of intermediate radius and average internal pressure with area reduction for $V_f = 10\ in/s$

decrease in P_i at higher reductions can be explained by looking at Table 5.5, for semi die angle of 4° and exit wire velocity of 20 in/s;

AR %	P_i @ entry Ksi	P_i @ exit Ksi	$P_{i(avg)}$ Ksi
10	108.32	97.36	103.42
30	120.14	75.91	98.4

Table 5.5: Variation of internal pressure with area reduction for $V_f = 20\ in/s$ and $\alpha = 4°$.

It is clear from Table 5.5, that for the same exit velocity the average internal pressure at 30% reduction becomes lower than that at 10%. This causes the shrink-fit pressure to decrease with increase in area reduction.

Figure 5.2 is same as Figure 5.1 except that the semi die angle in this case is 8°. The curve patterns are exactly the same, but the shrink-fit pressure is a little higher than that of the 4° die. Therefore same reasoning given in Tables 5.4 and 5.5 is applicable here.

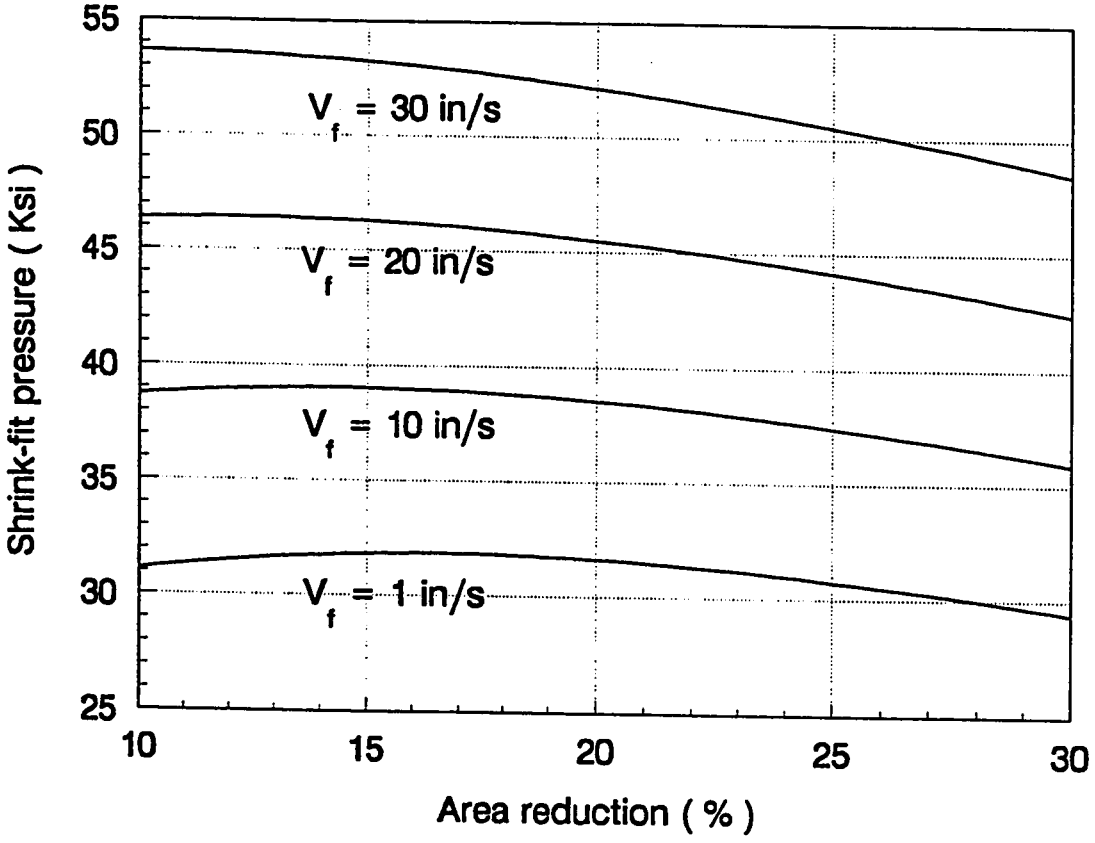

Figure 5.2: Variation of shrink-fit pressure with area reduction for $\alpha = 8°$.

The variation of the shrink-fit pressure with exit wire velocity is plotted for different area reductions in Figure 5.3. Semi die angles are 4° and 8° respectively. Each curve represents almost a linear relation between shrink-fit pressure and exit wire velocity. It is noted that, for a fixed insert and holder material, the influence of exit wire velocity on shrink-fit pressure is considerable. Also for higher velocities and at larger semi die angles, the rate of increase of shrink-fit pressure decreases a little as compared to that at lower velocities, causing a slight decrease in the slope of the curves, as can be observed in Figure 5.4.

Figure 5.5 shows the variation of shrink-fit pressure with semi die angle for 10% and 20% area reductions. The exit wire velocity is set at $1in/s$. Semi die angle is one of the most important parameter from the point of view of process mechanics. But it can easily be observed from the figure under consideration, that in the case of die design its influence on shrink-fit pressure is not significant for the specified wire velocity. The shrink-fit pressure increases only about 5% if the semi die angle is increased from 2° to 10°.

5.1.1 Comparison of Principal Stresses

In order to verify the assumption of uniform internal pressure at insert bore and uniform inner radius of the insert, made in the analytical approach, a comparison of the maximum principal stresses obtained from analytical and finite Element approach is presented in this section.

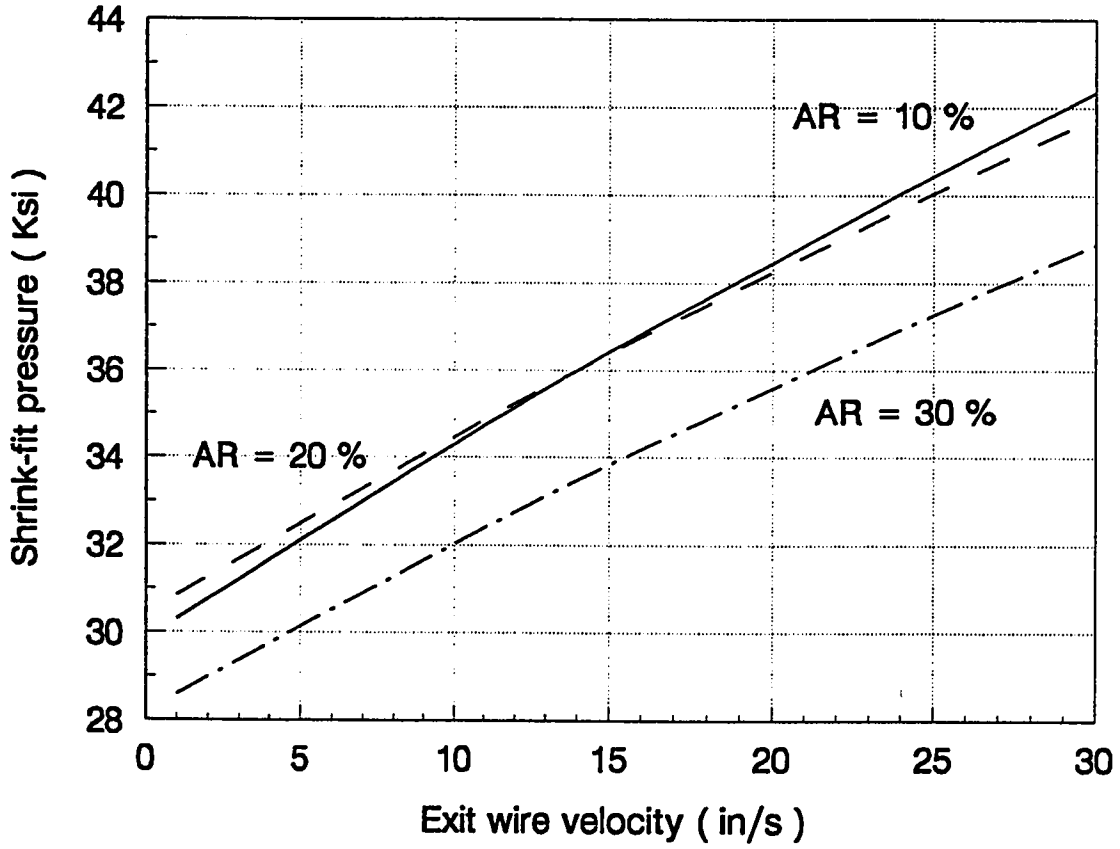

Figure 5.3: Variation of shrink-fit pressure with exit wire velocity for $\alpha = 4°$.

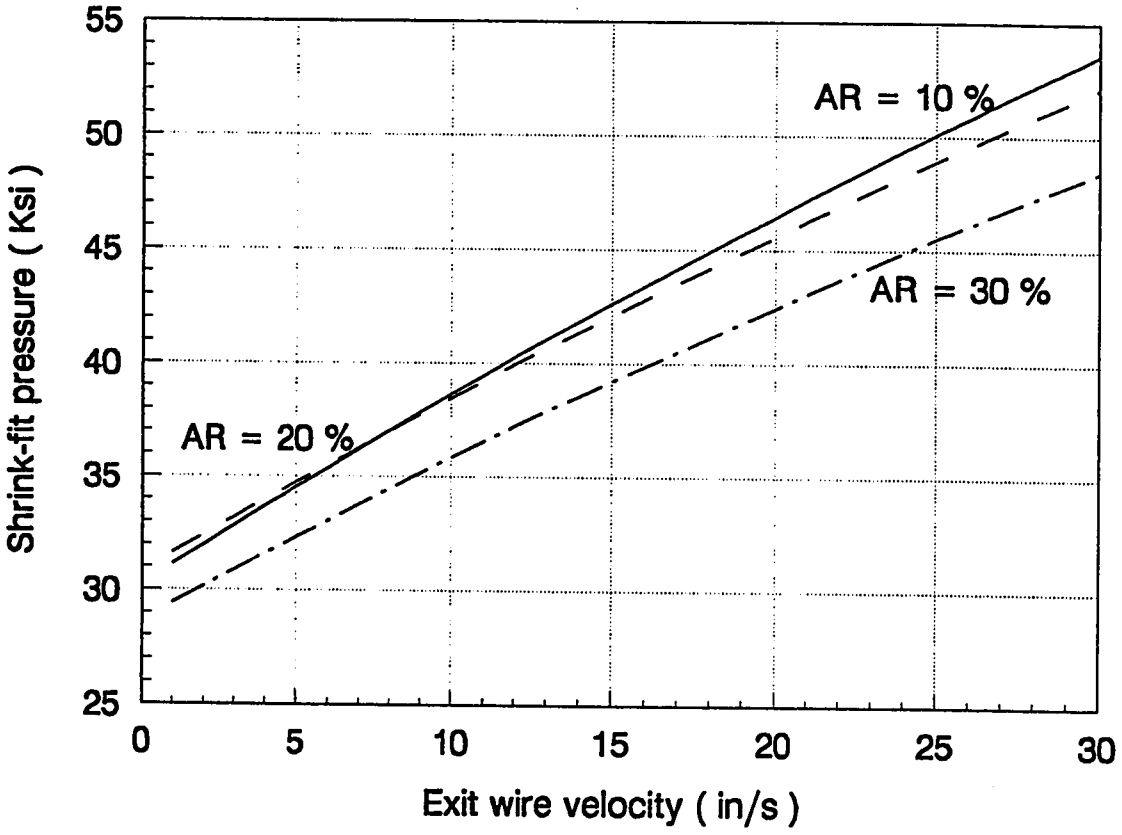

Figure 5.4: Variation of shrink-fit pressure with exit wire velocity for $\alpha = 8°$.

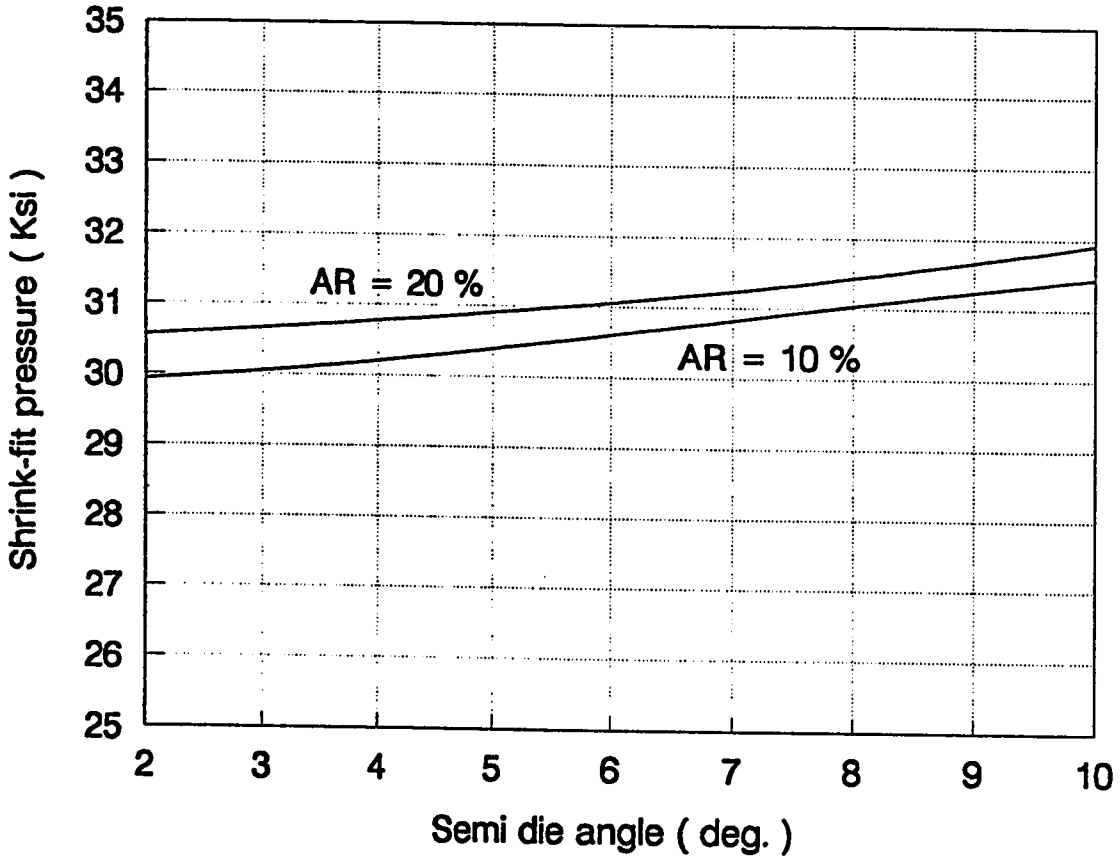

Figure 5.5: Variation of shrink-fit pressure with semi die angle for $V_f = 1\ in/s$.

Die dimensions
a = 0.3937 in
b = 0.9300 in
c = 2.2000 in
L = 0.2888 in

Holder yield strength	111 Ksi	87 Ksi
Solution procedure	Cristescu's model	Avitzur's model
Analytical	P_s = 35.12	26.95 Ksi
F.E.M	P_s = 37.02	27.85 Ksi

Table 5.6: Comparison of the analytical and Finite Element results.

To have the same die dimensions in all the models, i.e Cristescu, Avitzur and Finite Element model, different die holder materials are used, while the insert is made up of sapphire in all models. A detailed description of the results is presented in Table 5.6.

Figure 5.6 shows the variation of maximum principal stress at insert bore with the axial die length. Area reduction is 10% and a semi die angle of 4° is selected. In the most critical zone, i.e in the proximity of die exit, the assumption of constant internal pressure and constant inner radius holds very well. However, there is a significant difference between the analytical and Finite Element solution, as we approach the die entry. Since the actual principal stress at the die entry, obtained from the Finite Element model, is lower than that of the allowable one(18 Ksi). Therefore we can say that, the assumption of uniform internal pressure and a constant inner radius of the cylinder, is still valid. Die shapes and pressure distributions for the three

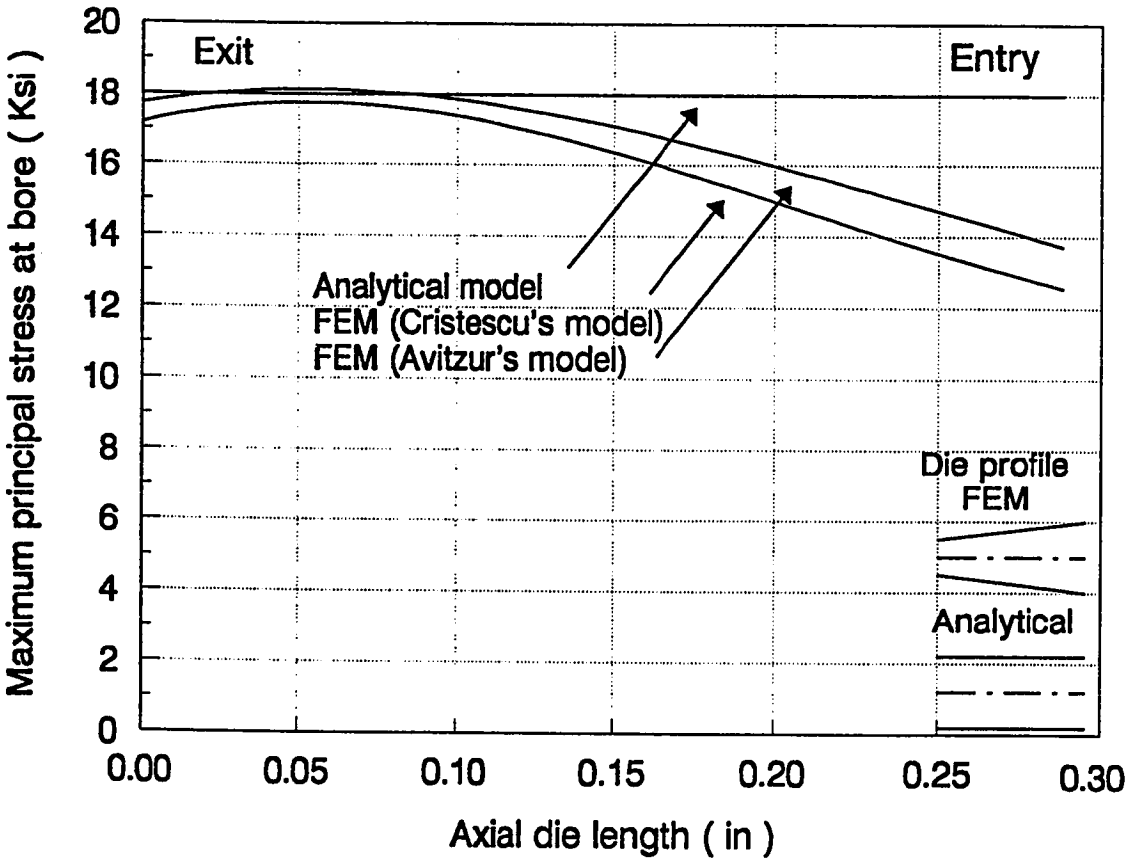

Figure 5.6: Variation of maximum principal stress with axial die length for AR = 10 % and $\alpha = 4°$.

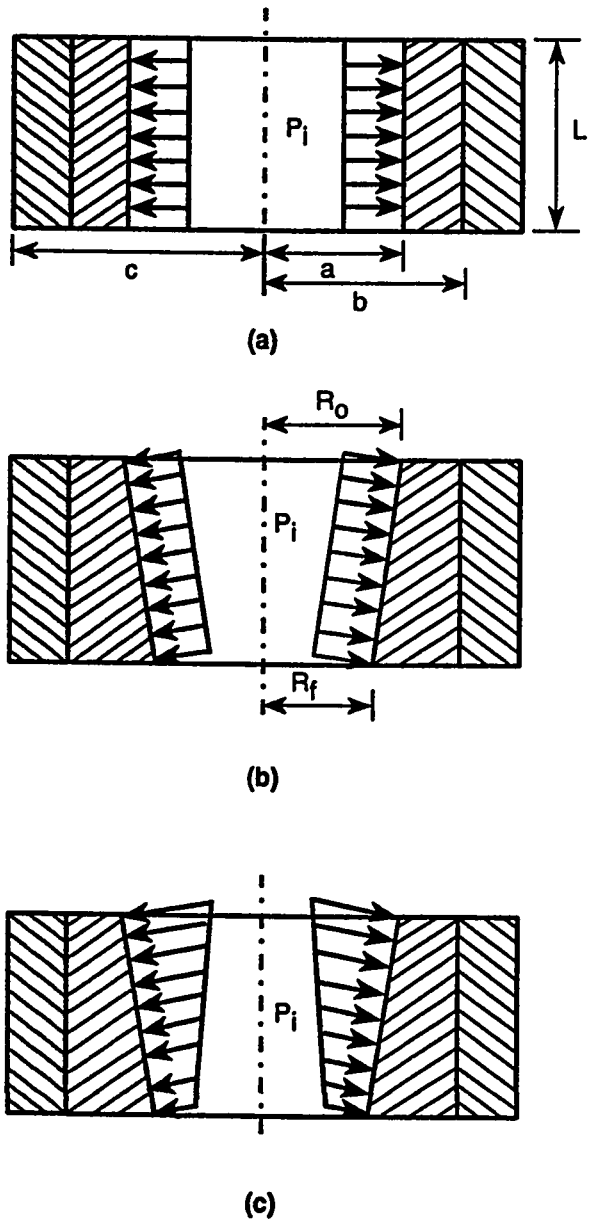

Figure 5.7: Pressure distribution and die profiles for (a) analytical model (b) Avitzur's model (c) Cristescu's model.

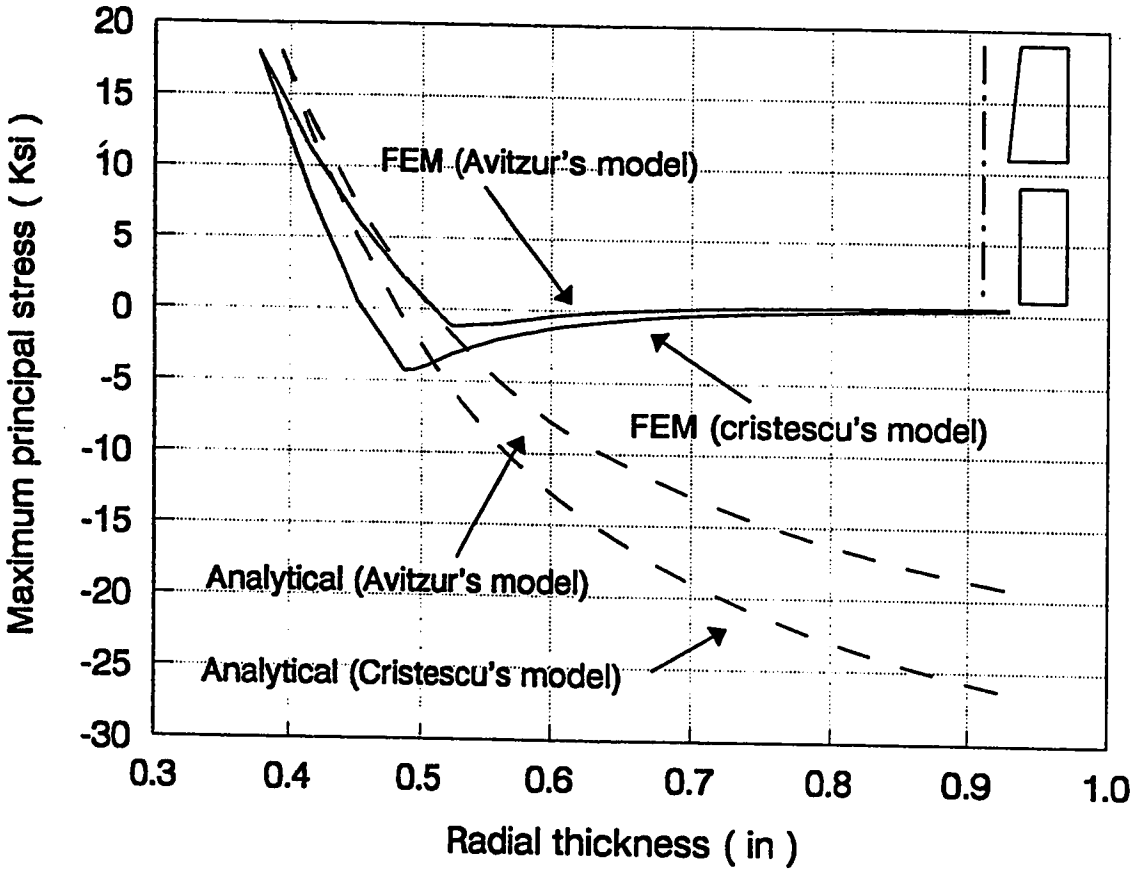

Figure 5.8: Variation of maximum principal stress with radial thickness for $AR =$ 10 % and $\alpha = 4°$.

models are shown in Figure 5.7.

From Lame's theory it is known that, for the problem under consideration, the maximum principal stress always acts at the bore of the cylinder. But for the sake of completeness a plot of maximum principal stress verses radial thickness is shown in Figure 5.8, for the same working conditions as shown in Figure 5.6.

5.2 Results of the Finite Element Approach

The Finite Element modeling is done for two mathematically contoured dies; cosine die and convex die. In the Finite Element approach, optimization of the die dimensions is carried out in a different way. A specified insert geometry with boundary conditions and internal pressure at bore is first fed into the computer program and the required external pressure is calculated. For a given holder material, the external radius of the holder is then calculated in a way, so that the overall radius ratio is less than 6 and the stress at the inner radius of the holder is equal to the allowable value. Materials for the insert and holder are same as used in the analytical approach.

It is important to mention here that we cannot make a direct comparison between Figure 5.1 and 5.9. Because in the analytical approach die dimensions are the output of the computer program, for any variation of the process parameters these are optimized by the computer program. Where as in the Finite Element approach we have to feed the insert geometry in advance to calculate the shrink-fit pressure, re-

quired to pre-stress the composite die.

Figure 5.9 shows the variation of shrink-fit pressure with area reduction for a cosine die. Velocities vary from $1in/s$ to $30in/s$. Radial thickness of the insert is set at $0.1in$. It is clear from the figure that area reduction have a significant effect on the shrink-fit pressure even for small velocities. This is due to the fact that at higher velocities, the internal pressure increases sharply which in turn requires more shrink-fit pressure. For higher velocities and higher reductions, the slope of the curve is less than that at lower reduction ratios. The reason for this decrease is that at higher reduction ratios, the variation of internal pressure is so great that the internal pressure at the die exit becomes very low, which reduces the rate of increase of the shrink-fit pressure.

Figure 5.10 is same as Figure 5.9 except that the radial thickness at entry is set at $0.3in$. The shrink-fit pressure at 10% area reduction is increased for all the velocities. Also the slope of all the curves is decreased, except for $30in/s$, as compared to Figure 5.9. The increase in shrink-fit pressure at lower reductions is due to the increase in radial thickness of the insert. As the radial thickness is increased, the reaction of the internal pressure, which is contributing in supplying the external pressure, will decrease. So that a greater amount of shrink-fit pressure is now required to constrain the maximum principal stress from exceeding the allowable limit. The decrease in slope of the curves, as compared to Figure 5.9 is also due to the increase in thickness. But the effect of increase in thickness is nullified at higher velocities.

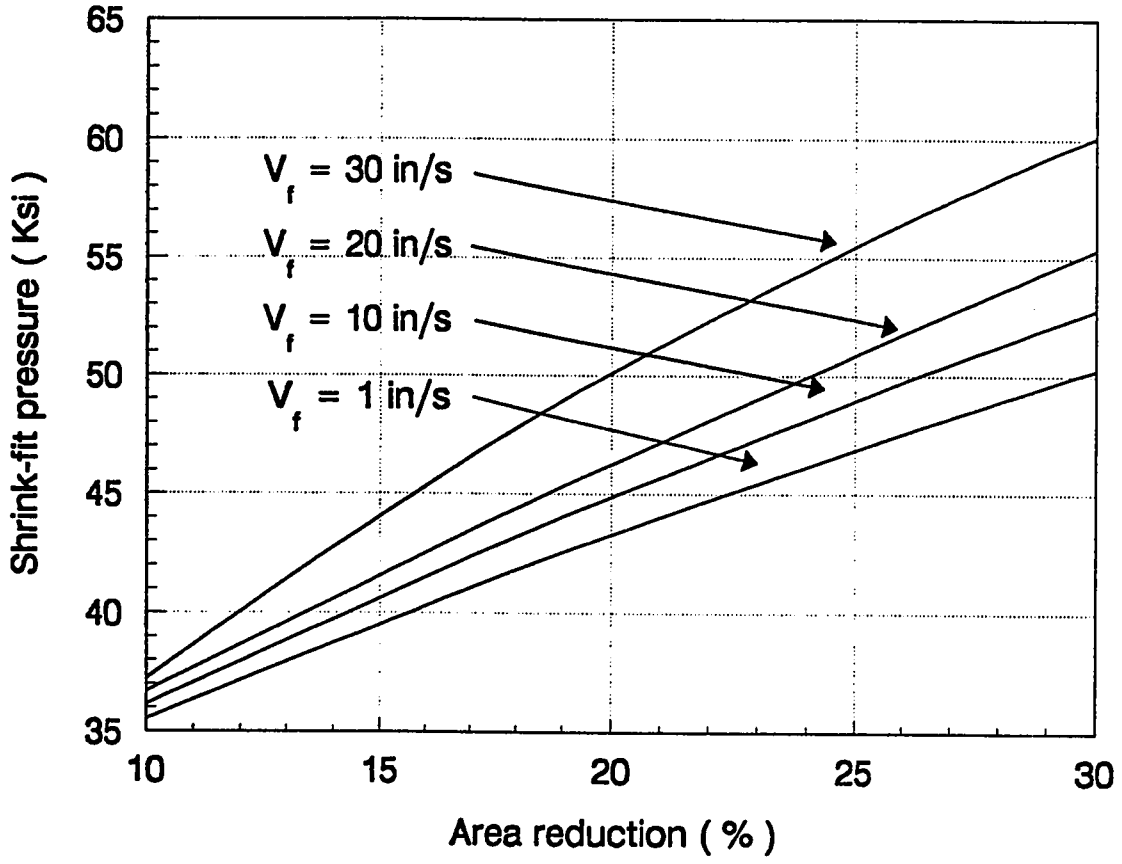

Figure 5.9: Variation of shrink-fit pressure with area reduction for cosine die, radial thickness at entry i.e $t_1 = 0.1\ in.$

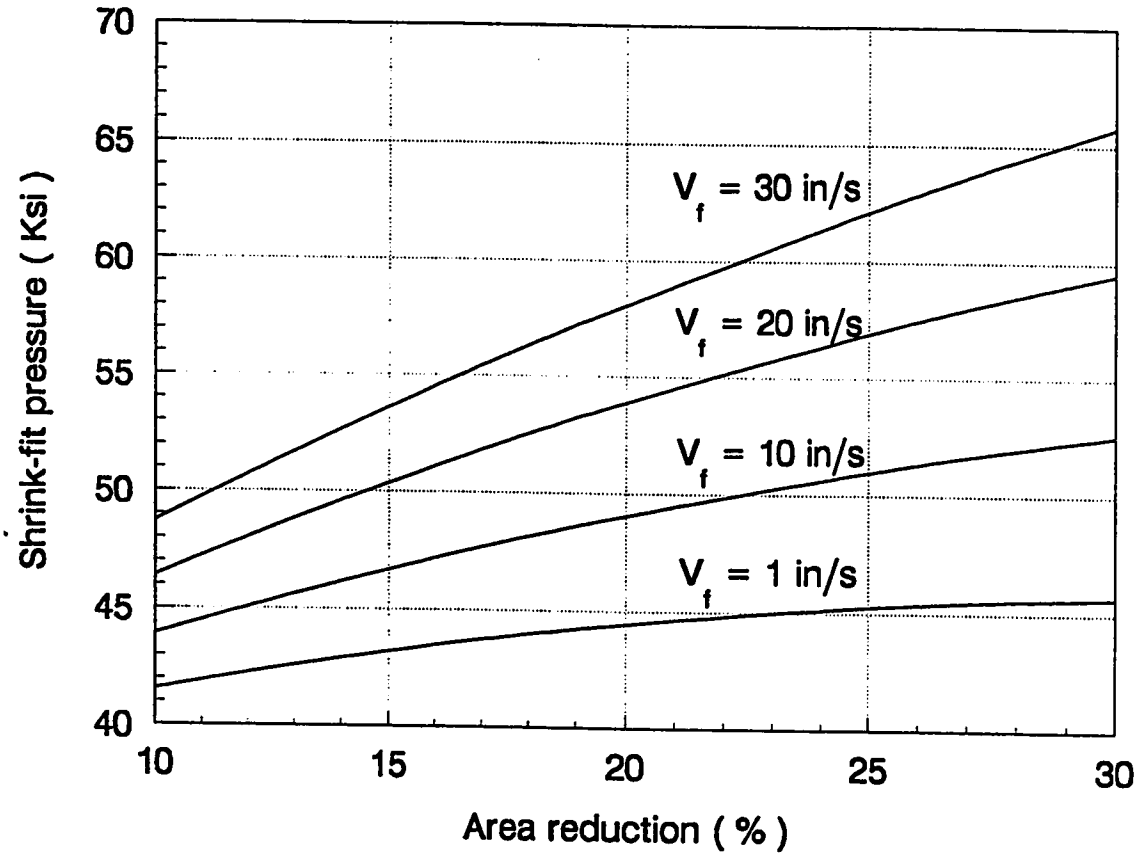

Figure 5.10: Variation of shrink-fit pressure with area reduction for cosine die, $t_1 = 0.3\ in.$

The reason for the decrease in slope at higher reductions is the same as explained for Figure 5.9.

Figure 5.11 shows the variation of shrink-fit pressure with wire exit velocity for three different reductions. The radial thickness at entry is $0.1in$. For low to moderate reductions, the exit wire velocity has no noticeable effect on shrink-fit pressure. For 10% area reduction, the increase in shrink-fit pressure is about 5% for which the velocity increases from $1in/s$ to $30in/s$. Again the same argument applies here, that at higher reductions the effect of exit wire velocity is significant because of higher internal pressure.

Figure 5.12 is same as Figure 5.11 except that the radial thickness at die entry is $0.3in$. The rate of increase of shrink-fit pressure for all area reductions is increased as compared to Figure 5.11. As mentioned earlier, this behavior of the shrink-fit pressure is due to the increase in thickness of the die.

Figure 5.13 shows the variation of shrink-fit pressure with die length for 10% and 20% area reduction. Since in the case of mathematically contoured dies the slope of the contoured radius is changed as we go from entry to exit of the die. Therefore, to see the effect of varying the die angle, length of the die is varied from 0.2 to 0.5 in. The radial thickness of the insert at entry is set at $0.4in$. Although, semi die angle is one of the important parameter from the view point of process mechanics. But it is observed from Figure 5.13 that in the case of die design it does not play any significant role. By varying the die length, it is seen that the internal pressure

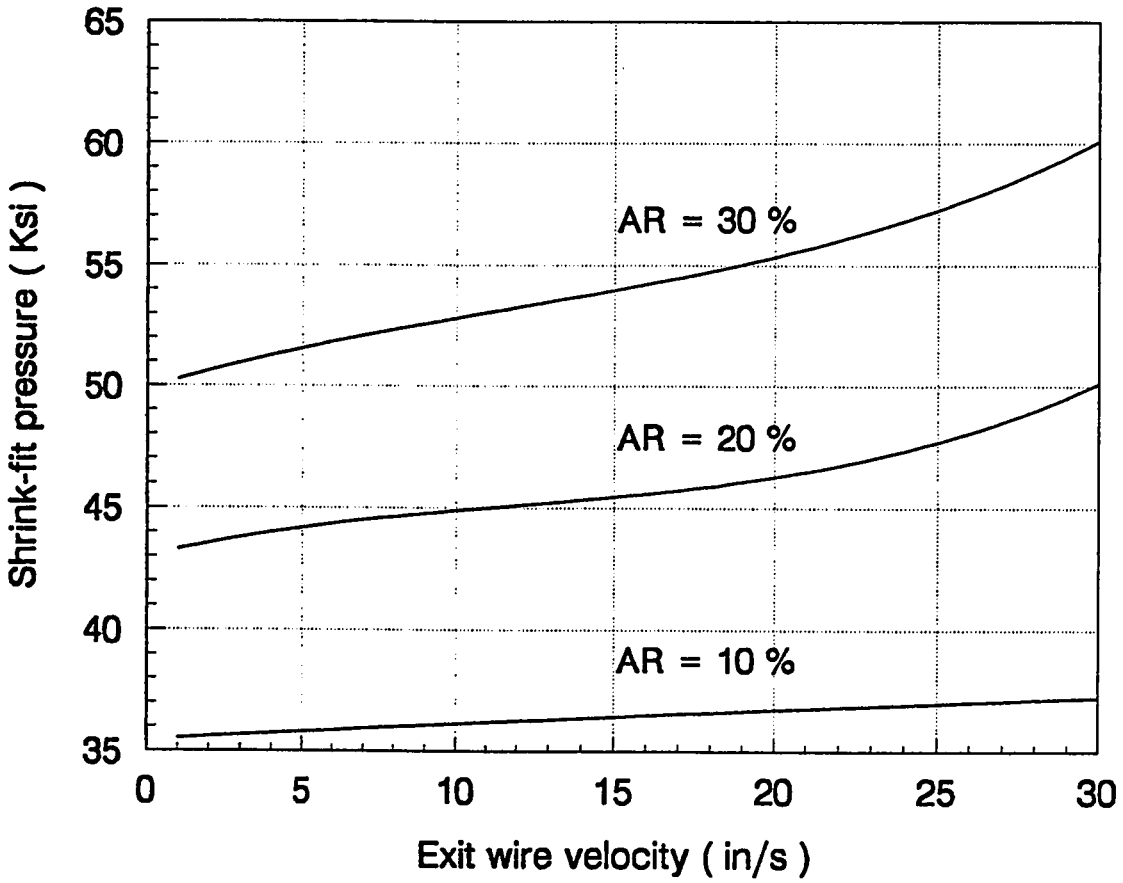

Figure 5.11: Variation of shrink-fit pressure with exit wire velocity for cosine die, $t_1 = 0.1$ *in.*

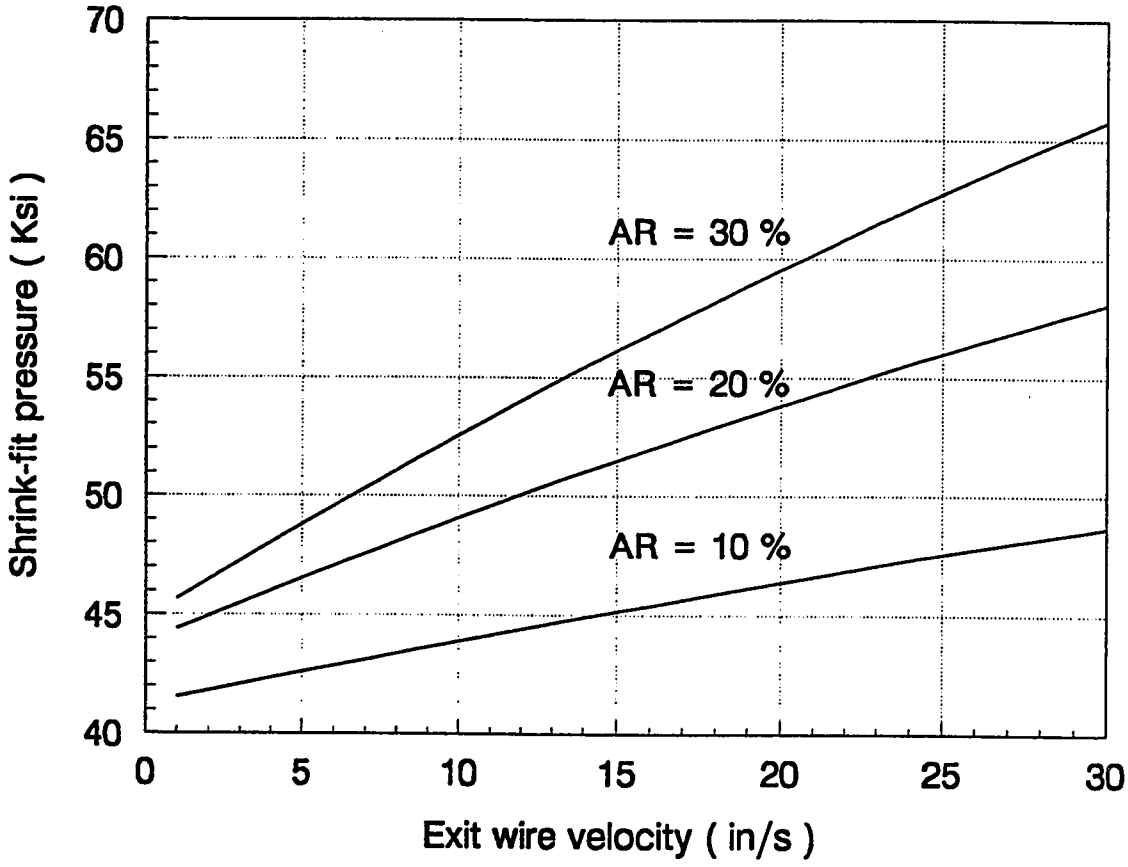

Figure 5.12: Variation of shrink-fit pressure with exit wire velocity for cosine die, $t_1 = 0.3\ in.$

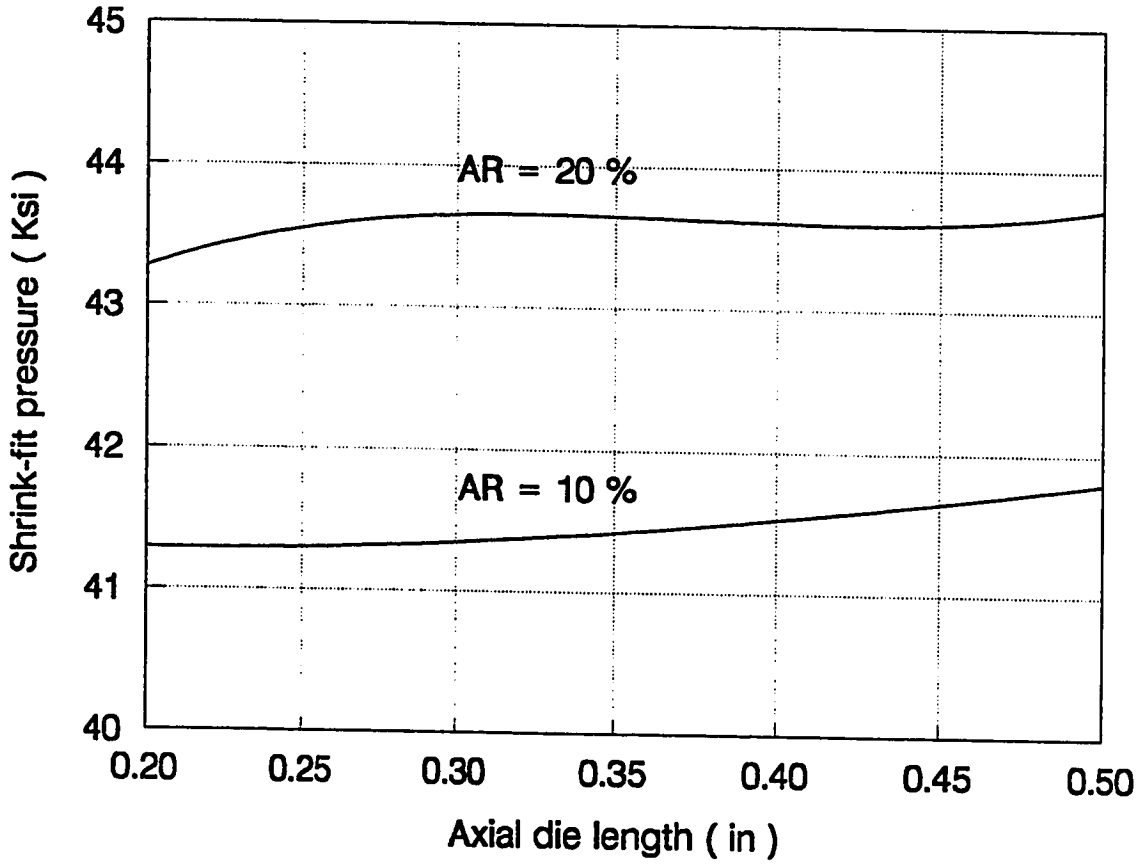

Figure 5.13: Variation of shrink-fit pressure with axial die length for cosine die, $V_f = 1\ in/s$.

variation is almost unchanged in every case. This is why, we do not see a noticeable change in shrink-fit pressure.

In order to investigate the variation of shrink-fit pressure by varying the insert radial thickness, a plot of shrink-fit pressure verses radial thickness at die entry is shown in Figure 5.14. Area reduction is varied from 10% to 30%. The curve for 10% area reduction shows lower shrink-fit pressure for small thickness. As the radial thickness is increased, the shrink-fit pressure becomes independent of it. This behavior is also found for the other two reductions. But for small radial thicknesses, the behavior of shrink-fit pressure is different in all cases. Table 5.7 shows this behavior for 0.1 *in* radial thickness.

AR %	P_o Ksi	n	P_s Ksi	ρ_1	ρ_2
10	69.75	0.4065	35.53	1.32	1.82
20	70.7	0.3497	43.30	1.40	1.84
30	69.75	0.2910	50.26	1.5	1.82

Table 5.7: Variation of external pressure, multiplying factor and radius ratios with area reduction.

The external pressure acting on the insert is almost same in all the reductions. The multiplying factor n is a function of material properties (different for all reductions) and radius ratios. Since ρ_1 is changing significantly, which in turn force n to decrease, and a major portion of the external applied pressure must have to act as the shrink-fit pressure for larger area reductions.

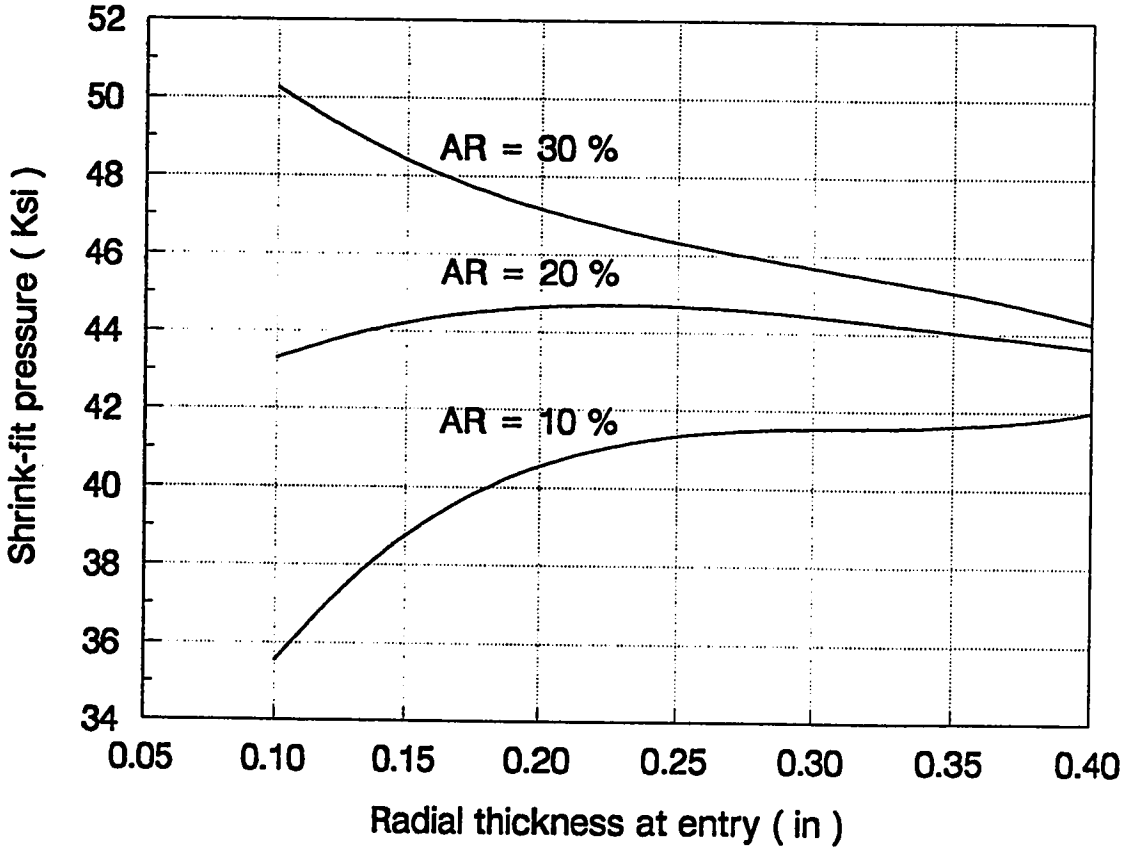

Figure 5.14: Variation of shrink-fit pressure with radial thickness at die entry for cosine die, $V_f = 1\ in/s$.

Figures 5.15 to 5.20 show the variation of shrink-fit pressure with different process parameters for a convex die. The variation of shrink-fit pressure with these process variables is almost similar to that of the cosine die, discussed above. The only difference between the two dies is that the shrink-fit pressure for convex die is approximately 3 to 5% lower than that of the cosine die, for a particular set of process variables. This small difference in shrink-fit pressure is attributed to the difference in die profile. Therefore same reasoning, as explained for cosine die is applicable in the case of convex die.

In order to be consistent with the analytical results, plots of maximum principal stress verses axial die length and radial thickness, for cosine and convex dies, are shown in Figures 5.21 and 5.22 respectively. The stress distribution in the radial direction is shown at that axial depth, where the maximum principal stress is equal the allowable tensile limit of the insert at the bore.

5.3 Comparison of the Analytical and Finite Element Approach

In order to verify, that the analytical approach is valid for small die angles and small reductions, a sample comparison between the two methods is presented in this section.

Figure 5.23 shows the variation of shrink fit-pressure with area reduction for two

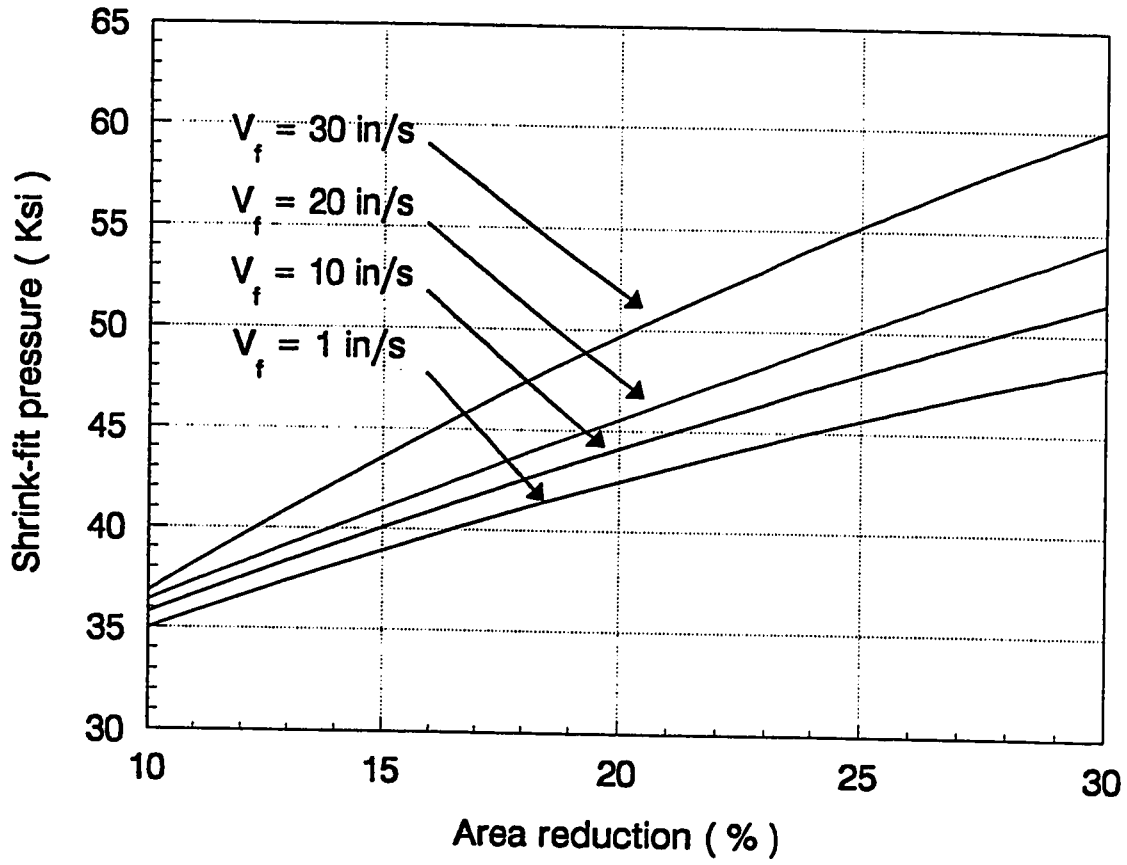

Figure 5.15: Variation of shrink-fit pressure with area reduction for convex die, $t_1 = 0.1\ in.$

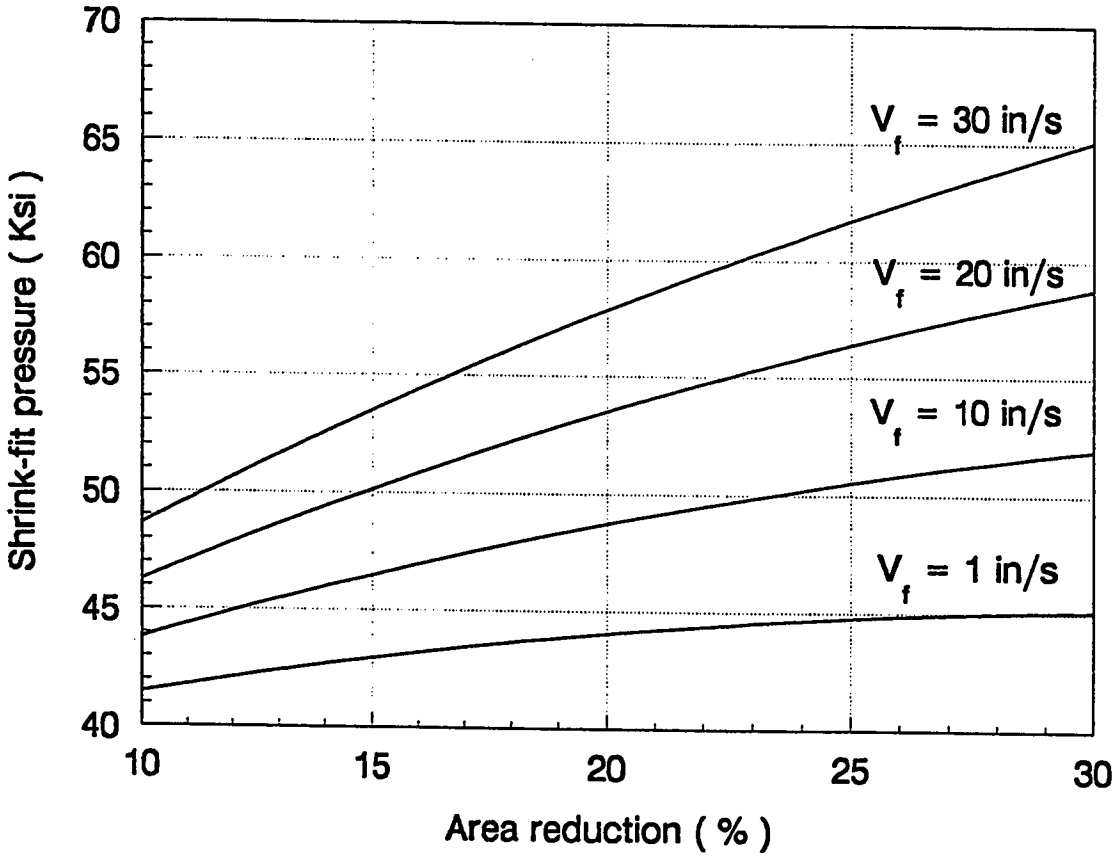

Figure 5.16: Variation of shrink-fit pressure with area reduction for convex die, $t_1 = 0.3\ in.$

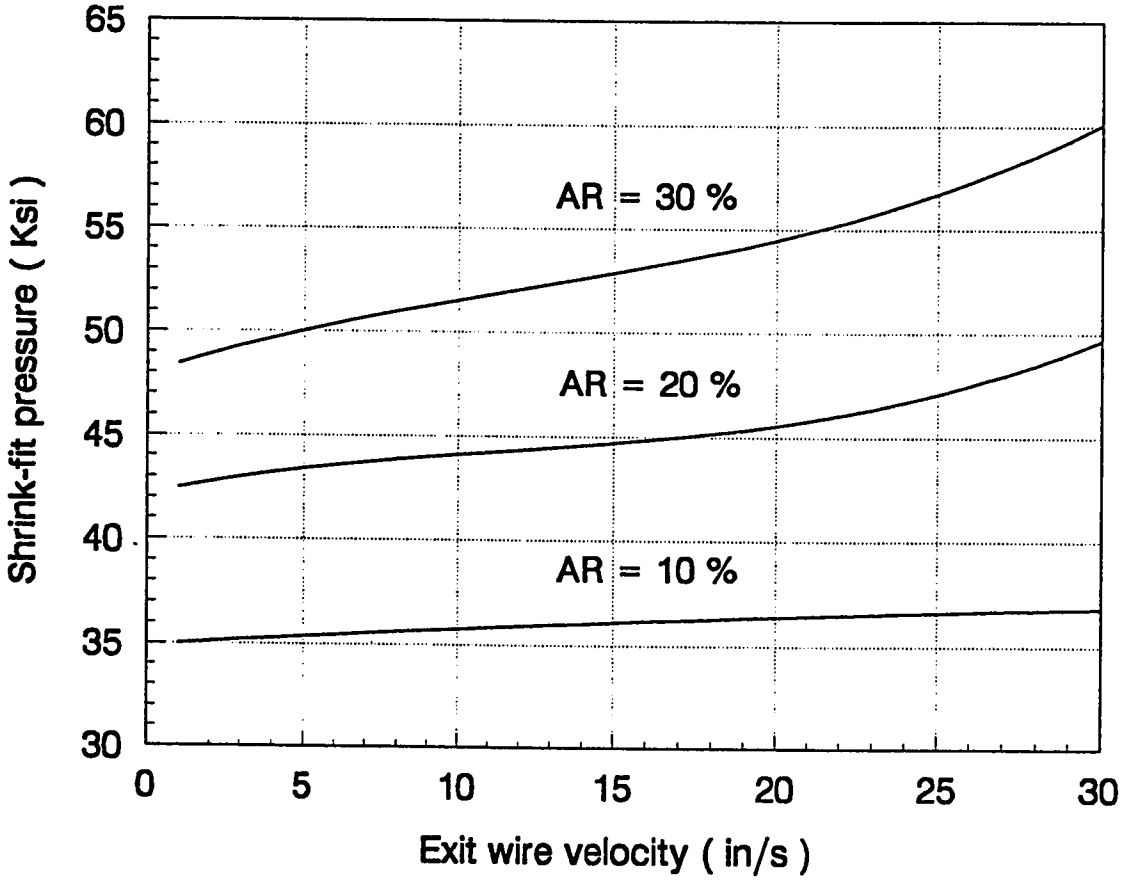

Figure 5.17: Variation of shrink-fit pressure with exit wire velocity for convex die, $t_1 = 0.1\ in.$

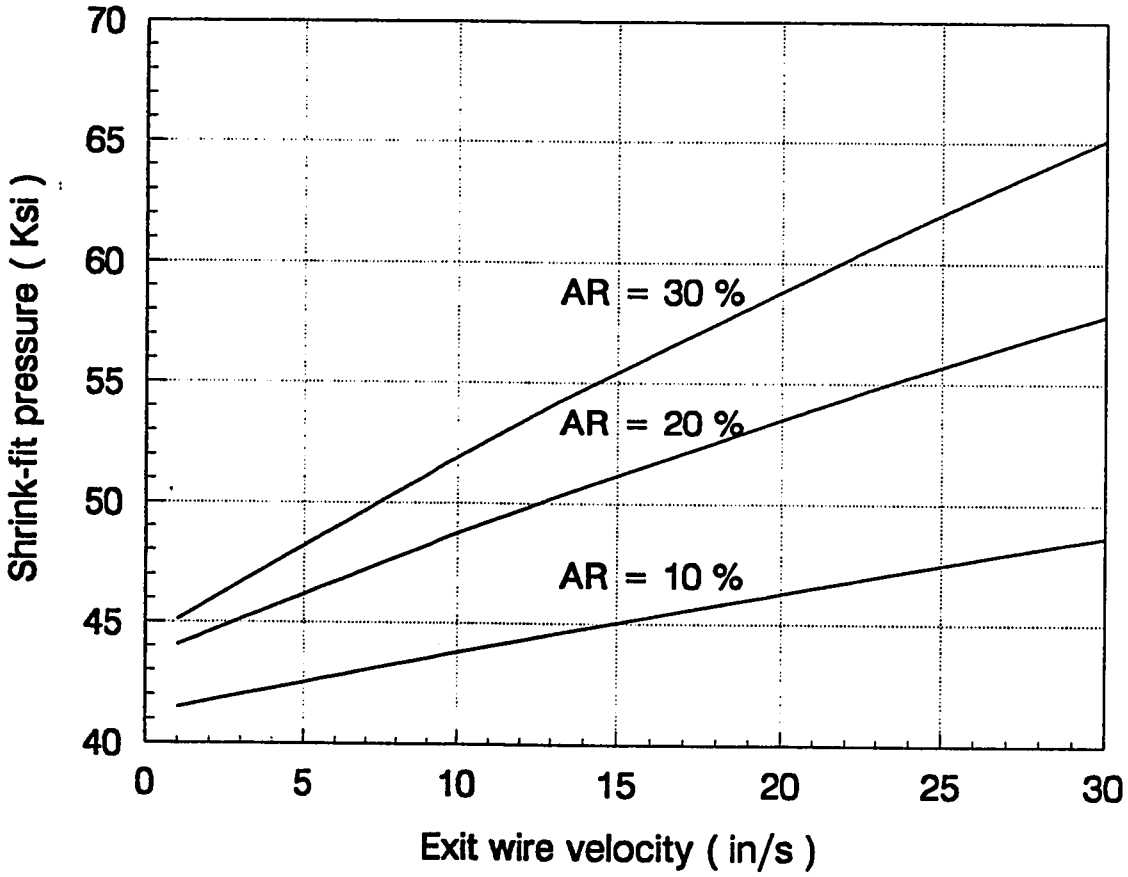

Figure 5.18: Variation of shrink-fit pressure with exit wire velocity for convex die, $t_1 = 0.3\ in.$

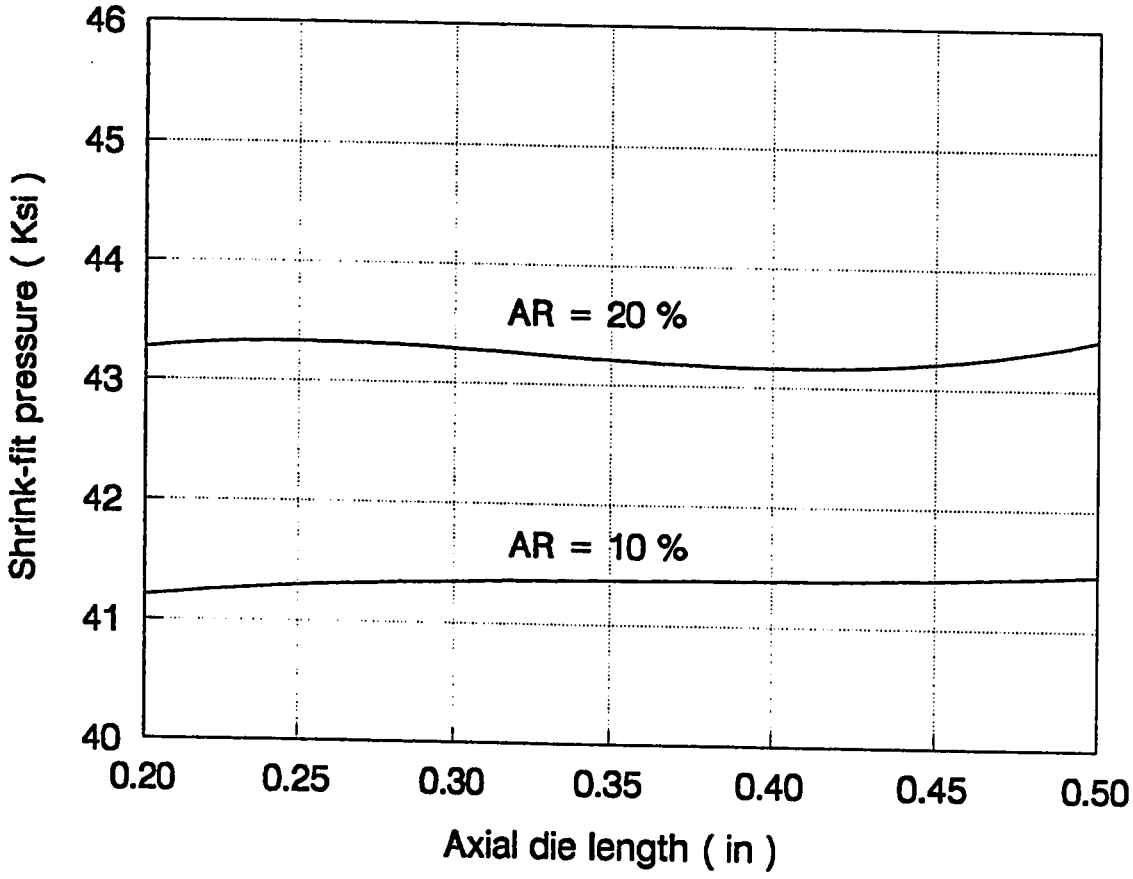

Figure 5.19: Variation of shrink-fit pressure with axial die length for convex die, $V_f = 1\ in/s$.

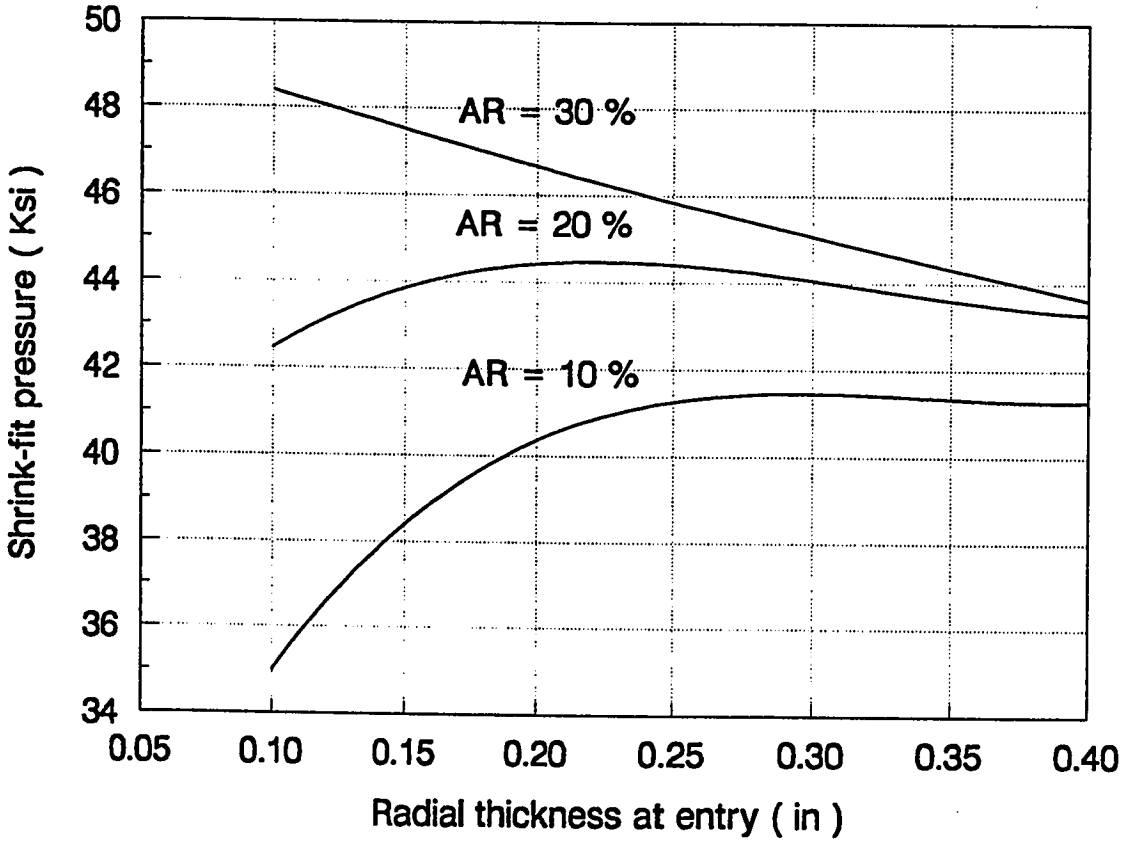

Figure 5.20: Variation of shrink-fit pressure with axial die length for convex die, $V_f = 1\ in/s$.

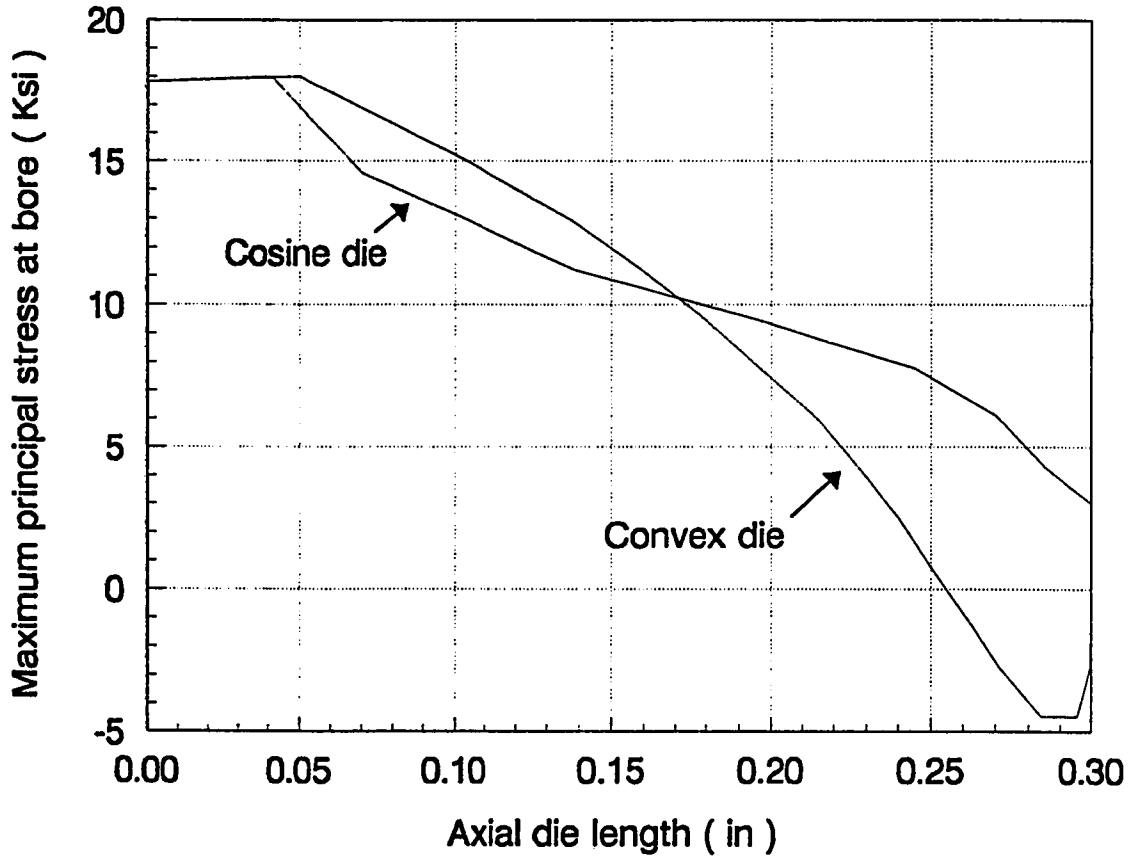

Figure 5.21: Variation of maximum principal stress at die bore for cosine and convex dies, $AR = 10\,\%$.

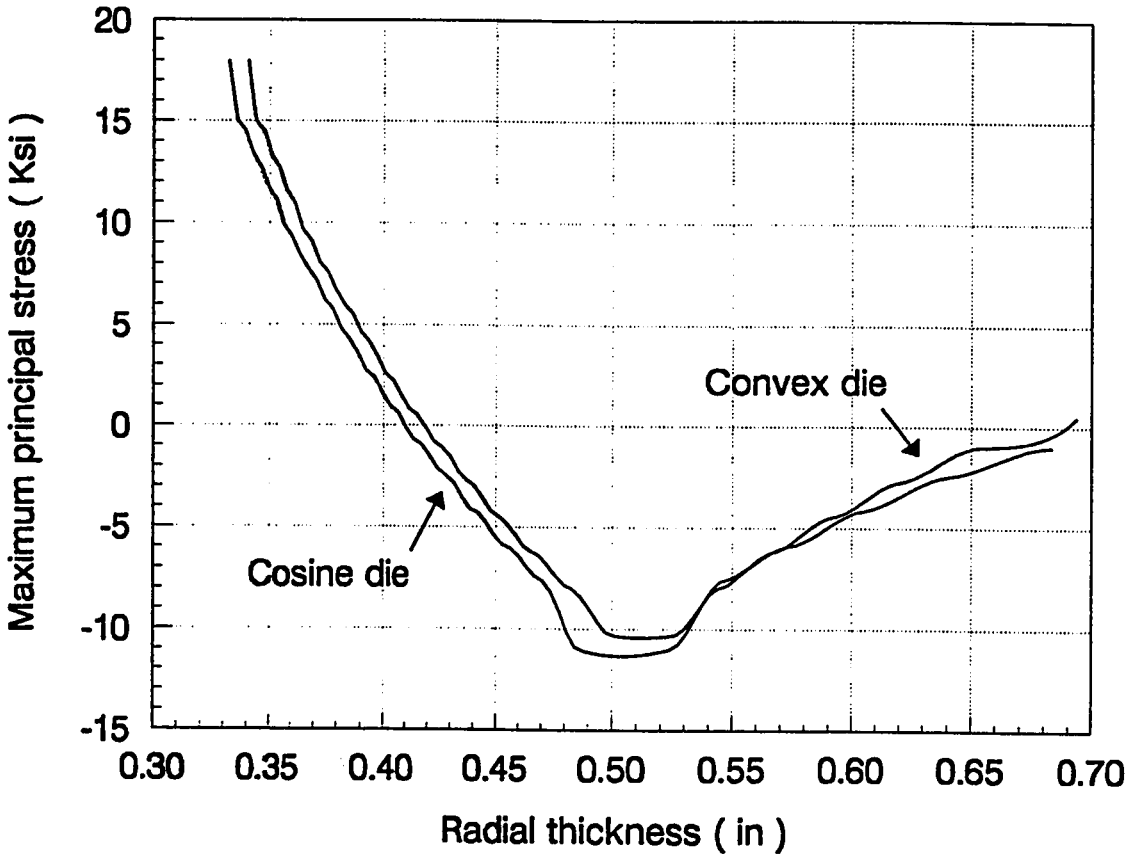

Figure 5.22: Variation of maximum principal stress in the radial direction for cosine and convex dies, $AR = 10\ \%$.

different exit wire velocities, i.e $1in/s$ and $20in/s$. Solid lines represent analytical solution where as the dotted lines represent analytical solution. To have the same optimized die dimensions for both the analytical and Finite Element solutions, one has to change the yield strength of the holder, at each reduction. The die dimensions and process parameters for the two velocities are shown in Table 5.8.

Die dimensions
a = 0.3937 in
b = 0.6937 in
c = 1.4000 in
L = 0.3000 in

Exit wire velocity	V_f = 1 in/s	V_f = 20 in/s
α = 2.85°, AR = 5 %		
Holder yield strength	Y = 135	152 Ksi
Analytical	P_s = 32.66	37.11 Ksi
F.E.M.	P_s = 33.40	38.50 Ksi
α = 3.85°, AR = 10 %		
Holder yield strength	Y = 140	163 Ksi
Analytical	P_s = 34.62	40.31 Ksi
F.E.M.	P_s = 37.25	43.40 Ksi
α = 7.89°, AR = 20 %		
Holder yield strength	Y = 145	185 Ksi
Analytical	P_s = 35.52	46.06 Ksi
F.E.M.	P_s = 41.18	52.74 Ksi
α = 12.10°, AR = 30 %		
Holder yield strength	Y = 142	196 Ksi
Analytical	P_s = 34.75	49.25 Ksi
F.E.M.	P_s = 43.17	59.27 Ksi

Table 5.8: Comparison of the analytical and Finite Element results.

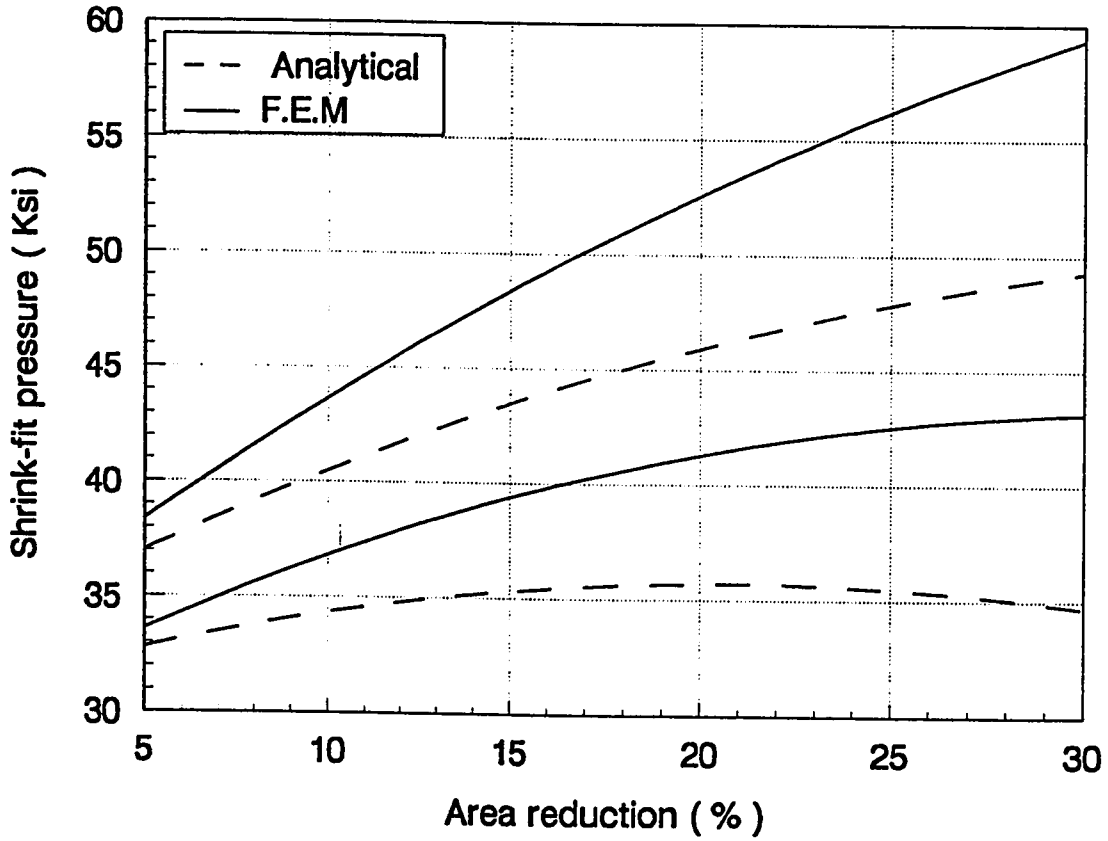

Figure 5.23: Variation of shrink-fit pressure with area reduction.

AR = 30 %			
V_f in/s	P_i @ entry Ksi	P_i @ exit Ksi	% decrease
1	112.52	67.0	-40.0
20	143.30	102.6	-28.4

Table 5.9: Percentage change in internal pressure at different exit wire velocities.

Let us first consider the case, where exit velocity is $1in/s$. For small reductions it is shown that both, the analytical and Finite Element, techniques agree very well. At 15% area reduction, the difference between the analytical solution and Finite Element solution is about 10%. At higher reductions, the analytical approach indicates a decrease in shrink-fit pressure, whereas the Finite Element curve has a positive slope throughout the specified range of area reduction. The lower value of shrink-fit pressure in the analytical solution is due to the fact that we are not taking into account, the variation of internal pressure. As mentioned previously that an average value of internal pressure is used in the analytical calculations. It is found that the average value of internal pressure is decreased, when reductions greater than 20% are considered. For exit wire velocity of $20in/s$, the trend is same for the Finite Element solution. But the curve of the analytical solution has a positive slope throughout the range of area reduction. This can easily be explained by looking at Table 5.9.

A 40 % decrease in internal pressure has occurred for exit wire velocity of $1in/s$, whereas for $20in/s$ this decrease is reduced to 28%. Therefore we can say that, for

higher reductions, a higher exit wire velocity helps to reduce the variation of internal pressure, which in turn increases the slope of the shrink-fit pressure curve.

Chapter 6

Conclusions and Suggestions

6.1 Conclusions

The problem of composite die design for wire drawing have been studied using analytical and Finite Element approach. A computer program is developed to integrate wire drawing process with wire drawing die design. This program produces good results for semi die angles of about 6° and small area reductions up to 15 %.

In the first part, an analytical approach is developed, based on Lame's thick wall cylinder theory. Die dimensions are optimized by taking into consideration, the strength of materials used. It is found that, if ceramic materials are pre-stressed then we can use them as a wire drawing die material. Variation of the shrink-fit pressure is studied by systematically varying some of the important process parameters. In order to create a link, which was not available until now, between wire

drawing process and wire drawing die design, a computer program is developed. Now the most important parameter, i.e internal pressure at die bore, from the point of view of die design is not an arbitrary value. It is the actual value which comes from a process model.

In the second part die design problem of contoured dies(cosine and convex die) is solved. Dies of such profiles are very useful because of there high drawing efficiency. Product strength, ductility, and surface finish is also improved considerably as compared to straight taper dies. Variation of shrink-fit pressure is studied by systematically varying some of the most important parameters, using a Finite Element software. It is found that the exit wire velocity is the parameter which significantly influence the shrink-fit pressure required to pre-stress the composite die. Area reduction also significantly influence the shrink-fit pressure. Although semi die angle is one of the most critical parameter from the point of view of process mechanics, but it is found that in the case of die design its influence on the shrink-fit pressure is not significant. Similarly, for contoured dies, the parameter equivalent to semi die angle, i.e die length L, shows no significant effect on shrink-fit pressure.

By comparing the analytical and Finite Element results it is found that the analytical approach produces good results for up to 15 % area reduction and a semi die angle of 6°. For higher reductions and semi die angle, the analytical approach can provide a preliminary design. For more accurate design one should make use of Finite Element approach.

6.2 Suggestions for Future Work

We have neglected the effect of thermal stresses in the present study. It will be interesting to see, how shrink-fit pressure behave when thermal stresses are taken into consideration?

A different pre-stress technique can be employed like wire wound technique, so that the shrink-fit pressure can also be varied according to the variation of internal pressure and then a comparison can be made between the current and the suggested techniques. Thus the more efficient technique can be identified.

A quantitative analysis of die life can also be performed to see the percentage increase in die life by applying pre-stress to this type of composite dies. These ideas can be extended to other metal forming processes.

Appendix A

Evaluation of the Factor (n)

Consider a composite cylinder consisting of two cylinders of equal length.

1. an insert with elastic constants E_1 and ν_1 , and of internal and external radii a and b respectively, where b/a is denoted by ρ_1.

2. a holder with elastic constants E_2 and ν_2 , and of internal and external radii b and c respectively, where c/b is denoted by ρ_2.

The conditions to be satisfied at the insert-holder interface are the continuity of radial stress and tangential strain. Considering first that the insert fits exactly into the holder with no shrink-fit pressure. Denoting the reaction of the internal pressure on the insert due to the holder by nP_i, the tangential strains, equation(3.3), at the contact surface i.e at $r = b$ are,

$$\epsilon_{ti} = \frac{u_1}{b} \quad \epsilon_{th} = \frac{u_2}{b} \tag{A.1}$$

where

ϵ_{ti} hoop strain of the insert

ϵ_{th} hoop strain of the holder

u_1 and u_2 can be found out using equation 3.7.

$$u_1 = \frac{1-\nu_1}{E_1}\left[\frac{P_i - \rho_1^2 nP_i}{\rho_1^2 - 1}\right] b + \frac{1+\nu_1}{E_1}\left[\frac{(P_i - nP_i)\rho_1^2}{\rho_1^2 - 1}\right]\frac{1}{b} \tag{A.2}$$

$$u_2 = \frac{1-\nu_2}{E_2}\left[\frac{nP_i}{\rho_2^2 - 1}\right] b + \frac{1+\nu_2}{E_2}\left[\frac{nP_i\rho_2^2}{\rho_2^2 - 1}\right]\frac{1}{b} \tag{A.3}$$

The two strains, equation (A.1), must be equal to maintain continuity at the interface. Hence P_i can be eliminated from equations (A.2) and (A.3). Substituting u_1 and u_2 in the respective strain equations and simplifying,

$$\begin{aligned}
\epsilon_{ti} &= \left[\frac{1}{\rho_1^2 - 1} - \frac{n\rho_1^1}{\rho_1^1 - 1}\right]\left(\frac{1-\nu_1}{E_1}\right) + \left[\frac{1}{\rho_1^2 - 1} - \frac{n}{\rho_1^1 - 1}\right]\left(\frac{1+\nu_1}{E_1}\right) \\
\epsilon_{ti} &= \frac{1}{\rho_1^2 - 1}\left[\frac{1-\nu_1}{E_1} + \frac{1+\nu_1}{E_1}\right] - \frac{n}{\rho_1^2 - 1}\left[\frac{\rho_1^2(1-\nu_1)}{E_1} + \frac{1+\nu_1}{E_1}\right] \\
\epsilon_{ti} &= \frac{2}{E_1(\rho_1^2 - 1)} - \frac{n}{\rho_1^2 - 1}\left[\frac{\rho_1^2(1-\nu_1) + (1+\nu_1)}{E_1}\right]
\end{aligned} \tag{A.4}$$

$$\begin{aligned}
\epsilon_{th} &= \frac{n}{\rho_2^2 - 1}\left[\frac{1-\nu_2}{E_2} + \frac{\rho_2^2(1+\nu_2)}{E_2}\right] \\
\epsilon_{th} &= \frac{n}{\rho_2^2 - 1}\left[\frac{\rho_2^2(1+\nu_2) + (1-\nu_2)}{E_2}\right]
\end{aligned} \tag{A.5}$$

equating equations (A.4) and (A.5)

$$n\left[\frac{\rho_1^2(1-\nu_1) + (1+\nu_1)}{E_1\rho_1^2 - 1} + \frac{\rho_2^2(1+\nu_2) + (1+\nu_2)}{E_2\rho_2^2 - 1}\right] = \frac{2}{E_1(\rho_1^2 - 1)}$$

$$n = \frac{2E_2(\rho_2^2 - 1)}{E_2(\rho_2^2 - 1)[\rho_1^2(1-\nu_1) + (1+\nu_1)] + E_1(\rho_1^2 - 1)[\rho_2^2(1+\nu_2) + (1-\nu_2)]}$$

letting $\phi = E_2/E_1$ and expanding

$$n =$$

$$\frac{2\phi(\rho_2^2 - 1)}{(\phi\rho_1^2\rho_2^2 - \phi\rho_1^2\rho_2^2\nu_1 + \rho_2^2\phi + \rho_2^2\phi\nu_1 - \phi\rho_1^2 + \rho_1^2\phi\nu_1 - \phi - \phi\nu_1 + \rho_1^2\rho_2^2 + \rho_1^2\rho_2^2\nu_2 + \rho_1^2 - \rho_1^2\nu_2 - \rho_2^2 - \rho_2^2\nu_2 - 1 + \nu_2)}$$

$$n =$$

$$\frac{2\phi(\rho_2^2 - 1)}{(1 - \nu_2 - \phi + \phi\nu_1)\phi_1^2 + (-1 - \nu_2 + \phi + \phi\nu_1)\rho_2^2 + (1 + \rho_2 + \phi - \phi\nu_1)\rho_1^2\rho_2^2 + (-1 + \nu_2 - \phi - \phi\nu_1)}$$

For simplicity let

$$\beta = 1 - \nu_2 - \phi - \phi\nu_1$$

$$\delta = 1 + \nu_2 + \phi(1 - \nu_1)$$

$$\gamma = -[1 - \nu_2 + \phi(1 + \nu_1)]$$

$$\psi = -[1 - \nu_2 + \phi(1 + \nu_1)]$$

Hence

$$n = \frac{2\phi(\rho_2^2 - 1)}{\psi + \beta\rho_1^2 + \gamma\rho_2^2 + \delta\rho_1^2\rho_2^2} \qquad \text{(A.6)}$$

Appendix B

Calculation of Interference (Δ)

From equation (3.7), the radial displacements u_1 and u_2 of the outside of the insert and the inside of the holder respectively, due to the interference pressure P_s, are;

$$u_1 = \frac{-bP_s}{E_1(\rho_1^2 - 1)}\left[\rho_1^2(1-\nu_1) + 1 + \nu_1\right] \tag{B.1}$$

$$u_2 = \frac{-bP_s}{E_2(\rho_2^2 - 1)}\left[1 - \nu_2 + \rho_2^2(1+\nu_2)\right] \tag{B.2}$$

Thus the required interference is given by the following equation;

$$\frac{\Delta}{b} = \frac{u_2 - u_1}{b} = P_s\left[\frac{\rho_1^2(1-\nu_1) + 1 + \nu_1}{E_1(\rho_1^2 - 1)} + \frac{1 - \nu_2 + \rho_2^2(1+\nu_2)}{E_2(\rho_2^2 - 1)}\right] \tag{B.3}$$

simplifying the above expression we get;

$$\frac{\Delta}{b} = \frac{2P_s}{nE_1(\rho_1^2 - 1)} \tag{B.4}$$

Nomenclature

a	inner radius of the inner cylinder(insert)
b	intermediate radius
c	outer radius of the outer cylinder(holder)
e	element number
E	modulus of elasticity
E_1	modulus of elasticity of the insert
E_2	modulus of elasticity of the holder
E_{ijkl}	material properties tensor
$f(\alpha)$	a function of semi die angle
f_c	allowable compressive strength of the insert
f_t	allowable tensile strength of the insert
F	body force
K	shear yield stress of the work material
K_h	work hardening coefficient of the work material
L	axial die length of the conical portion
m	node number
m_f	constant friction factor
n	multiplying factor for internal pressure

n_h	work hardening exponent of the work material
N^m	shape function for node m
p_i^m	force at node m in direction i
P_i	internal pressure on the insert
P_o	external pressure on the insert
P_s	shrink-fit pressure on the insert
q_n	generalized coordinates
r	radius from the apex of the cone
r_f	radius from the apex of the cone to die exit
r_m	mean radius of the cylinder
r_o	radius from the apex of the cone to die entry
R	die profile radius from the center line of the die
R_f	final wire radius
R_o	initial wire radius
t	radial thickness of the cylinder
t_1	radial thickness of the insert at entry
u	nodal displacements of the element
u_i^m	displacement of node m, in direction i
u_r	radial displacement of uniform cylinder
u_1	radial displacement of the insert

u_2	radial displacement of the holder
V	volume of an element
V_f	exit wire velocity
$W^{(e)}$	virtual internal work of an element
$W_p^{(e)}$	elemental work of the external forces
Y	yield strength of the holder material
Y_m	mean flow stress of the work material
x, y, z	cartesian coordinates
α	semi die angle
δ_{ij}	kronecker delta
Δ	shrink-fit interference
η_v	viscosity coefficient of the work material
ϕ	ratio of the modulus of elasticity
σ_b	back stress(back pull)
σ_d	drawing stress
σ_h	maximum compressive stress on the insert
σ_r	radial stress
σ_t	tangential stress
σ_i	principal stress in i direction
τ_{rz}	frictional shear stress

ϵ	tensile strain
ϵ_{ij}	strain tensor of an element
ϵ_r	radial strain
ϵ_t	tangential strain
ϵ_{th}	hoop or tangential strain of the holder at intermediate radius
ϵ_{ti}	hoop or tangential strain of the insert at intermediate radius
ν	Poisson's ratio
ρ_1	radius ratio of the insert
ρ_2	radius ratio of the holder
ρ_3	over all radius ratio
ζ, η, ξ	local coordinates of an element

Bibliography

[1] R. S. Rao, M. L. Devenpeck, P. K. Wright, E. J. Appleby, C. Y. Lu, and O. Richmond. New strip drawing experiments using transparent sapphire dies. *International Journal of Mechanical Science*, 27(11):725–740, 1985.

[2] J. G. Wistreich. Investigation of the mechanics of wire drawing. *Proceedings of the Institution of Mechanical Engineers.*, 169:654–678, 1955.

[3] B. Avitzur. *Metal Forming:Processes and Analysis.* McGraw-Hill Book Company, 1968.

[4] B. Avitzur. Analysis of wire drawing and extrusion through conical dies of large cone angle. *ASME Journal of Engineering for Industry ser. B*, 86:305–316, November 1964.

[5] R. Davies and E. R. Austin. *Developments in High Speed Metal Forming.* Industrial Press Inc., 1970.

[6] N. Cristescu. Plastic flow through conical converging dies using a viscoplastic constitutive equation. *International Journal of Mechanical Science*, 17:425–433, 1975.

[7] N. Cristescu. Drawing through conical dies-an analysis compared with experiments. *International Journal of Mechanical Science*, 18:45–49, 1976.

[8] J. Tirosh and S. Kobayashi. Kinetic and dynamic effects on the upper-bound loads in metal-forming processes. *ASME Journal of Applied Mechanics*, 43:314–318, June 1976.

[9] G. Camenschi, N. Cristescu, and N. Sandru. High speed wire drawing. *Archives of Mechanics*, 31(5):741–755, 1979.

[10] N. Sandru and G. Camenschi. Viscoplastic flow through inclined plates with application to the strip drawing. *Letters Applied Engineering Science*, 17:773–784, 1979.

[11] R. A. Kohser and D. J. Chronister. Wire and rod drawing - the process and the product. *Proceedings of the North American Metalworking Research Conference(NAMRC)*, pages 100–106, May 1979.

[12] N. Cristescu. On the optimum die angle in fast wire drawing. *Journal of Mechanical Working Technology*, 3:275–287, 1980.

[13] A. Vannes and P. Thierry. Effects of die characteristics on the strength and residual stresses during wire drawing. *Journal of Mechanical Working Technology*, 5:251–266, 1981.

[14] D. Durban. Rate effects in steady forming processes of plastic materials. *International Journal of Mechanical Science*, 26(4):293–304, 1984.

[15] O. Richmond and M. L. Devenpeck. A die profile for maximum efficiency in strip drawing. *Proceedings of the 4th U. S. National Congress on Applied Mechanics*, 2:1053–1057, June 1962.

[16] M. L. Devenpeck and O. Richmond. Strip-drawing experiments with a sigmoidal die profile. *ASME Journal of Engineering for Industry ser. B*, 87:425–428, 1965.

[17] S. K. Samanta. A new die profile with high process efficiency. *Applied Science Research*, 25:54–64, 1971.

[18] O. Richmond. Theory of streamlined dies for drawing and extrusion. *Mechanics of the Solid State*, pages 154–167, 1968.

[19] J. Frisch. A conversational mode for direct numerical machine tool control. *Papers presented at the 13th International Machine Tool Design and Research Conference*, pages 161–166, 1973.

[20] E. M. Pietri and J. Frisch. Metal flow through various mathematically contoured extrusion dies. *Proceedings of the North American Metalworking Research Conference(NAMRC)*, pages 99–104, May 1977.

[21] S. I. Oh. Finite element analysis of metal-forming processes with arbitrarily shaped dies. *International Journal of Mechanical Science*, 24(8):479–493, 1982.

[22] C. H. Lee and S. Kobayashi. New solutions to rigid-plastic deformation problems using a matrix method. *Transactions ASME Journal of Engineering for Industry*, 95:865–873, August 1973.

[23] S. Herbert. Wire drawing dies - a new technology gains ground. *Industrial Diamond Review*, 41(486):237–241, May 1981.

[24] K. E. Glen and T. Maxwell. Die design and automatic finishing increase die life. *Wire Journal*, 13(12):68–71, December 1980.

[25] H. Peter. The manufacture and use of diamond wire drawing dies. *Industrial Diamond Review*, 41(483):63–66, February 1981.

[26] Finnigan. Diamond dies for wire drawing. *Industrial Diamond Review*, pages 31–33, January 1987.

[27] M. R. Kennelly. Die design for better performance. *Wire Journal International*, 17(12):42–47, December 1984.

[28] H. L. D. Pugh. *The Mechanical Behavior of Materials Under Pressure.* Applied Science Publishers Ltd, 1971.

[29] W. R. D. Manning and S. Labrow. *High Pressure Engineering.* International Book Co. Ltd., 1971.

[30] I. L. Spain and Paauwe. *High Pressure Technology.* Marcel Deckker Inc., 1977.

[31] U. Guven. Stress distribution in shrink-fit with elastic-plastic hub exhibiting variable thickness. *International Journal of Mechanical Science*, 35(1):39–46, 1993.

[32] R. R. Guntur and A. K. Sheikh. Saving weight with shrink fits. *Machine Design*, 62(15):99–102, july 1990.

[33] F. J. Cunha and A. D'Ambra. Cylindrical component stress analysis. *Heating/Piping/Air Conditioning*, 59(11):96–98, November 1987.

[34] J. L. Frater and R. Zinolabedini. Stress analysis of dies having multiple shrink rings. *Journal of Materials Shaping Technology*, 7(2):67–80, 1989.

[35] J. L. Frater. Application of finite element method to the prestressed tooling. *Journal of Materials Shaping Technology*, 7(1):49–55, 1989.

[36] K. Lang. On the stress distribution in prestressed extrusion dies under nonuniform distribution of internal pressure. *International Journal of Mechanical Science*, 27(3):169–175, 1985.

[37] J. Gronbaek and T. Wanheim. Optimum design of ribbon and wire wound cylinders for metal forming dies. *ASME Journal of Engineering for Industry*, 99(3):733–737, August 1977.

[38] E. D. Doyle, J. G. Horne, and D. Tabor. Frictional interactions between chip and rake face in continuous chip formation. *Proceeding of the Royle Society London series-A*, 366(1725):173–183, 1979.

[39] P. K. Wright. Frictional interactions in machining: Comparisons between transparent sapphire and steel cutting tool. *Journal of Metals Technology*, 8:150, 1981.

[40] R. S. Rao, M. L. Devenpeck, P. K. Wright, O. Richmond, E. J. Appleby, and C. Y. Lu. Observations of die work interfaces through transparent sapphire dies. *Proceedings of the TMS-AIME Fall Meeting and ASM Metal Congress St. Louis 25-28*, pages 65–78, October 1982.

[41] C. Y. Lu, E. J. Appleby, R. S. Rao, M. L. Devenpeck, P. K. Wright, and O. Richmond. A numerical solution of strip drawing employing measured boundary conditions obtained with transparent sapphire dies. *Proceedings of the International Conference on Numerical Methods in Industrial Forming Processes, Swansea, U. K.*, pages 735–746, 1982.

[42] E. J. Appleby, C. Y. Lu, R. S. Rao, M. L. Devenpeck, P. K. Wright, and O. Richmond. Strip drawing: A theoretical-experimental comparison. *International Journal of Mechanical Science*, 26(5):351–362, 1984.

[43] R. S. Rao. Verification of strip drawing analysis using new sapphire dies. *ASME Journal of Engineering for Industry*, 112(4):379–382, November 1990.

[44] B. Crossland and D. J. Burns. Stress distribution in shrink-fit with elastic-plastic hub exhibiting variable thickness. *Proceedings of the Institution of Mechanical Engineers*, 175:1083–1098, 1961.

[45] G. L. DePoorter. *ASM Metals Handbook Volume-2 Properties and selection.* ASM International, 1990.

[46] W. H. Cubberly. *ASM Metals Reference Book.* American Society for Metals, Metals Park, Ohio, 1981.

[47] N. Cristescu and I. Suliciu. *Viscoplasticity.* Martinus Nijhoff Publishers, 1982.

Vita

- Rasheed Ahmed Butt
- Born in Karachi, Pakistan
- Received Bachelor's degree in Mechanical Engineering from the N.E.D. University of Engineering and Technology, Karachi, Pakistan in June, 1990.
- Completed Master's degree requirements at King Fahd University of Petroleum and Minerals, Dhahran, Saudi Arabia in January, 1994.